

**The synthesis of star copolymers for the delivery of
macromolecular guest & photodynamic therapy**



Alaa Kadhim

PhD Thesis

March 2018

The synthesis of star copolymers for the delivery
of macromolecular guest & photodynamic therapy

Alaa Fadhil Kadhim

A thesis submitted for the degree of Doctor
of philosophy

Department of Chemistry

The University of Sheffield

Sheffield S3 7HF

England

March 2018

To Mum and Dad,

Thanks for your endless love

Acknowledgments

I would like to express my sincere gratitude to Dr. Lance Twyman for his guidance in all the time of my research and writing up. I could not have imagined having a better supervisor for my Ph.D study.

As a part of my scholarship, I had the opportunity to travel to Singapore working with carcinoma cells. This would not be possible without the help and guidance I have received from Dr. Haishan Wang, my sincere thanks also goes to him. Special thanks go to Dr. Helen Bryant and Luke Mckenzie, who have accepted to collaborate with us and completed the cell works. Without their precious support it would not be possible to conduct this research.

To my group members-Azrah, Abdullah, Bunian, Devanshi, Fatema, Greg, Hamza, Ibrahim, Jawad, Mang, Saimra and Talal- thanks for the stimulating discussions, and for all the fun we have had in the last four years. I would like to thank Heather, Nick, Peter, Simon and the department of Chemistry for providing the essential laboratory and technical support towards my research work.

Last but not the least, I would like to thank my family: my parents and to my sisters and brother in law for supporting me spiritually throughout my writing this thesis and my life in general.

Table of Figures

FIGURE 1.1: EXAMPLE FOR CONTROLLED DRUG DELIVERY. ^[7]	24
FIGURE 1.2: CURVE OF DRUG CONCENTRATION IN PLASMA OVER TIME AFTER A SINGLE DOSE ^[16]	25
FIGURE 1.3: DRUG CONCENTRATIONS IN PLASMA AFTER DELIVERY BY CONVENTIONAL INJECTION IN A CHRONIC DISEASE ^[17]	26
FIGURE 1.4: POLYMER FUNCTIONALIZED TO INTERACT WITH SPECIFIC TARGETS ^[24-26]	27
FIGURE 1.5: ENDOCYTOSIS IS THE PROCESS BY WHICH MOLECULES ENTER INTO CELLS. ^[30] FIRSTLY, THE CELL MEMBRANE FOLDS' INWARDS RESULTS IN THE FORMATION OF A SMALL VESICLE CALLED ENDOSOME. THIS ENDOSOME THEN MERGES WITH A LYSOSOME AND FORMS A SECONDARY LYSOSOME, WHICH CONTAINS AN ACIDIC INTERNAL ENVIRONMENT WITH ENZYMES WHERE THE LINKER MOLECULES BREAK AND RELEASE THE DRUG. ^[31]	29
FIGURE 1.6: SCHEMATIC REPRESENTATION SHOWING THE ANATOMICAL AND PHYSIOLOGICAL CHARACTERISTICS OF HEALTHY AND MALIGNANT TISSUE IN TERM OF THE VASCULAR PERMEABILITY AND RETENTION OF SMALL AND LARGE MOLECULES (EPR EFFECT). ^[27]	31
FIGURE 1.7:EXAMPLES OF COVALENT AND NON-COVALENT ENCAPSULATION ^[37]	32
FIGURE 1.8: FREE SURFACTANT MOLECULES BELOW CMC (LEFT) AND ABOVE CMC FORMING A MICELLE (RIGHT)	33
FIGURE 1.9: STEP GROWTH POLYCONDENSATION.....	36
FIGURE 1.10: SELF-CONDENSING VINYL POLYMERIZATION	36
FIGURE 1.11: RING OPENING POLYMERIZATION.....	37
FIGURE 1.12: EXAMPLES OF PORPHYRIN (I-IV) AND NON-PORPHYRIN BASED PS SYSTEMS (V-VII).....	39
FIGURE 1.13:CHEMICAL STRUCTURE OF PHOTOFRIN, A MIXTURE OF HEMATOPORPHYRIN DIMERS AND OLIGOMERS	40
FIGURE 1.14: CHEMICAL STRUCTURE OF CHLORINE E6.....	41
FIGURE 1.15: FORMATION OF PDT ROS THROUGH TYPE 1 AND 2 [62].....	42
FIGURE 2.1: THE CHEMICAL STRUCTURE OF THE PORPHYRIN CORED HYPERBRANCHED POLYMER (HBP 15) AS A MACRO-GUEST	49
FIGURE 2.2: POSSIBLE SELF-ASSEMBLY OF PORPHYRIN-CORED STAR COPOLYMERS	50
FIGURE 2.3: POTENTIAL PORPHYRIN DERIVATIVE TO BE USED AS A CORE IN DRUG DELIVERY SYSTEMS FOR PDT APPLICATIONS THPP 12 AND TDHPP 13	51
FIGURE 3.1: CHEMICAL STRUCTURE OF THE TRIMETHYLOLPROPANE 1 ,EPSILON-CAPROLACTONE 2 AND GLYCIDOL 3 SELECTED FOR THE PROPOSED COPOLYMERS.	54
FIGURE 3.2: ¹ H NMR SPECTRA OF SPCL ₆₀ -HPG ₉₀ IN CDCl ₃	57
FIGURE 3.3: ¹ H NMR SPECTRA OF SPCL ₆₀ -HPG ₉₀ IN D ₂ O.....	57

FIGURE 3.4: CMC DETERMINATION OF SPCL ₆₀ -HPH ₉₀	63
FIGURE 3.5: CMC LEVEL OF TMP-HPG ₉₀	64
FIGURE 3.6: TREND TO SHOW THE INCREASE IN THE CONCENTRATION OF THE ENCAPSULATED HBP 11 WITHIN DIFFERENT SIZE OF STAR COPOLYMERS AND ONE CONTROL	70
FIGURE 3.7: SCHEMATIC REPRESENTATION SHOWING WHERE THE ENCAPSULATION OF THE MACROMOLECULAR GUEST (TAPP-HBP 15) WITH A) HPG AND B) STAR COPOLYMER HAPPEN.....	71
FIGURE 4.1: POTENTIAL PORPHYRIN DERIVATIVE TO BE USED AS A CORE IN DRUG DELIVERY SYSTEMS FOR PDT APPLICATIONS THPP 12 AND TDHPP 13	75
FIGURE 4.2: DELOCALIZATION OF THE HYDROXYL LONE PAIR WITH THE AROMATICITY OF THE PORPHYRIN RING	84
FIGURE 4.3: STRUCTURES OF S-THPP-HPG 28 AND S-TDHPP-HPG 29	88
FIGURE 4.4: PLOTS OF THE HYDRODYNAMIC DIAMETER OBTAINED FOR VARIOUS CONCENTRATIONS OF A) S-THPP ₁ -PCL ₄₀ -HPG ₆₀ 31 , B) S-THPP-HPG 28 AND C) THPP-HPG IN DEIONISED WATER.....	94
FIGURE 4.5: PLOTS OF THE INTENSITY RATIO OF I ₁ /I ₃ AGAINST LOG CONCENTRATION OF A) SPPCL-HPG 41 , B) S-THPP-HPG 31 AND C) THPP-HPG IN DEIONISED WATER.	96
FIGURE 4.6: % CELL VIABILITY OF THE PHOTOTOXICITY SRB ASSAY OF MCF-7 CELLS TREATED WITH DIFFERENT CONCENTRATIONS OF A) COMPOUND 41 AND B) COMPOUND 33 AT DIFFERENT LED DOSES OF ZERO (DARK), 5 MINUTES LED (0.84 J/cm ²) AND 10 MINUTES LED (1.65 J/cm ²).....	98
FIGURE 4.7: % CELL VIABILITY OF THE DARK TOXICITY SRB FOR OF MCF-7 CELLS WITH AND WITHOUT REMOVAL OF THE MEDIA FOR 10 MINUTES	99
FIGURE 4.8: % CELL VIABILITY OF THE DARK TOXICITY SRB ASSAY OF MCF-7 CELLS TREATED WITH DIFFERENT CONCENTRATIONS OF A) COMPOUND 31 AND B) COMPOUND 33	100
FIGURE 4.9: PHOTOTOXICITY OF MCF-7 CELLS TREATED WITH DIFFERENT CONCENTRATIONS OF A) COMPOUND 31 AND B) COMPOUND 33	100
FIGURE 4.10: GRAPH SHOWING THE DARK TOXICITY OF THE THPP-SET COMPOUNDS IN EJ CELLS AT 100 μM	101
FIGURE 4.11: DARK TOXICITY OF THPP AT DIFFERENT CONCENTRATIONS IN EJ CELL LINE	102
FIGURE 4.12: DARK TOXICITY OF TDHPP MOLECULE AND TDHPP-CORED POLYMER AT 100 μM	103
FIGURE 4.13: PHOTOTOXICITY OF THPP-SET COMPOUNDS USING EJ CELL LINE AT A LIGHT DOSE OF 10 mW/cm ²	103
FIGURE 4.14: PHOTOTOXICITY OF TDHPP-SET COMPOUNDS USING EJ CELL LINE AT A LIGHT DOSE OF 10 mW/cm ²	104
FIGURE 5.1: THE CHEMICAL STRUCTURE OF PACLITAXEL	111

FIGURE 5.2: BEER LAMBERT PLOT OF PTX IN MeOH: PBS (3:7)	112
FIGURE 5.3: PTX TOXICITY TO BLADDER CELL LINE AT DIFFERENT INCUBATION TIMES.....	116
FIGURE 5.4: STRUCTURE OF S-THPP ₁ -PCL ₄₀ -HPG ₆₀ 31	116
FIGURE 5.5: TOXICITY OF DIFFERENT CONCENTRATIONS OF THE STAR COPOLYMER TO BLADDER CELL LINE (NO PTX ENCAPSULATION)	117
FIGURE 5.6: CYTOTOXICITY OF PTX ENCAPSULATED WITH STAR COPOLYMER	117
FIGURE 5.7: STRUCTURE OF PTX INDICATING THE ELECTROPHILIC SITES.....	118
FIGURE 5.8: POSSIBLE PTX-MICELLE FORMATION	119

Table of Table

TABLE 3.1: SUMMARY OF THE ESTIMATED MN VALUES BY GPC AND ¹ H NMR SPECTROSCOPY, AND THE EXPECTED MN OF THE HYDROPHOBIC SEGMENT OF STAR POLYMERS (SPCL)	58
TABLE 3.2: SUMMARY OF THE ESTIMATED MN VALUES BY GPC AND ¹ H NMR, AND THE EXPECTED MN OF THE OF THE STAR CO- POLYMERS (SPCL-HPG)	59
TABLE 3.3: MOLECULAR WEIGHT CHARACTERIZATION OF HPG POLYMERS.....	62
TABLE 3.4: TABLE SHOWING THE ENCAPSULATION OF TAPP-HBP 15 WITHIN THE HOST POLYMERS AT 10MG/ML.....	69
TABLE 4.1: SUMMARY OF THE AVERAGE MOLECULAR WEIGHT OF PORPHYRIN-CORED POLYGLYCEROLS USING DIFFERENT TECHNIQUES	81
TABLE 4.2: SUMMARY OF THE AVERAGE MOLECULAR WEIGHT OF PORPHYRIN-CORED POLYGLYCEROLS USING DIFFERENT TECHNIQUES	89
TABLE 4.3: MOLECULAR WEIGHT OF THE INITIAL STAR POLYMERS DETERMINED BY DIFFERENT TECHNIQUES	89
TABLE 4.4: MOLECULAR WEIGHT OF THE STAR COPOLYMERS DETERMINED BY DIFFERENT TECHNIQUES	90
TABLE 4.5: SUMMARY OF CMC LEVELS OBTAINED FOR POLYMERS AND THEIR DIAMETER AT THE CMC LEVEL	95
TABLE 4.6: COMPOUNDS LABELLING	101
TABLE 4.7: TABLE TO SHOW THE CONFOCAL IMAGES FOR NAKED PORPHYRIN (THPP (TH)), COMPOUND 1 (THPP-HPG), COMPOUND 3 (S-THPP-HPG 33) AND COMPOUND 5 (SPPCL ₄₀ -HPG ₆₀ 41).....	105
TABLE 4.8: TABLE TO SHOW THE CONFOCAL IMAGES FOR NAKED PORPHYRIN (TDHPP (TD)), COMPOUND 2 (TDHPP-HPG), COMPOUND 4 (S-TDHPP-HPG 34) AND COMPOUND 5 (SPPCL ₁₀ -HPG ₃₅ 43).....	106

TABLE 5.1: CHARACTERISATION OF PTX IN MeOH: PBS (3:7)	111
TABLE 5.2: THERMODYNAMIC AND KINETIC SOLUBILITY OF PTX IN WATER	113
TABLE 5.3: ENCAPSULATION RESULT OF PTX WITH STAR COPOLYMERS AND HPGS	115

List of abbreviation

Standard Abbreviations

^{13}C NMR

Å

ADME

API

ATRP

CDD

CMC

D₂O

d₆ -DMSO

Da

DB

DCM

DDS

DLS

DMF

EPR

ES-MS

FDA

FT-IR

GPC

HBP

Standard Abbreviations

Carbon Nuclear Magnetic Resonance Spectroscopy

Angstrom

absorption, distribution, metabolism, excretion

Active pharmaceutical ingredients

Atom Transfer Radical Polymerisation

Controlled Drug Delivery

Critical Micelle Concentration

Deuterated Water

Deuterated Dimethyl Sulphoxide

Dalton

Degree of Branching

Dichloromethane

Drug Delivery System

Dynamic Light Scattering

Dimethylformamide

the enhanced permeability and retention

Electrospray Ionisation Mass Spectrometry

Food and Drug Administration

Fourier Transform Infrared Spectrophotometry

Gel Permeation Chromatography

Hyperbranched Polymer

HMW	High Molecular Weight
HPD	Hematoporphyrin derivative
HPG	Hyperbranched polyglycerols
K	Kilo
K ₂ CO ₃	Potassium Carbonate
LWM	Low Molecular Weight
M	Molar
Mn	Number Average Molecular Weight
mTHPC	M-tetrahydroxyphenyl chlorine
MW	Molecular Weight
Mw	Weight Average Molecular Weight
nm	Nanometre
NPe6	Mono-L-aspartyl chlorine e6
°C	Degree Celsius
OH	Hydroxyl
PCL	Polycaprolactone
PCL	Poly(caprolactone
PD	Pharmacodynamics
PDI	Polydispersity Index
PDT	Photodynamic therapy
PEG	Polyethylene Glycol
PK	Pharmacokinetics
ppm	Part Per Million

PS	Photosensitizers
ROP	Ring Opening Polymerisation
ROS	Reactive oxygen species
SEC	Size Exclusion Chromatography
TDHPP	Tetrakis(3,5-dihydroxyphenyl)-porphyrin
TDMPP	Tetrakis(3,5-dimethoxyphenyl)-porphyrin
THF	Tetrahydrofuran
THPP	Tetrakis(4-hydroxyphenyl)-porphyrin
TMP	Trimethylolpropane
UV/Vis	Ultraviolet-Visible Light Spectrophotometry

Contents

ACKNOWLEDGMENTS	4
List of abbreviation	9
Abstract	16
1. Introduction	21
1.1. NOVEL DRUG DELIVERY SYSTEM.....	21
1.1.1 <i>Controlled Drug Release Method</i>	24
1.1.2 <i>Time-Controlled: Modified-Release Formulation</i>	25
1.1.3 <i>Controlled Distribution</i>	27
1.1.4 <i>The enhanced permeability and retention (EPR) effect</i>	29
1.1.5 <i>Drug encapsulation</i>	31
1.1.6 <i>Polymeric system: synthesis and application</i>	32
1.2 PHOTODYNAMIC THERAPY.....	37
1.2.1 <i>Photosensitizers agents (PSs)</i>	38
1.2.2 <i>Therapeutic irradiation</i>	41
1.2.3 <i>Photophysics</i>	41
1.2.4 <i>Photochemistry</i>	42
1.2.5 <i>Mechanisms of cell death in PDT</i>	43
1.2.6 <i>Use of Nanoparticles</i>	44
2. Aims and Objectives	46
2.1 SYNTHESIS OF STAR COPOLYMERS FOR LARGE DRUG DELIVERY SYSTEM	46
2.1.1 <i>General Design of the Proposed Drug Delivery System (Star Copolymers) and control systems</i> 46	
2.1.2 <i>Control system</i>	48
2.1.3 <i>Testing the macro-encapsulation potential of the star copolymers</i>	48
2.2 PORPHYRIN-CORED STAR COPOLYMERS FOR PHOTODYNAMIC APPLICATION	49
2.3 CHEMO-PHOTODYNAMIC COMBINATION THERAPY	51
3. Synthesis of star copolymers for large drug delivery systems	53
RESULT AND DISCUSSION	ERROR! BOOKMARK NOT DEFINED.
3.1 SYNTHETIC CONSIDERATIONS	53
3.2 ONE-POT SYNTHESIS OF THE POLY (E-CAPROLACTONE)-B-POLYGLYCEROLS (PCL-HPG).....	54
3.3 ANIONIC RING OPENING POLYMERIZATION OF FORMING POLY (E-CAPROLACTONE).....	55
3.4 THE STRUCTURAL CHARACTERISATION OF SPCL-HPG AMPHIPHILIC COPOLYMERS.....	56
3.5 ONE-POT SYNTHESIS OF HYPERBRANCHED POLYGLYCEROLS (HPG).....	59
3.6 CHARACTERISATION OF HYPERBRANCHED POLYGLYCEROLS.....	61
3.7 AGGREGATION OF STAR COPOLYMERS	62
3.8 SELECTION OF A SUITABLE MACROMOLECULAR GUEST	64

3.9	THE SYNTHESIS OF A PORPHYRIN CORED FUNCTIONALIZED HBP (LARGE MOLECULE).....	65
3.10	ENCAPSULATION OF A LARGE HYDROPHOBIC MACROMOLECULAR.....	68
3.11	SUMMARY.....	71
4.	Porphyrin cored star copolymers for photodynamic therapy.....	74
	RESULT AND DISCUSSUIO.....	74
4.1	SYNTHESIS AND CHARACTERISATION OF PORPHYRIN PHOTSENSITIZERS.....	74
4.1.1	<i>Tetrakis(4-hydroxyphenyl)-porphyrin (THPP 12)</i>	75
4.1.2	<i>Tetrakis(3, 5-dihydroxyphenyl)-porphyrin</i>	78
4.2	SYNTHESIS OF PORPHYRIN-CORED HYPERBRANCHED POLYGLYCEROLS (HPG).....	80
4.3	PORPHYRIN STAR POLY(ε-CAPROLACTONE)-POLYGLYCEROL COPOLYMERS.....	82
4.4	SYNTHESIS OF PORPHYRIN INITIATORS.....	84
4.4.1	<i>Acetonide-porphyrin</i>	84
4.4.2	<i>Spacer-porphyrin (S-porphyrin)</i>	87
4.4.3	SYNTHESIS OF SPACER-PORPHYRIN-CORED HYPERBRANCHED POLYGLYCEROLS.....	88
4.5	SYNTHESIS OF PORPHYRIN STAR POLY(ε-CAPROLACTONE)-POLYGLYCIDOL COPOLYMERS (SPPCL-HPG)....	89
4.6	MICELLE FORMULATION.....	93
4.6.1	<i>Dynamic light scattering</i>	93
4.6.2	<i>Fluorescence technique</i>	95
4.7	IN VITRO STUDY (CYTOTOXICITY AND PHOTOTOXICITY).....	97
4.8	CELL WORK USING MCF-7.....	97
4.9	MTT ASSAY USING EJ CELL LINES.....	101
4.9.1	<i>Intracellular localisation</i>	104
4.10	SUMMARY.....	107
5.0	Chemo-Photodynamic Combination Therapy.....	110
5.1	<i>Kinetic/Thermodynamic Solubility of PTX in water</i>	112
5.2	ENCAPSULATION OF PTX IN THE POLYMERIC MICELLES.....	113
5.3	<i>Encapsulation results</i>	114
5.4	IN VITRO STUDY.....	115
5.4.1	<i>Control experiment to determine PTX toxicity to bladder cell line</i>	115
5.4.2	<i>Polymer toxicity to bladder cell line</i>	116
5.5	ENCAPSULATION OF PTX USING KINETIC METHOD	121
5.6	SUMMARY.....	123
6.0	Conclusion and Further-work.....	126
7.0	Experimental.....	130
7.1	GENERAL CONSIDERATION.....	130
7.1.1	<i>Reagents, solvents and general equipment</i>	130
7.1.2	<i>Nuclear magnetic resonance spectroscopy</i>	130
7.1.3	<i>UV-Vis Spectroscopy</i>	130
7.1.4	<i>IR Spectroscopy</i>	130
7.1.5	<i>Thermal analysis</i>	131
7.2	SYNTHESIS OF PORPHYRIN MOLECULES.....	131
7.2.1	<i>5,10,15,20-Tetrakis(4-hydroxyphenyl)-21H,23H-porphine (THPP 12)</i>	131

7.2.2	<i>Tetrakis (3, 5-dimethoxyphenyl)-21H, 23H-porphyrin (TDMPP 18)</i>	132
7.2.3	<i>Tetrakis (3, 5-dihydroxyphenyl)-21H, 23H-porphyrin (TDHPP 13)</i>	133
7.3	SYNTHESIS OF PORPHYRIN INITIATOR	134
7.3.1	<i>Spacer-porphyrin (S-TDHPP 27)</i>	134
7.3.2	<i>Spacer-porphyrin S-THPP 26</i>	135
7.4	SYNTHESIS OF TAPP CORED POLY (3, 5-DIACETOXYBENZOIC ACID) 15	136
7.4.1	<i>Synthesis of 3, 5-diacetoxybenzoic acid (13)</i>	136
7.4.2	<i>Synthesis of 4-acetoxybenzaldehyde (7)</i>	136
7.5	SYNTHESIS OF TETRAKIS (4-DIACETOXYPHENYL)-21H, 23H-PORPHYRIN (TAPP 12)	137
7.6	SYNTHESIS OF TAPP CORED POLY (3, 5-DIACETOXYBENZOIC ACID) (15).....	138
7.7	GENERAL PROCEDURE FOR SYNTHESIS OF HYPERBRANCHED POLYGLYCEROL	139
7.7.1	<i>Synthesis of trimethylolpropane (TMP) core hyperbranched polyglycerol</i>	140
7.7.2	<i>Synthesis of porphyrin core hyperbranched polyglycerol</i>	140
7.7.3	<i>Synthesis of (porphyrin with spacer) core hyperbranched polyglycerol</i>	141
7.8	GENERAL PROCEDURE FOR SYNTHESIS OF AMPHIPHILIC COPOLYMERS BASED ON POLY(CAPROLACTONE) AND POLYGLYCEROLS	143
7.8.1	<i>Synthesis of trimethylolpropane (TMP) cored star poly (caprolactone)-block- hyperbranched TMPPCL-b-HPG</i>	144
7.8.2	<i>Synthesis of porphyrin cored star poly (caprolactone)-b-hyperbranched</i>	146
7.9	CRITICAL AGGREGATION CONCENTRATION (CAC).....	148
7.10	CELL CULTURE.....	148
7.10.1	<i>Imaging</i>	149
7.10.2	<i>Light and dark toxicity – MTT assay</i>	149
8.0	References	151

Abstract

Traditional delivery systems use polymeric structures that contain internal voids or specific functionality that can be used to encapsulate smaller molecules, protecting them from external environments and delivering them to specific sites. Although considerable success has been achieved in the delivery of small organic molecules, these systems are not suitable for the delivery of (larger) biomolecular drug moieties. This project has addressed this issue by constructing and studying nano-sized macromolecular carriers with the capacity to form and maintain a large volume of free internal space. A star polymeric core was synthesised to generate a suitable environment that can be used to encapsulate large macromolecular guest. The synthesis of the star copolymers involved a multi-step reaction process using a single pot procedure. Initially, a core functionalized with hydroxyl end groups (trimethylol propane TMP) was used as an initiator to ring open and polymerize caprolactone. The resulting hydrophobic star polymers (star poly(caprolactone) (SPCL)) which possessed a nucleophilic end group, were used to initiate a second ring opening polymerization (ROP) using a branched hydrophilic monomer (glycidol). Three star copolymers (SPCL-HPGs) were prepared with different chain length and similar size of the capping group (SPCL₁₅-HPG₉₀, SPCL₃₅-HPG₉₀ and SPCL₆₀-HPG₉₀) in order to study the effect of the chain length upon encapsulating large molecule. Hydrophilic HPG was synthesised as the only control system of our proposed drug delivery system. The aggregation was then studied using pyrene as probe. The study showed that both the star copolymer (SPCL₆₀-HPG₉₀) and the control (TMP₁-HPG₉₀) aggregate and form micelles at 10-20 µg/mL and 150 µg/mL, respectively. Having synthesised successfully the proposed drug delivery system and the control, a model macromolecular guest, a synthetic mimic of hemoglobin, was selected for the encapsulation. It is proposed that encapsulation of the synthetic mimic of hemoglobin (TAPP-HBP **15**) within the core of the star copolymers improved its water solubility and making it artificial blood product. The guest was synthesised

successfully with an average molecular weight of 18K Da. Upon encapsulation, significant amount of the guest was loaded within the star copolymers than the control system by 10 factors. The encapsulation of the guest is thought to happen with the aggregated structure of the polymer rather than within the structure of the host. This was concluded because although the HPG does not have hydrophobic segment, it has encapsulated the large guest.

The second part of the project discussed the synthesis of star copolymers with porphyrin core for photodynamic therapy (PDT). PDT is one of the outstanding protocols for cancer treatment, which involves the combined action of photosensitizer (PS), once accumulated into cancer cells, and irradiation with the light of appropriate wavelength. Porphyrins and their derivatives have been used extensively in PDT. Although PDT is an alternative therapeutic method to traditional cancer treatment, there are still a number of problems, which limit its clinical application. These include selectivity, solubility and therapeutic efficiency. In this study, the solubility of porphyrins in aqueous solution was enhanced significantly via covalent incorporation within aggregated water-soluble polymers (porphyrin cored star copolymers). Two porphyrin molecules with hydroxyl end group were selected as a core for the star copolymer, these are: tetrakis(3,5-dihydroxyphenyl) porphyrin (TDHPP), and tetrakis(4-(hydroxyphenyl)porphyrin (THPP). However, TDHPP and THPP were very unreactive initiators and did not polymerise with the caprolactone until a spacer was added to the porphyrin so that the lone pair of their terminal hydroxyl group cannot be part of the porphyrin conjugation system. Thus, two star copolymers were synthesised from spacer-porphyrin (S-THPP-PCL-HPG) and S-TDHPP-PCL-HBP). The control (porphyrin-HPG) were synthesised from porphyrins with and without spacer units. The particle size of all the aggregated polymers was between 100-200 nm determined by DLS. As such, favourable/selective delivery via the enhanced permittivity and retention effect (the EPR effect) was expected. The polymers were analysed for their PDT behaviour via a simple MTT assay, using EJ bladder carcinoma cell

line. The relative viability of the polymers and its controls in the dark were higher than 0.8 at 100 μM except the THPP-HPG polymer which had viability of 0.2.

Under light irradiation (10 mW/cm^2), significant toxicity was observed at 1 μM for the free THPP and at 10 μM for the free TDHPP porphyrin. While phototoxicity of the polymers, considerable cell death was obvious at polymers concentration of 10 μM for the THPP cored polymers except the star copolymer, which did not show any significant toxicity at this concentration. The phototoxicity of TDHPP cored polymers were significant for TDHPP-HPG and S-TDHPP-HPG at 100 μM for and poor for the star copolymer at the same concentration. The intracellular localisation of the molecules porphyrin cored polymers into the EJ cells was imaged by confocal microscopy. Both of the free porphyrin (THPP and TDHPP) molecules diffused within the cell at 10 μM . Porphyrin cored HPG polymers also diffused within the cells but as the spacer was added the diffused the fluorescence decreased. The porphyrin-PCL-HPGs star copolymers showed no diffusion into the cells. Thus, porphyrin-cored HPG polymers was deemed to be promising photosensitizers for photodynamic therapy (PDT) rather than the star copolymers.



Chapter 1

Introduction to drug delivery systems

1. Introduction

The graded development of drug delivery system started with the use of polymeric carriers to enhance drug stability and modify the release characteristics. Polymers range from their use as binders and film coating agents in tablets to viscosity and flow controlling agents in liquids, suspensions and emulsions; to disguise the unpleasant taste of a drug, enhance drug stability and of modify the release characteristics. Today, modern drug delivery systems have benefited many patients by enabling them receive safer and more effective doses of medicines that are desired to fight a variety of human diseases. However, still there are many fatal diseases that are not yet cured and threatening human life due to the problem encountered by formulation scientists in drug delivery approaches. For this reason, new formulations are being developed to achieve a complete therapeutic effect of the existing drug molecules; among these, polymeric materials in novel drug delivery approaches are of highly interest.

1.1. Novel Drug Delivery System

A Drug Delivery System (DDS) is defined as a formulation or a device that enables the administration of a therapeutic substance to desired body location and provides timely release of therapeutic agent. The way a drug is delivered can affect its efficacy. Though, the very slow progress in the effectiveness of curing difficult diseases, demand a growing need for a multidisciplinary approach to the delivery of therapeutics to their targets. From this, new development on controlling the pharmacokinetics (PK) and pharmacodynamics (PD) is being studied. PK studies investigate the system in which drugs move through the body. It rules the route of administration and can be broken down into four different areas (ADME): adsorption of the drug, distribution of the drug molecules, metabolism of the parent drug and excretion/elimination of the drug and its metabolites. It is vital to keep a balance between these processes which ensures the drug stays in the body long enough to show its therapeutic effect but not so long that it is regarded as being toxic. PD studies the relationship between the drug

concentration at the site of action and the resulting effect of it on the body. This is controlled by the way the drug interacts with its target site including the mechanism of action, pharmacological response, and affinity to the site of action. Previous studies have shown that the drug is most effective when its stereoelectronic structure is complementary with the stereoelectronic structure of the target site. ^[1]

The drug that possesses the pharmacological activity is called the Active pharmaceutical ingredients (APIs). Being small in quantity, the API is usually unable to be administered on its own. Therefore, some aiding substances called excipients are added in the API and a dosage form is formed that makes it easier to be administered to a patient. Emulsifiers, dyes, lubricants, diluents, supporters, and chemical stabilizers are some of the commonly used excipients. Once considered inert, the excipients are now known to be selected carefully as they can affect the speed and extent of drug absorption and, hence, the drug bioavailability. Immense research is being conducted in the field of an effective drug delivery system development. Such a delivery system is desired to be made that not only provides a controlled drug release and absorption, with special consideration to the poorly water soluble drugs, but also offers a dosage form that is convenient for the patient and allows easier administration of drug.

The high molecular weight carriers for example micelles, hyperbranched polymers and dendrimers, are known to form the basic components of the drug delivery systems. The API reaches its site of action by the help of these carriers where the API is either attached to the carrier's surface in the form of a prodrug or present within the polymer's inner core. The carrier polymers not only protect the APIs from the harmful effects of the outer environment, which renders it pharmacologically ineffective but also prevents the unnecessary interactions of the APIs with the macromolecules such as proteins that are responsible to hinder the drug to reach its target site of action. An ideal polymeric carrier must have a structure that allows it to release the drug at a desired rate and should have the properties like biodegradability. The polymeric

carriers adopt certain pathways to be eliminated from the body. Renal clearance (involving the kidneys) and metabolic clearance are the two pathways by which the polymers leave the body. Usually, the substances with a low molecular weight (approximately less than 50 KDa, which may be subject to change based on chemical structure)^[2-3] can easily pass the renal glomerular membrane and, hence, any polymer with a molecular weight lower than this value can effectively be excreted out from the body. It is important to note that the molecular weight is the most important factor to be considered in case of substances that are not biodegradable.

The chemical structure of the polymer, which includes the degree of hydrophobicity, covalent bonds between monomers, etc., is the most important factor in ideal polymer design that must be considered in case of biodegradable polymers. The reason behind this selection is the effect of chemical structure on the other important features like speed and degradation of the polymer and, hence, at the rate and site of drug release. Different linkers are used in cases where polymer is not biodegradable to release the drug moiety. For example, L. Erdmann et al reported that hydrolytic degradation of poly(anhydride ester) yield two equivalents of salicylic acid (SA) and one equivalent of sebacic acid. Local release of SA found to promote healing. Drug is covalently attached to the polymer via linkers.^[4a] These linkers break in response to specific conditions such as presence of an acidic medium or different enzymes and, thus, release of the drug. Similarly, different target molecules can be used that are attached to the surface of the polymer to achieve a directed drug delivery. Also, the use of smart polymers in making of carriers is gaining importance. These smart polymers are known to carry numerous benefits, which can be modulated by providing certain stimulations. The stimulations are known to alter the structure of the polymer, hence, allowing the release of drug at a controlled time and place. Some of the major benefits associated with the use of this smart polymer include improved pharmaceutical profile and drug stability, maximum biocompatibility with minimum side effects and facilitated accumulation of the drug for an extended period at a specific target site.

A rational model for pharmacologically active polymers was first proposed by Ringsdorf in 1975. [4b] The Ringsdorf model mainly involves of a biocompatible polymer backbone conjugated to three components: a solubilizer, to ensure water solubility, a drug, bound to the polymeric backbone via a linker, and a targeting moiety to provide transport to a desired physiological location or bind to a specific biological target.

1.1.1 Controlled Drug Release Method

Controlled-release systems aim to improve drug therapy. [5-6] The basic rationale of controlled drug delivery system is to optimize the pharmacokinetic and the pharmacodynamics properties of drug in such a way that its utility is maximized through reduction in the side effects and cure or control of condition in the shortest possible time by the most suitable route.

Controlled Drug Delivery (CDD) occurs when a polymer is judiciously combined with a drug or other active agent in such a way that the active agent is released from the bulk material in a pre-designed manner. The purpose behind controlling the drug delivery is to achieve more effective therapies while eliminating the potential for both under and overdosing. An example of Controlled drug delivery was shown in figure 1.1.

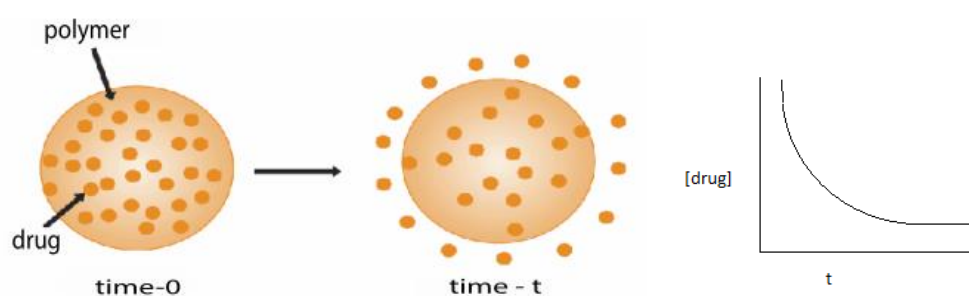


Figure 1.1: Example for Controlled Drug Delivery.[7]

Different types of drug classes like anti-inflammatory agents, [8-10] antibiotics, [11] chemotherapeutic drugs, [12] immunosuppressants, [13] anaesthetics, [14] and vaccines [15] can be formulated in the form of controlled release drug delivery systems in order to get the distribution or time-controlled drug delivery. This type of drug delivery is essentially beneficial

when either the drug reacts with the non-target tissues in its normal distribution path causing potential side effects or when the degradation makes it unable for the drug to reach its specific site of action.

1.1.2 Time-Controlled: Modified-Release Formulation

As the name indicates, in these formulations, the release of the drug is controlled. The drug is released at a controlled rate and ultimately achieves the desired therapeutic concentration at the target site. Figure 1.2 shows the case of a singly administered dose of a drug showing the achievement of an immediate (short-term) therapeutic concentration of the active ingredient.

[18]

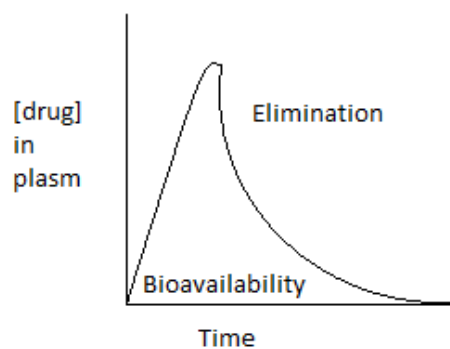


Figure 1.2: Curve of drug concentration in plasma over time after a single dose ^[16]

It can be seen from figure 1.2 that the drug continues to be absorbed until it reaches its maximum concentration (or till the desired bioavailable dose gets absorbed) followed by a slow and steady fall in drug absorption which is shown by the gradual decreases drug concentration in the plasma. ^[19] This gradual drop actually shows the elimination phase of the drug, which is dependent on both the metabolism and excretion. The minimum concentration of drug that is required to get desired pharmacological effects is called the effective (therapeutic) concentration whereas the concentration above which there are chances of occurrence of side effects or toxic effects is called the maximum safe concentration. Between the effective

(therapeutic) concentration and the maximum safe concentration lies the area which is termed as the therapeutic window and the drug concentration must lie in this therapeutic window to give the desired therapeutic effects. Figure 1.3 shows a chronic treatment case where multiple doses are administered at regular intervals. It is in this case where there are higher chances of under or over dosing due to alterations in the API concentrations. The drug concentrations higher than the desired therapeutic concentrations cause toxic effects whereas lower than the desired concentrations lead to therapeutic failure.

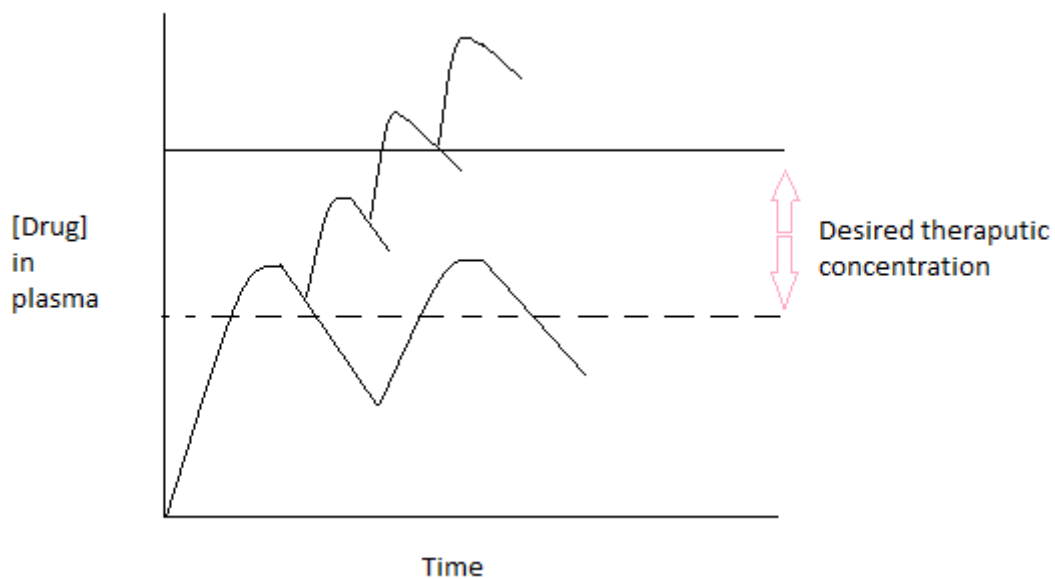


Figure 1.3: Drug concentrations in plasma after delivery by conventional injection in a chronic disease^[17]

Strict adherence to the drug administration pattern is required in case of chronic treatments to prevent the events of drug toxicity. Half-life is an important factor that must be considered in case of these multiple dosing treatments. Half-life is actually the time that is taken by a drug to reduce its concentration by one half after reaching the systemic circulation. Multiple drug doses are generally administered at the intervals of two times the half-life of the drug in systemic circulation. The modified-release formulation, on the contrary, is believed to deliver the drug

at a speed or at a site (other than the administration site) that is determined before the actual administration of the drug.

1.1.3 Controlled Distribution

Drug carriers with a controlled distribution system are used in case of controlled drug distribution, which allows the distribution of drug at the desired target site. Different methods are being employed in order to achieve controlled drug distribution.

Use of molecular tracking devices is one of the most commonly used methods to get targeted drug distribution. Research in molecular biology has established that certain receptors are over expressed in diseased tissues as in case of cancer. If these receptors on the targeted diseased tissues are recognised, then the surface of the nano- and micro-drug-polymers complex can be modified by attaching receptor recognition elements or tracking devices; hence, a controlled drug distribution at a specific target site can be achieved (see figure 1.4). Antibodies ^[20-21], carbohydrates ^[22] and simple electrically charged species are some of the commonly used tracking devices ^[23].

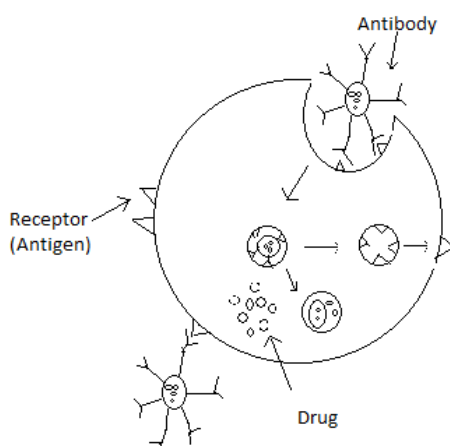


Figure 1.4: Polymer functionalized to interact with specific targets ^[24-26]

Another approach to achieve a controlled distribution is by the use of hydrogels. In this approach, the drug is either encapsulated or absorbed in a hydrogel, which is then released by

diffusion through the hydrogel system. An interesting feature of this approach is that the release of drug from the hydrogel is triggered by different external stimulus, which are studied and explained extensively by Qiu et al. and Gupta et al. ^[27-28]

Following different controlled drug release models/systems are studied: the pH-dependent system where ionisable groups are present in the hydrogel structure, which responds to changes in pH by showing attraction and repulsion among the molecules of its structure, hence, stopping and allowing the drug release respectively, electrical signals-controlled drug release systems where electrical signals cause changes in the pore size and permeability and hence the release of drug were studied as well as the temperature-dependent hydrogel systems. In addition to that, specific substances-dependent drug release systems where the concentration of substances in the external environment (like glucose, urea and morphine) alters the drug release and systems bearing specific linker molecules ^[29] that are degraded in the presence of acidic environment (for example the endosomal acidic environment and tumor tissues) or specific enzyme (for example the lysosomal environment containing proteolytic and hydrolytic enzymes) cause drug release were also studied.

Endocytosis ^[30] is the process by which molecules enter into cells. Firstly, the cell membrane folds' inwards results in the formation of a small vesicle called endosome. This endosome then merges with a lysosome and forms secondary lysosome, which contains an acidic internal environment with enzymes where the linker molecules break and release the drug. ^[31]

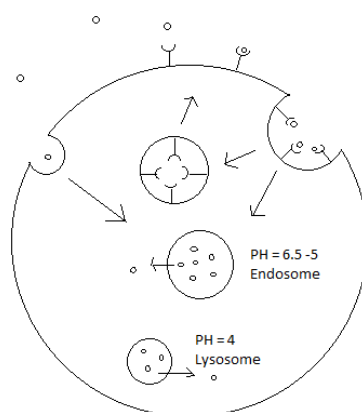


Figure 1.5: Endocytosis is the process by which molecules enter into cells. ^[30] Firstly, the cell membrane folds inward results in the formation of a small vesicle called endosome. This endosome then merges with a lysosome and forms a secondary lysosome, which contains an acidic internal environment with enzymes where the linker molecules break and release the drug. ^[31]

It is the specific environment of the endosome, lysosome or the tumor tissue where the linkers are cleaved in order to release the drug, not under normal circumstances ^[32], like the labile acid linkers such as cis-aconityl or hydrazone which specifically degrade in the acidic tumour tissue or endosomal environment. ^[33] Similarly, protein-containing linkers can be destroyed when in the lysosome as lysosome bears the enzyme responsible for the cleavage of the peptide bond. The breakage of the linker molecule is followed by the drug release that is then diffused into the cytosol of the cell, figure 1.5. Peptides and oligosaccharides are the linker molecules used most commonly in controlled drug release systems. Some of the important linkers included in the linker library by VectraMed include lysosomal endoproteases, Cathepsin B from the Cathepsin family, which mainly target the cancer tissues. ^[34] Prostate Specific Antigen targets the prostate tumours and the Proline peptidases, which are highly abundant in case of pulmonary hypertension and during inflammation.

1.1.4 The enhanced permeability and retention (EPR) effect

Nano-delivery systems must have certain criteria when used in the desired application. The delivery system should have a certain particle size, hydrophobicity and surface charge to overcome physiological barriers (biological structures or physiological mechanisms) that

prevent nanoparticles from reaching their targets. The biological barriers are prevented when the nanoparticles show effective extravasation over the vasculature, improved cellular uptake, prolonged vascular circulation time and endosomal or lysosomal escape.

In the recent past, polymeric carriers of antineoplastic drug molecules have been widely studied. ^[35] These polymeric carriers accumulate (passively) around tumours tissue due to differences in the biochemical and physiological characteristics of normal and cancerous tissue. The passive accumulation of therapeutic in tumour tissue is known as the enhanced permeability and retention (EPR) effect, which was first reported by Maeda *et al.* ^[36] (Figure 1.6). Usually small molecules diffuse through the endothelial cell wall to normal and cancerous tissues. Nevertheless, macromolecules can reach only malignant tissues because the walls of the endothelial cells of these tissues are fenestrated, resulting in pores that allow macromolecules to cross. Malignant tissue has other features include increased vascularity (angiogenic process) and poor lymphatic drainage and, which both lead to the retention of macromolecules. Therefore, therapeutic compounds can be delivered to the site of action in a safe and efficient manner by either an active or a passive process. The former includes the use of peripherally conjugated targeting moieties for enhanced delivery to the site of action. The passive process refers to transport through leaky capillary fenestrations into malignant tissues via passive diffusion because of the EPR effect.

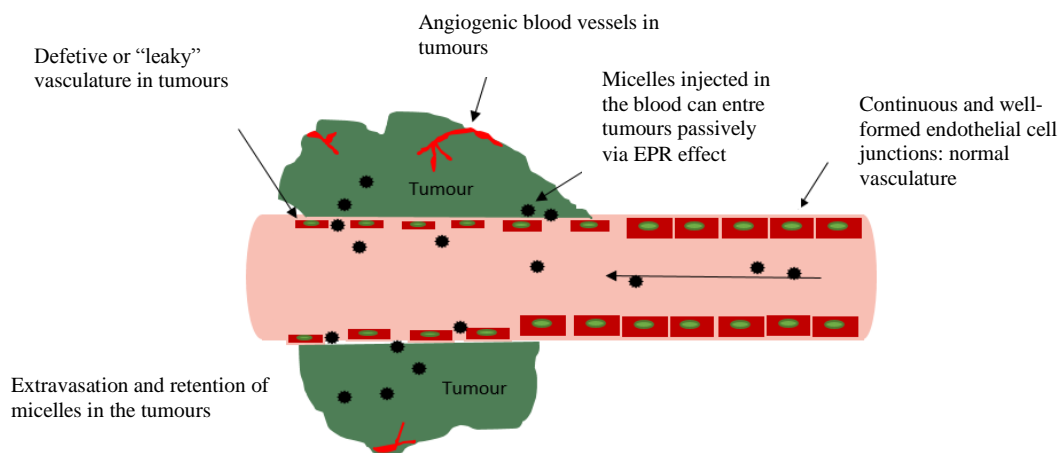


Figure 1.6: Schematic representation showing the anatomical and physiological characteristics of healthy and malignant tissue in term of the vascular permeability and retention of small and large molecules (EPR effect).^[27]

When macromolecules reach the tumour tissue, they are either endocytosed (receptor-mediated endocytosis) or phagocytosed (internalization without the mediation of receptor) by the tumour tissues forming endosome (vesicle). Since the pH in these endosome vesicles (6.5- 5.0) is lower than that of the extracellular matrix (7.2-7.4), acid-labile linkers are hydrolysed and hence releasing the encapsulated drug molecule. In the final step a secondary lysosome is formed as a result of the endosome being absorbed by a lysosome. The secondary lysosome includes hydrolytic and digestive enzymes, which are active in acidic environments.

1.1.5 Drug encapsulation

There are two different type of encapsulating a drugs within polymeric carriers; these are non-covalent and covalent encapsulation (Figure 1.7). In the former case the drug is physically entrapped within the structure of a polymer. This approach may retain the chemical integrity and pharmacological properties of the drug molecule; however, it provides little *in vivo* evidence of therapeutic benefit as there is no control over the release of the drug molecule. The alternative approach is to covalently link the drug molecule to the surface of the polymer as part of a pendant group in what is called a polymer-drug conjugate. The idea of conjugating a drug to a water-soluble polymer was first proposed by Ringsdorf in 1970.^[4b] Drugs can be

connected to the backbone either directly or via linkers or spacers. The biodegradable linkage provides an alternative to solubilisation and electrostatic association. The drug can be released via chemical or enzymatic cleavage of hydrolytically labile bonds.

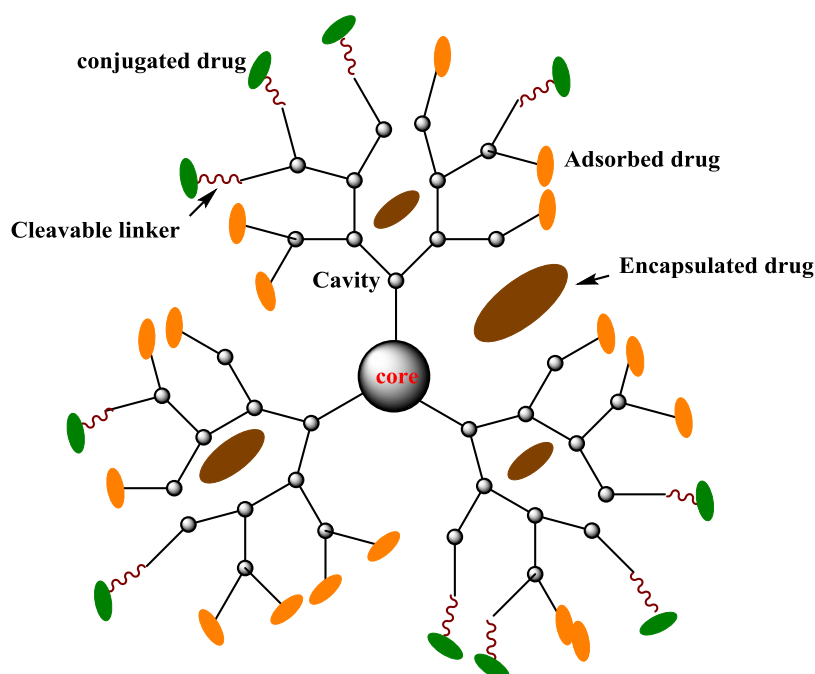


Figure 1.7: Examples of covalent and non-covalent encapsulation ^[37]

1.1.6 Polymeric system: synthesis and application

1.1.6.1 Amphiphilic copolymers

In aqueous media molecules containing a hydrophobic and hydrophilic segment (amphiphilic) form aggregates called micelles or self-organisation. In amphiphilic polymers, hydrophilic part forms the outer shell in contact with water, while the hydrophobic part is sequestered in the interior. Micelles form only when the concentration of the amphiphilic copolymer is greater than the critical micelle concentration (CMC) ^[38]. The formation of micelles is monitored by the rapid change in the chemical and physical properties. Below the CMC, micelles are totally absent, Figure 1.8. The use of amphiphilic copolymers as drug carriers involves the incorporation of low molecular weight drugs in the interior region for improving therapeutic

efficacy. Accordingly, the core of polymeric micelles (hydrophobic domain) help the encapsulation of hydrophobic drug molecules either via covalent or non-covalent interactions.

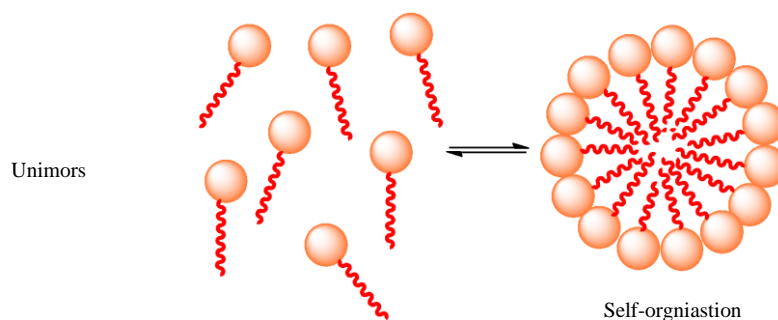


Figure 1.8: Free Surfactant Molecules below CMC (left) and above CMC forming a micelle (right)

There are number of advantages for using micellar systems as drug carriers. One of which is their capability of encapsulating hydrophobic drugs, thereby permitting circulation through the blood due to the solubility and stability of the complex in physiological environment. In addition, the drug molecule will be safe from embolization by enzymes or another bioactive species. Moreover, micelles have long half-life in the body for being large and hence they cannot be filtered from kidney. Therefore, the drug molecule activity remains in the blood circulatory system for a long time after injection. The renal route because of their composition and structure slowly excretes these polymeric structures.

The outer layer in polymeric micelles responsible for interactions with biostructures (such as cells and proteins), and these interaction controls the pharmacokinetics and biodistribution of the drug molecule. Example of the outer layer is polar poly(ethylene oxide) (PEO) that forms the shell of the micelle and protects its interior. Polymer micelles have been widely studied for improving the solubility and selectivity of poorly soluble and toxic chemotherapeutic drugs though passive mechanism (EPR effect) or active mechanism for enhanced delivery to the site of action. ^[39]

1.1.1.1 Dendritic Polymers

Dendritic macromolecules, which refer to dendrimers and hyperbranched polymers, are highly branched molecules with three-dimensional dendritic architecture coined by Tomalia et al. Dendritic polymers constructed from multifunctional monomers and that possess a high degree of branching which leads to large number of functionalised end groups. These end groups are designed to facilitate solubility in a solvent, which can dramatically affect the overall properties of the branched system. Accordingly, these polymers have attracted much interest from the pharmaceutical industry who is trying to develop and tailor their behaviour.

Hyperbranched polymers, in comparison to dendrimers, possess high polydispersity. Their highly branched architecture and chemical tenability makes them efficient drug carrier systems. In 2011, Kolhe et al has researched the potential use of hyperbranched polymers as drug delivery agents.^[40] The research consists of the encapsulation of both hyperbranched polyol and polyglycerol. These two polymers could form conjugates with large numbers of ibuprofen molecules when the ester linkages occur between the polymers and the drug. The hyperbranched polymers achieved high loading and showed a significant therapeutic effect in *in vivo* studies. Another study for the hyperbranched polyglycerol has been carried to encapsulate the hydrophobic anticancer drug, tamoxifen. This study showed that the solubility of the drug allows 12 times more to be transported into an aqueous phase in comparison to the free drug molecule.^[41] These two studies proved that hyperbranched polymers can be used as a potential drug delivery agent.

1.1.1.2 Synthesis of Hyperbranched Polymer

In 1952, Flory highlighted the synthesis of hyperbranched polymers from AB_n monomers (where $n \geq 2$) for forming highly branched soluble polymers.^[40] In contrast to dendrimers, the synthesis of hyperbranched polymers is a one-pot process,^[40-41] which, results in a significant time advantage over the synthesis of dendrimer. Consequently, hyperbranched polymers can

be prepared in large quantities. Unlike dendrimers, hyperbranched polymers possess a broad molecular weight distribution rather than a monodisperse product. Hyperbranched polymers can be prepared using three synthetic approaches: step growth polycondensation of AB_n monomers and $A_2 + B_3$ monomer^[84,85]; self-condensing vinyl polymerization^[86-88]; and ring-opening polymerization^[89-91].

1.1.1.2.1 Step Growth Polycondensation

This type of polymerisation of AB_n monomers (where $n \geq 2$) has been widely used for preparing a wide range of polymeric products including polyphenylenes,^[41] polyesters,^[42a] polyethers^[42b] and polyamides.^[42c] Branching units of hyperbranched polymers are produced each time both B functionalities of one molecule react with a function of A groups contained on others. There also possibilities that only one B functionality react which results in some linear character in the hyperbranched polymer (Figure 1.9). The AB_2 type of monomer is popularly used due to their ease of preparation at low cost. Other type of monomers that contain as many as six B type functionalities (AB_6) have been reported in the synthesis of polyester and polysiloxanes. Many other possibilities exist such as using A_2 and B_3 monomers but these reactions are difficult to control. The drawback of this method is unwanted side reactions such as cross-linking which may cause gelation during the synthesis. Gelation makes the product insoluble in organic solvents, which, in turn leads to significant difficulties in purification of the desired product. In addition, this approach is less commercially viable due to the importance of synthesizing the AB_n monomers before their polymerization.^[43]

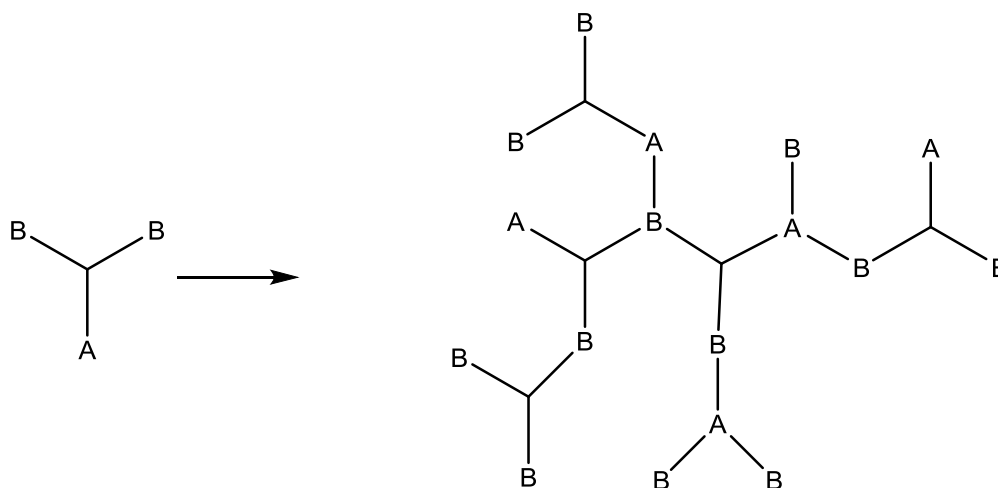


Figure 1.9: Step growth polycondensation

1.1.1.2.2 Self-condensing Vinyl Polymerisation

The self-condensing vinyl polymerisation (SCVP) approach was introduced by Fréchet and co-workers in 1995. ^[44] SCVP uses use of one vinyl group and one initiating moiety (AB* monomers) to produce hyperbranched polymers (Figure 1.10). The activated species can be a radical, anion, cation or carbanion. In order to avoid side reactions that may cause gelation, living or controlled polymerisation systems are employed.

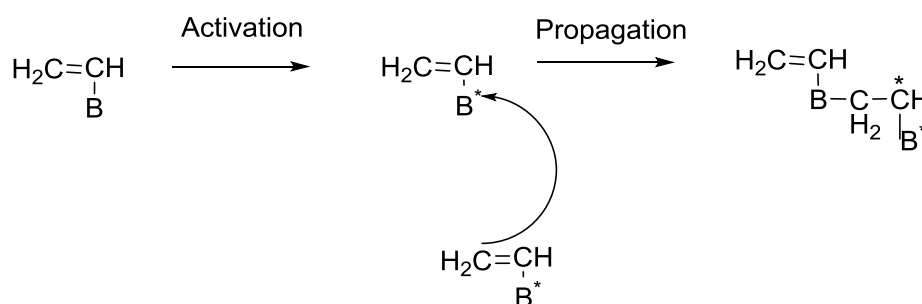


Figure 1.10: Self-condensing vinyl polymerization

1.1.1.2.3 Ring-opening Polymerisation

This approach was first developed by Suzuki for the ring-opening multi-branching polymerisation of latent AB(B) monomers. ^[45] The terminal function of a polymer acts as a reactive centre on which further cyclic monomers bond to form a larger polymer chain through

ionic propagation. In this synthetic method, each additional monomer step forms another reactive centre, shown schematically for ring opening polymerisation of glycidol below in Figure 1.11. Examples of hyperbranched polymers produced by this method are polyamines, polyethers and polyesters.

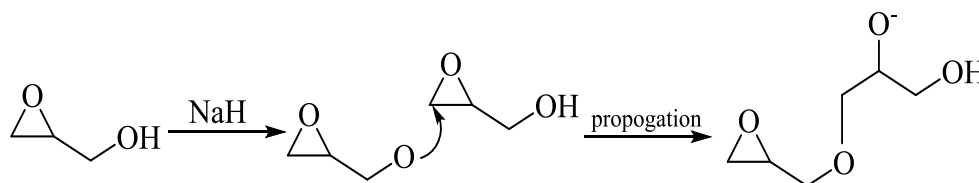


Figure 1.11: Ring opening polymerization

1.2 Photodynamic therapy

Photodynamic therapy, often known as photochemotherapy, ^[50] is a treatment involving a photosensitizing agent and a light of specific wavelength used in conjunction with molecular oxygen to cause cell death. PDT has proven to be effective in treat many medical conditions, including microbial cells (bacteria, fungi and viruses), acne, wet age-related macular degeneration, psoriasis and atherosclerosis. ^[48] It also treats malignant cancers ^[49] including lung, esophageal, bladder, and gastric tumours. In 1990, PDT utilized Photofrin as a photosensitizing agent for cancer treatment. The major drawback of the FDA approved PDT agents (photosensitizers) is skin sensitization as a side effect of the treatment and poor light absorption near the IR region. ^[51] Therefore, it is vital to develop new PDT agents that can also these limitations while achieving the target criteria for effective PDT treatment. The mechanism of PDT involves different components; defining and exploring them help in understating the mechanism. Basically, a PS agent is administrated, and then activated by light of a specific wavelength. The presence of molecular oxygen activates the PS and can create the photodynamic reaction, which is tumour and vascular ablative. In this review, each component will be considered individually, and how can affect the mechanism of PDT.

1.2.1 Photosensitizers agents (PSs)

Both dyes and pigments reflect absorbed light into certain wavelength that result in the precipitation of the colour. The difference between PSs and dyes is that PSs are able to transfer the energy of absorbed light electronically to adjacent molecules or used in photochemical reactions. ^[52] PSs are a key component of PDT, which used in the treatment of some cancer and other medical conditions. They are divided into porphyrin and non-porphyrin based molecules. Sample of porphyrin-based PS molecules include chlorins, bacteriochlorins, phthalocyanines, and pupurins. ^[53,54] example of non-porphyrin based PS molecules include anthracyclines, cyanines, hypericin, psioalens and phenothiazinium molecules (Nile blue analogs, methylene blue, toluidine blue and acridines).^[51] Figure show 3.1 shows examples of porphyrin and non-porphyrin based PS. In PDT, the ideal PS should satisfy the key target criteria including high selectivity toward tumours, production of reactive oxygen species or free radicals, near the IR light, high molar extinction coefficient, absorption, optimal of ADME (absorption, distribution, metabolism, excertion) and absence of dark toxicity.^[59-61]

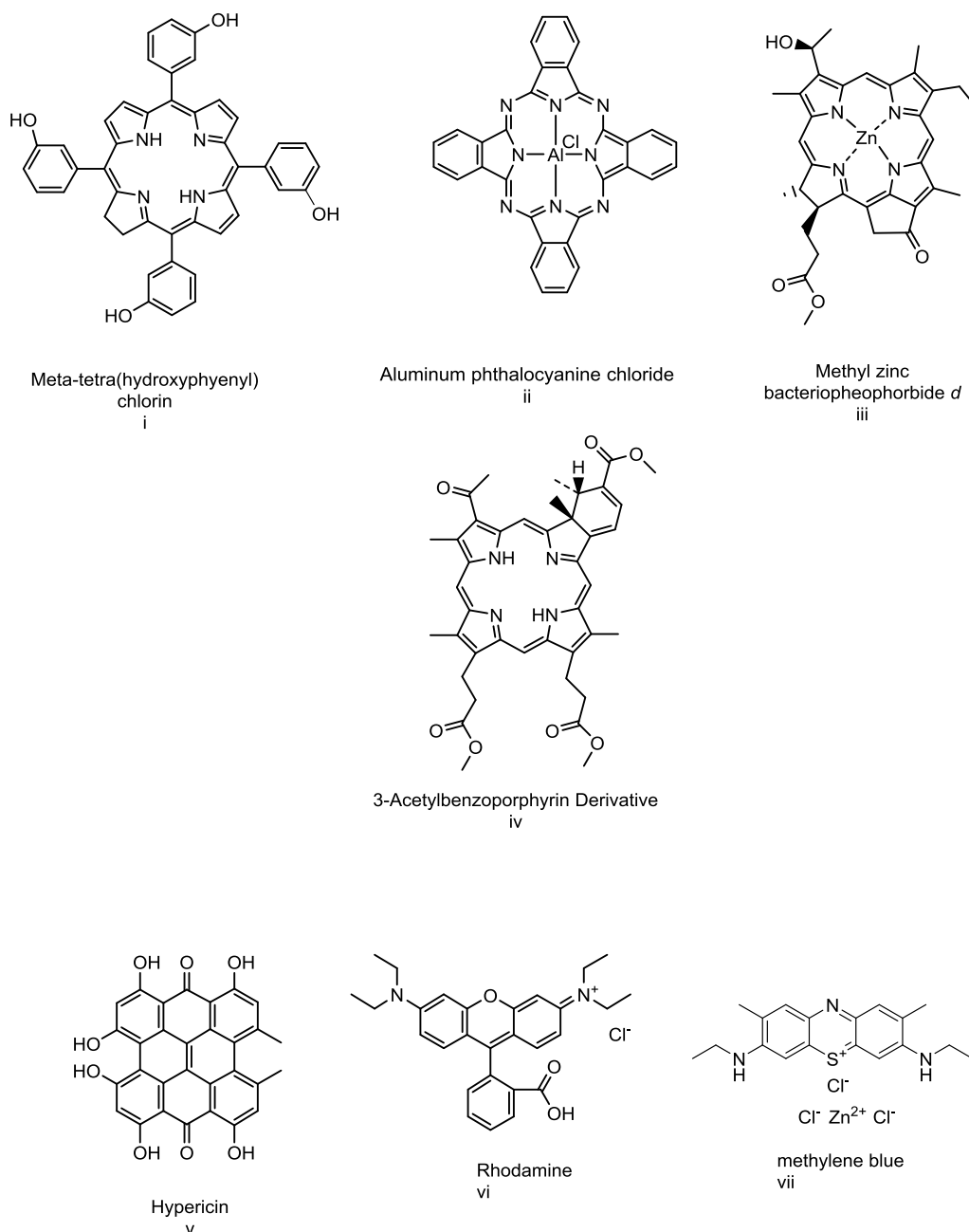


Figure 1.12: Examples of porphyrin (i-iv) and non-porphyrin based PS systems (v-vii)

1.2.1.1 Hematoporphyrin derivative (HPD)

HPD (Photofrin) was the first PS brought to the market, by Dougherty in the 1970's. HPD is a collection of several monomers, dimmers, and polymers of hematoporphyrin that all necessary for effective PDT. This PS considered safe and does not cause pain when activated with light allowing reliable and easy outpatient treatment. However, the treatment time of the HPD

requires 20 minutes or more per lesion. HPD can cause severe skin burns if the patient unintentionally exposed to sunlight.

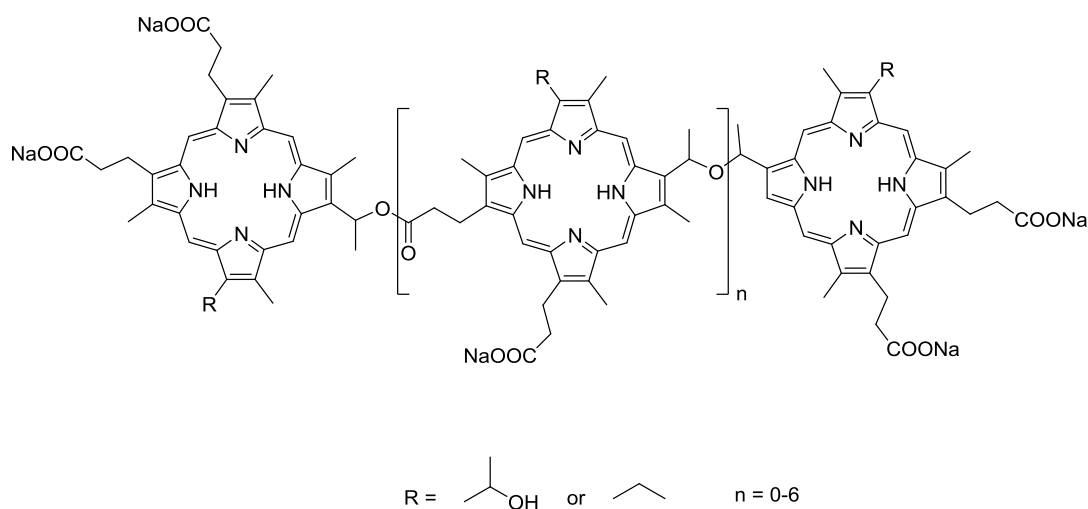


Figure 1.13: Chemical structure of Photofrin, a mixture of hematoporphyrin dimers and oligomers

1.2.1.2 M-tetrahydrophenyl chlorine (mTHPC)

This PS produces fast and significant photodynamic reaction with treatment time measured in seconds. However, the treatment is painful and so the activation of the drug done while the patient under anesthesia. In addition, patients treated with this drug stay in a dark room for 24 hours to avoid skin burn that can happen by the expose with strong light. Still, the drug has found a place in treating primary and recurrent head and neck cancers because of its high effectiveness.

1.2.1.3 Mono-L-aspartyl chlorine e6 (NPe6)

Chlorine e6 is a very effective PDT agent, does not have the dark toxicity common with mTHPC, and treatment allowed for few hours after infusion. Unlike the photofrin and mTHPC, this drug treat patient in the same day that makes it very convenient for patients and practitioners.

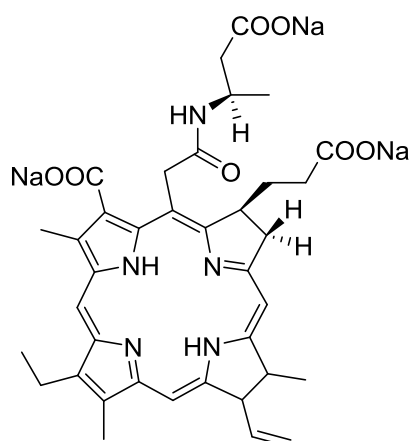


Figure 1.14: Chemical structure of chlorin e6

1.2.2 Therapeutic irradiation

Each PS has a specific wavelength of light and for effective activation; the intensity of light should be higher than 630 nm.^[55] Clinically, excitation at wavelength in the IR region can lead to deeper penetration. The therapeutic irradiation window, preferred range of wavelength, has been reported to be 630-800 nm by some^[56] and 650-950nm by other^[57]. PS with high molar absorptivity (>20,000) can reduce the required dose of the PS for PDT treatment.^[58]

1.2.3 Photophysics

The process of light absorption and energy transfer are the two most significant aspects of PDT, see illustration in figure 3.2. The ground state of PS (two electrons with opposite spins) in the low energy molecular orbital known as singlet state PS. Upon absorption of light in the form of photons, one of these electrons is boosted into a high energy orbital keeping its spin from the first excited singlet state $^1P^*$. This species has very short lifetime (in nanoseconds) and can lose its energy by emitting light or by internal conversion. Intersystem crossing process occurs when the spin of the excited singlet state $^1PS^*$ inverts to produce long-lived excited triplet state ($^3P^*$) (microseconds) that has electron spins in parallel conformation. The loss of energy of the $^3P^*$ by emission of light (phosphorescence) is known as "spin-forbidden" process where the PS move directly from a triplet to a singlet state.^[62]

1.2.4 Photochemistry

In PDT, PS efficiently populates an excited triplet state when irradiated with light near the IR region. This triplet state ($^3\text{PS}^*$) can produce toxic reactive oxygen species (ROS) such as free radicals or $^1\text{O}_2$ in two different pathways (Fig. 2). In type 1, the $^3\text{PS}^*$ reacts directly with cell membrane or molecule to produce a radical anion or radical cation, respectively. In turn, these radicals further react with oxygen to generate reactive oxygen species. Otherwise in Type 2 reactions, the $^3\text{PS}^*$ can transfer its energy directly to molecular oxygen in its ground state to produce excited state singlet oxygen. Both Type 1 and Type 2 reactions can occur simultaneously, and the ratio between these processes depends on the type of PS used, the concentrations of substrate and oxygen.

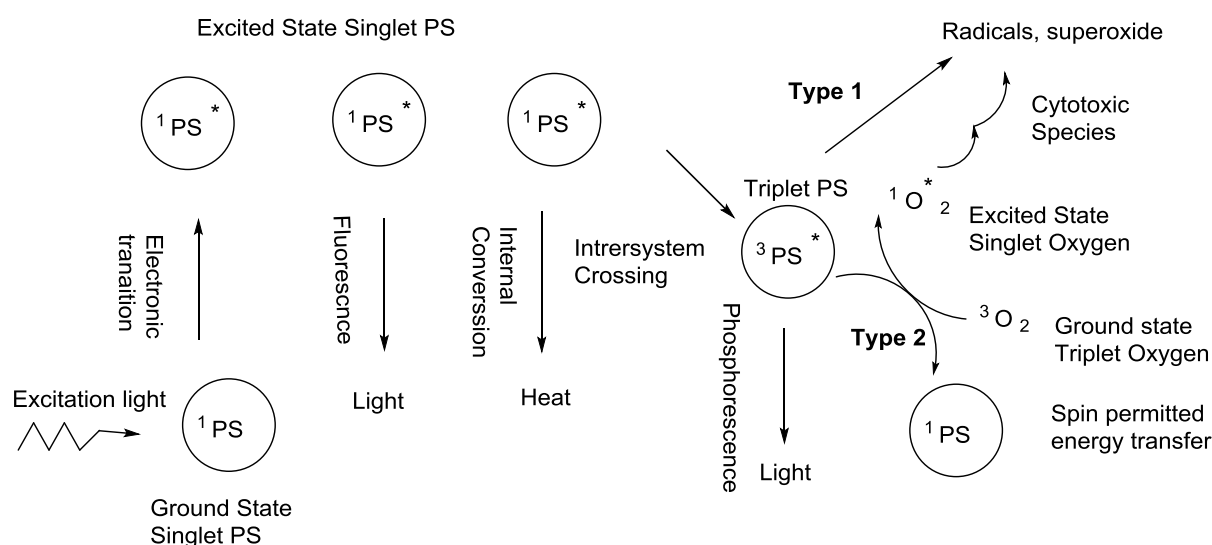


Figure 1.15: Formation of PDT ROS through type 1 and 2 [62]

Both Type 1 and Type 2 reactions can occur simultaneously, and the ratio between these processes depends on the type of PS used, as well as the concentrations of substrate and oxygen. Due to the high reactivity and short half-life of singlet oxygen and hydroxyl radicals, only

molecules and structures that are proximal to the area of its production (i.e. areas of PS localization) are directly affected by PDT and are subsequently destroyed.^[62]

1.2.5 Mechanisms of cell death in PDT

Photodynamic therapy can lead to cell death via pathways including apoptosis and necrosis. Necrosis is an unprogrammed cell death pathway that can be induced by injury, infection, heat, cancer, infarction, toxins, and inflammation.^[63] It is quick method of degradation that can be characterized by damage to organelles, cytoplasm swelling, and disruption of the cell membrane. Necrosis takes place when high doses of light are being used. Unlike necrosis, apoptosis can be characterised morphologically as single cells which surrounded by other normal-looking cells and is distinguished by cell shrinkage. *In vitro*, apoptotic cells degraded into multiple membrane enclosed spherical vesicles. However, *in vivo*, these vesicles can be scavenged by phagocytes whereas inflammation can be prevented^[63]. Recent studies have shown that autophagy plays a role in PDT^[64]. Autophagy is a vital transportation process through lysosomal degradation pathways that associated with cell survival, development, and differentiation. Toxic oxidized protein can be developed when proteins undergo irreversible ROS damage, autophagy will be activated to remove these toxic species. In the case of failure to stimulate these mechanisms, accumulation of oxidized macromolecules will take place and the functions of the cells will be compromised which ultimately leads to cell death^[65]. The effectiveness of PDT depends on the location at which light has been delivered. PDT can also lead to tumour death by deprivation of oxygen and nutrition PSs differ in terms of biodistribution and pharmacokinetics. After their injection into the blood stream, they can bind to endothelial cells, then bind to the extracellular matrix or then accumulate within the tumour cells. The cytotoxicity induced by the absorbed light is thus restricted to the area of irradiation^[66].

1.2.6 Use of Nanoparticles

The selectivity of PS was increased by using a molecule having high affinity to cancer cells, such as folic acid ^[67-68] or antibodies ^[69], peptides, LDLs, and polymers ^[70]. Third-generation PSs is one approach designed to target subcellular compartments such as mitochondria ^[71]. The second approach includes utilising nanoparticle-based drug delivery methods in PDT. The usage of nanoparticles in PDT studies has very attractive following reasons: (1) monomeric form of PSs can be used within nanoparticles; (2) lower levels of the PSs can be used for PDT; (3) hydrophobic PTD agents have been approved by the FDA and nanoparticles can boost the selectivity of these compounds to reduce side effects after treatment as well as aggregation problems; (4) applying strategies such as pH sensitivity, thermal sensitivity, peptide or antibody tags in nanoparticle system can boost selectivity more efficiently; (5) passive targeting through EPR system by making nanoparticles with a diameter of less than 200 nm; (7) increase in cell uptake ^[72-73]. Examples of some of the nanoparticles that have been used in PDT studies so far include micelles, polymeric micelles, carbon nanodots ^[74], liposomes ^[75] quantum dots, gold nanoparticles ^[76-77], cationic vesicles ^[78], hydrogels ^[79], and dendrimer nano particles ^[80-81], TiO₂^[82].

In summary, polymeric material have been used widely as drug carrier to improve the effectiveness and reduce the toxicity of drug molecules. In this research, new drug delivery system is constructed to deliver small and large drug molecule and also for PDT.



Chapter 2

Aims and Objectives



2. Aims and Objectives

2.1 Synthesis of star copolymers for large drug delivery system

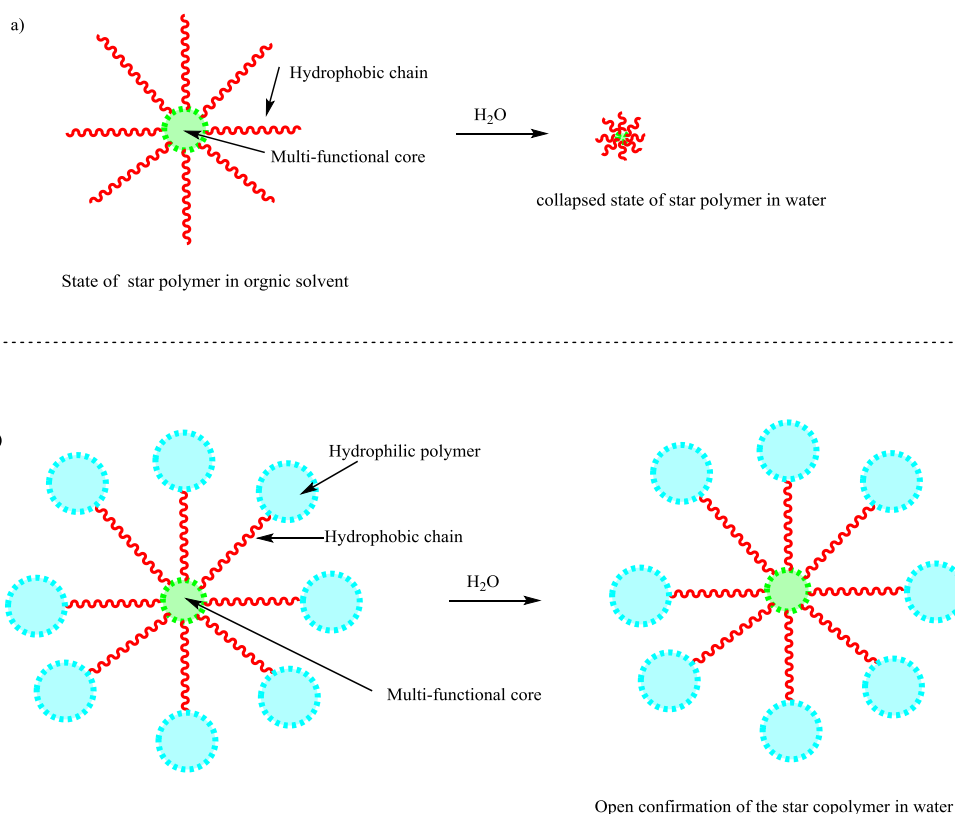
Advances in biology, molecular genetics and human genomics are starting to generate new pharmacologically active biomolecules. However, these emerging biomolecules are much larger than traditional drug molecules and undergo rapid degradation in a biological environment, often resulting in severe toxicity. Therefore, the application of these pharmacologically active biomolecules as therapeutic drugs will require the use of new delivery systems.

The aim of this project is to generate a general delivery system that can be used to deliver large drug molecules; including biomolecules (peptides, proteins, RNA etc.). This delivery system will consist of a large star shaped polymer that possesses many long arms, each terminated with a large globular polymeric unit. These terminal units are designed to interlock and help prevent the internal arms from collapsing (steric stabilisation). Thus, the internal arms are prevented from collapsing/coiling, leaving large amounts of internal space. Large drug molecules can occupy this “free” space. In addition, the polymers are designed to degrade slowly in a neutral solution but rapidly in acidic solution. This controlled degradation can be exploited to trigger drug release under certain conditions.

2.1.1 General Design of the Proposed Drug Delivery System (Star Copolymers) and control systems

This project will start by constructing nano-sized macromolecular carriers with the capacity to form and maintain a large volume of free internal space. The general design is shown schematically in scheme 2.1 b. A star polymeric core will be used to generate a suitable environment that can be used to encapsulate large drug molecules. Without any further functionalization, there is nothing to stop the arms from simply collapsing or coiling in aqueous

solution (significantly reducing the level of free space), scheme 2.1 a. To prevent this, hydrophilic highly branched polymer (HBP) will be added to the ends and used as steric capping groups to lock the structure in an open conformation and therefore maximising the internal space, scheme 2.1, b.



Scheme 2.1: A cartoon representation of the proposed drug delivery system

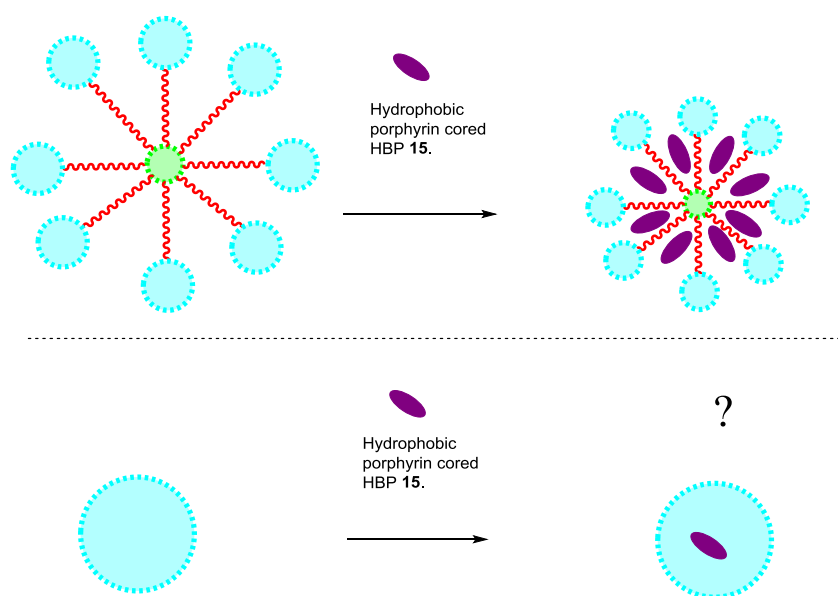
To optimise the desired amount of internal space and capping density, allowing specific drug molecules to efficiently enter and leave the delivery system, the size of the terminal capping groups and the length of the internal arms is optimised. This will be achieved experimentally by varying the size of the terminal groups and the length of internal polymer arms. Care must be taken to obtain a balanced system. For example, small capping groups may not provide enough water solubility to the hydrophobic star polymer, whereas large capping groups can maximise delivery times (by trapping drugs within the interior spaces), but they can also make it very difficult to get significant amounts of drug into the delivery system.

2.1.2 Control system

Since the proposed delivery system consist of two segments (hydrophobic chains and hydrophilic capping groups), the two parts should be investigated independently as control systems. However, the hydrophobic star polymer or single chain does not have any water solubility, as illustrated in the main aim, scheme 2.1 a, hence, only the hydrophilic HPG will be studied as a control system of the proposed drug delivery system.

2.1.3 Testing the macro-encapsulation potential of the star copolymers

Having establish the parameters and properties for possible aggregations, encapsulation of a model macromolecular drug using a hydrophobic macromolecule will be investigated. A synthetic mimic of haemoglobin which is water insoluble will be chosen to improve its solubility in water. Specially, encapsulation of porphyrin cored hyperbranched polymer (HBP 15, figure 3.3) within the star copolymers and the control system will be tested.



Scheme 2.2 : A cartoon representation of the aqueous solubilisation of hydrophobic HBP upon encapsulating with the proposed star copolymer and/or the control (hydrophilic polymer).

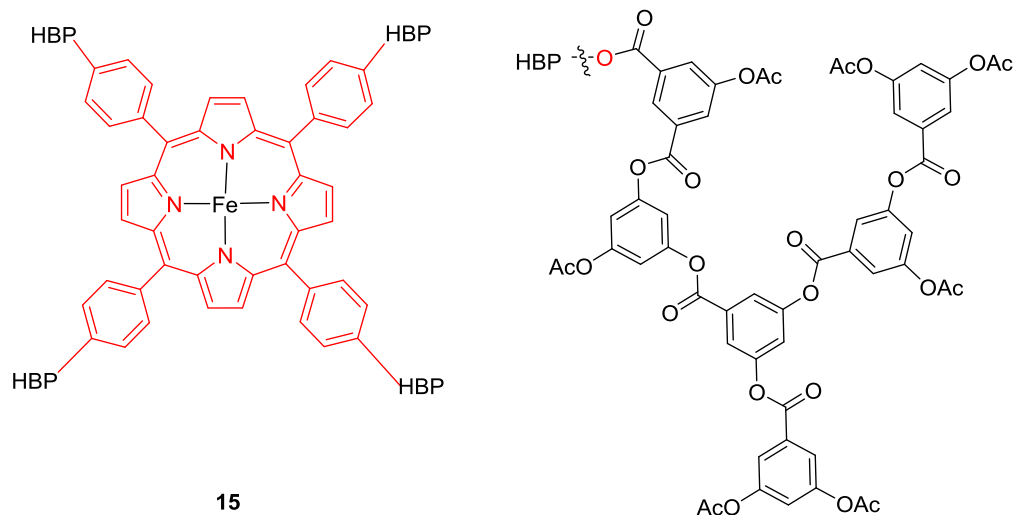


Figure 2.1: The chemical structure of the porphyrin cored hyperbranched polymer (HBP 15) as a macro-guest

2.2 Porphyrin-cored star copolymers for photodynamic application

In a previous study carried out by the Twyman group, different porphyrin molecules were successfully encapsulated within dendritic molecule. These systems showed good encapsulation results that could potentially be investigated for PDT. However, the encapsulated porphyrin molecules may be released from the delivery system at any time before reaching the target, reducing their selectivity. As such, it was desirable to develop a delivery system where the PS was covalently attached within a macromolecular delivery system.

In this study, star copolymers comprising a porphyrin at the central core and a number of hydrophobic arms, each terminated with hydrophilic units, were synthesised. Specifically, each copolymer arm comprises an inner hydrophobic poly(ϵ -caprolactone) arm attached to a porphyrin core. The outer layer is a hydrophilic hyperbranched polyglycerol unit, covalently attached to the poly(ϵ -caprolactone) arms. In aqueous solution, the proposed amphiphilic star copolymers should aggregate to form micelles with diameters 10–200 nm. These large self-assembled molecules would satisfy the EPR effect and be effective PDT agents, figure 2.2.

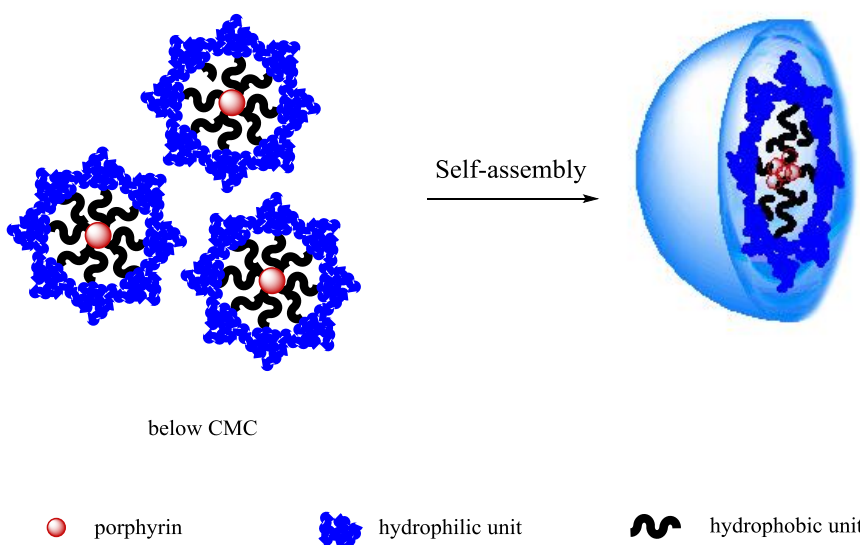


Figure 2.2: Possible self-assembly of porphyrin-cored star copolymers

As a control, a simpler porphyrin hydrophilic hyperbranched polyglycerol will be used, as well as experiments using just the porphyrin core. The main aim is to solubilise and protect a porphyrin PS within an amphiphilic molecule that could self-assemble into a large structure that could clarify the mechanism of the EPR effect by these molecules. Tetrakis(4-hydroxyphenyl)-porphyrin (THPP **12**) and tetrakis(3,5-dihydroxyphenyl)-porphyrin (TDHPP **13**), were selected as the porphyrin core for use within the delivery system, figure 2.3. These possess nucleophilic hydroxy groups that enable a ring opening polymerisation (ROP) to take place at the caprolactone and/or glycidol.

Upon successful synthesis of the proposed delivery system, the dark toxicity, phototoxicity and porphyrin uptake will be evaluated using appropriate cell lines. The phototoxicity of the porphyrin polymers for different concentrations will be evaluated using different light doses.

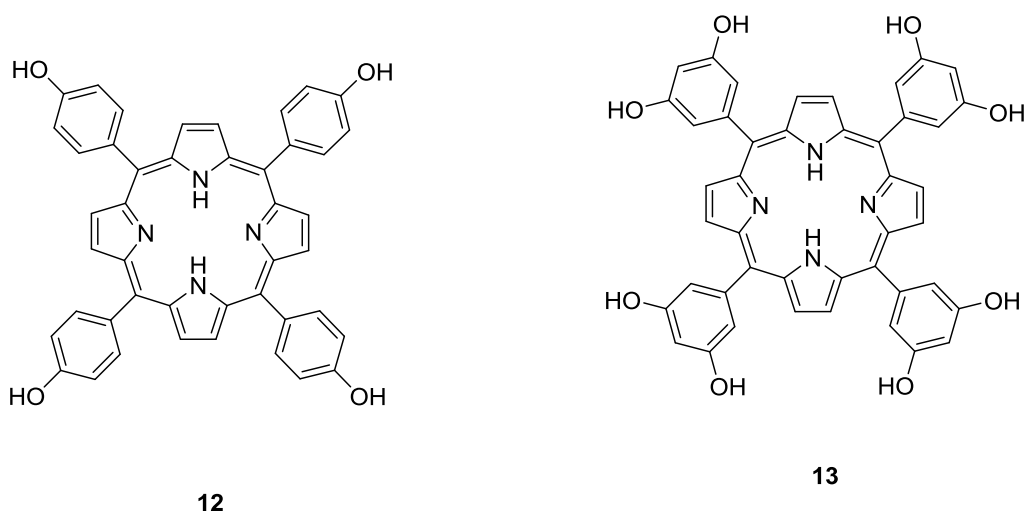


Figure 2.3: Potential porphyrin derivative to be used as a core in drug delivery systems for PDT applications THPP 12 and TDHPP 13

2.3 Chemo-Photodynamic Combination Therapy

Cancer is an inclusive term, first assigned by the ancient Romans, for a large group of diseases involving abnormal cell growth with the potential to spread to adjacent tissues, resulting in uncontrolled cell proliferation and loss of cellular differentiation. There are over 10 million new cases of cancer every year and over 6 million annual deaths from cancer. Nowadays, cancer is mostly treated by therapy involving the modulation of a single target. A tumour-targeting drug delivery system consists of a tumour detection moiety and cytotoxic molecule (chemotherapeutic molecule) combined directly, via encapsulation or through conjugation. Photodynamic therapy (PDT) is a treatment that involves the combined action of photosensitisers and light of specific wavelength to treat various cancers. The combination of these two therapies, chemotherapy and PDT, make cancer treatment more effective.

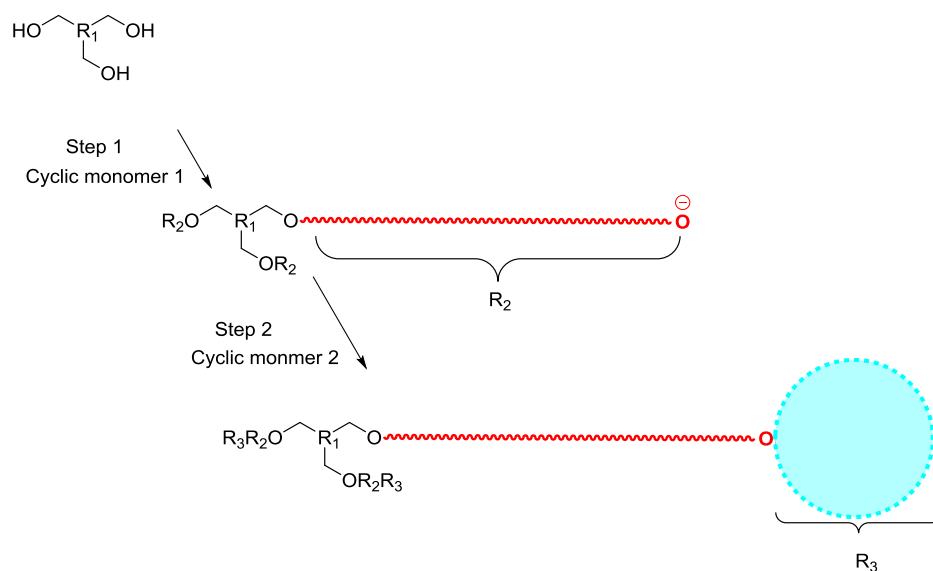
The present project investigates the use of combined anticancer therapies where both photosensitiser and chemotherapeutic molecules are included in one drug delivery system; one molecule being covalently attached to the corona (photosensitiser) and the other being non-covalently attached to the system (chemotherapeutic molecule).

In the previous chapter, porphyrin molecules and photosensitisers were attached covalently to a hydrophilic hyperbranched polymer or to star copolymers for their use in photodynamic therapy (PDT). In this chapter, the potential of the self-assembled porphyrin-delivery systems to encapsulate lipophilic chemotherapeutic drug molecules (such as a paclitaxel) into the core region of the micelle is investigated. Such drug delivery systems which combine PDT and chemotherapy strategy can offer fast and effective treatment for cancer, especially for those in the last stage of cancer.

3. Synthesis of star copolymers for large drug delivery systems

3.1 Synthetic considerations

Construction of the drug delivery system proposed in the previous chapter began with a multi-step reaction using a single-pot procedure. A core functionalized with hydroxyl end groups was proposed as an initiator to ring open and polymerize ϵ -caprolactone. The resulting hydrophobic star polymers were predicted to possess a nucleophilic end group that could then be used to initiate a second ring opening polymerization (ROP) using a branched hydrophilic monomer (Scheme 3.1).



Scheme 3.1: Reaction design of the proposed drug delivery system, where R_2 represents the hydrophobic arms resulting from the polymerisation of the caprolactone monomer with nucleophilic hydroxyl end groups of the core (R_1). R_3 is the hydrophilic branched polymer resulting from another ROP of another monomer.

The three components (core, monomer 1, and monomer 2) chosen for our proposed delivery system are shown in Figure 3.1. The branched unit trimethylolpropane (TMP) **1** was functionalised with three hydroxyl groups and is a suitable core for a simple three-armed star polymer.

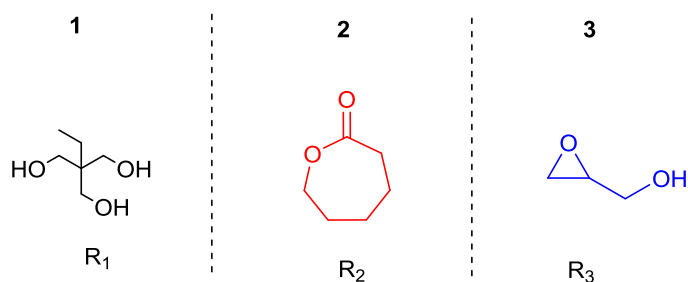
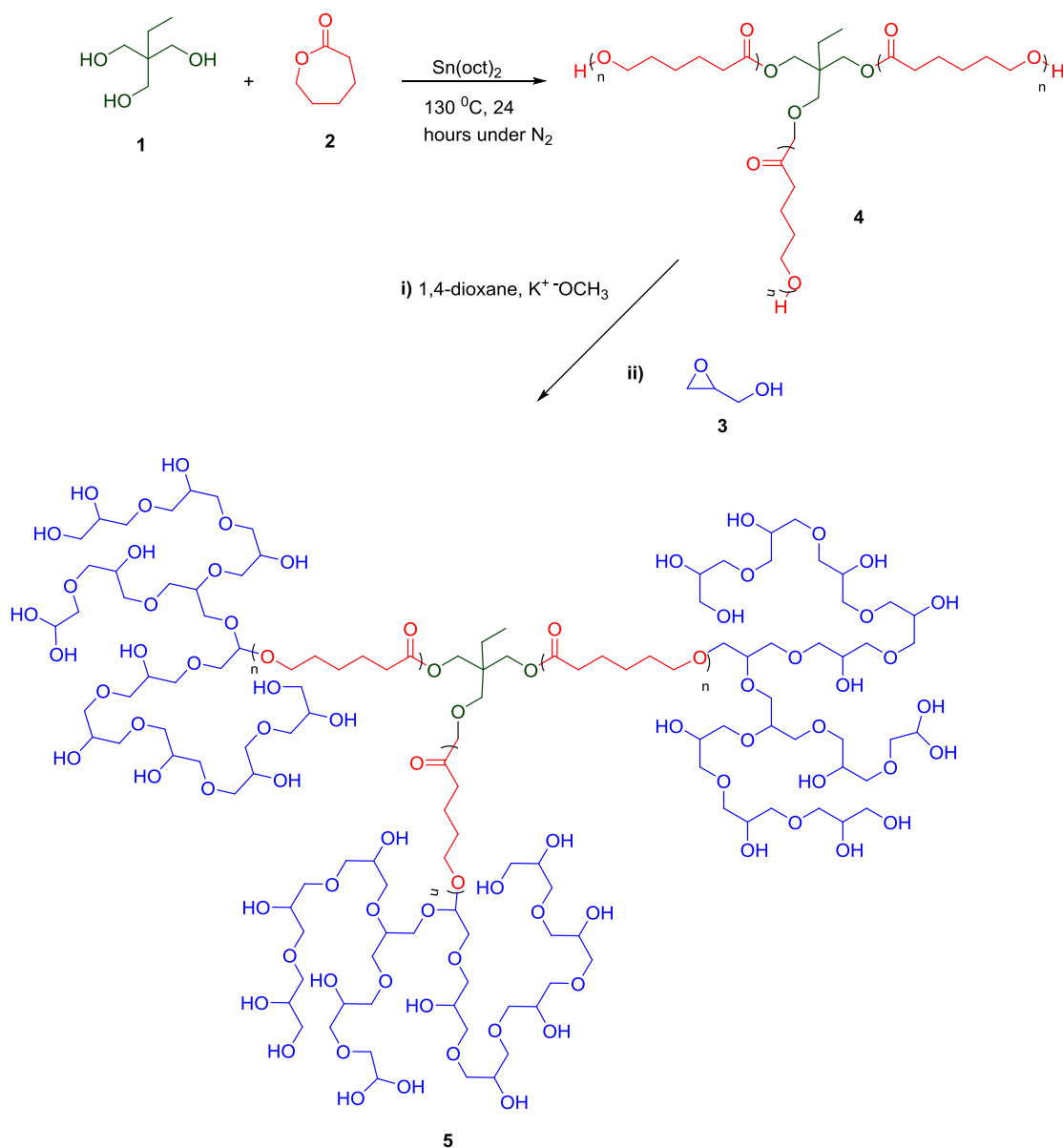


Figure 3.1: Chemical structure of the trimethylolpropane **1**, epsilon-caprolactone **2** and glycidol **3** selected for the proposed copolymers.

The hydrophobic component selected for the arms was ϵ -caprolactone (ϵ -CL) **2**, which would result in PCL arms. Poly(caprolactone) (PCL) has the advantages of being approved for human use and being biodegradable and compatible with a wide range of other polymers.^[45] The terminal hydrophilic hyperbranched polymer group would be formed by reacting the hydroxyl end group of PCL with glycidol **3** to obtain a hydrophilic polymer.

3.2 One-pot synthesis of the poly (ϵ -caprolactone)-b-polyglycerols (PCL-HPG)

Amphiphilic SPCL-HPG **5** star copolymers were synthesized in two steps using a one-pot synthesis (Scheme 3.2). In the first step, poly (ϵ -caprolactone) (PCL) **4** was synthesised using 0.05% w/w tin(II)-ethyl hexanoate to catalyse the ring-opening polymerization (ROP) of ϵ -CL **2** formed by the hydroxyl-functionalised core **1** in the bulk at 130 °C. The target molecular weight for PCL depended on the molar ratio of ϵ -CL **2** to the core hydroxyl groups. The next step was subsequently started by reducing the temperature and adding 1,4-dioxane. Potassium methoxide was used to deprotonate the hydroxyl groups of PCL **4**, followed by the slow addition of glycidol **3**. The molar ratio of glycidol to the terminal hydroxyl groups of the PCL was also varied to adjust the size of the HPG ends. In this work, three star copolymers were prepared with different chain lengths and similar size of the capping group to study the effect of the chain length on encapsulating large molecules.

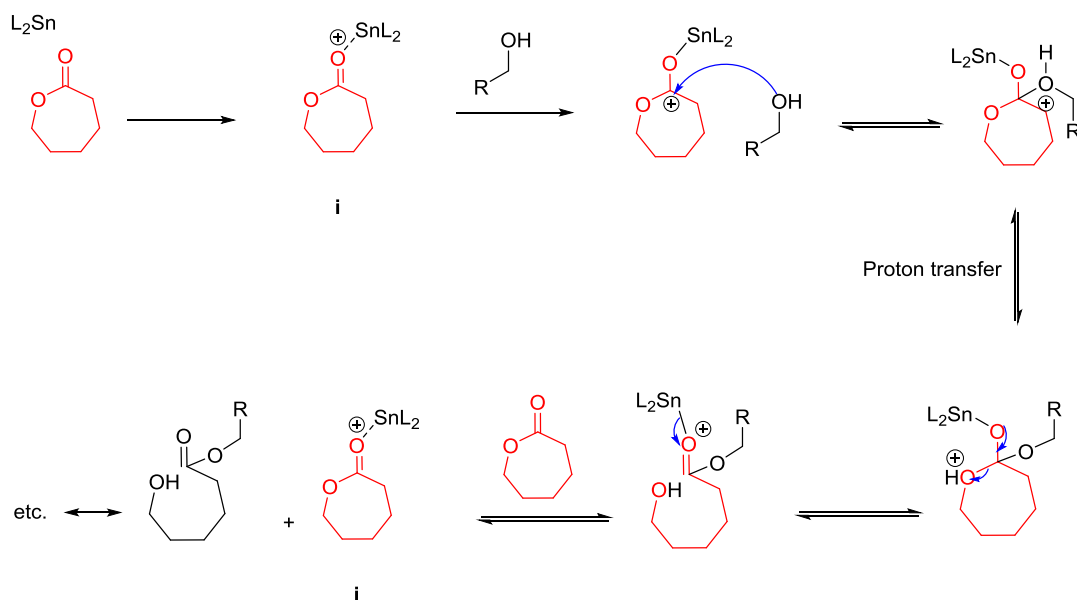


Scheme 3.2: Reaction scheme of synthesising amphiphilic copolymer 5 based on poly (ϵ -caprolactone) and polyglycerols (SPCL-HPG)

3.3 Anionic ring opening polymerization of forming poly (ϵ -caprolactone)

The reaction mechanism for the ring opening of ϵ -CL 2 is shown in Scheme 3.3. To increase its electrophilicity, the tin atom of Sn(oct)₂ initially coordinates with the ϵ -CL 2 carbonyl oxygen atom through its non-binding electron pair. This results in an increased susceptibility to nucleophilic attack by the hydroxyl group. This is then followed by proton transfer and acyl oxygen cleavage, resulting in the formation of a PCL molecule with an alcohol-derived ester-end group and a caprolactone-derived hydroxyl. The process then begins again at **i** where a tin

atom coordinates with a second monomer molecule. The stannous octoate molecule continually transfers from one growing polymer chain to another; however, unlike the hydroxyl group concentration, the concentration of the stannous octoate does not affect the molecular weight of the polymer.



Scheme 3.3: Proposed steps mechanism for the ring opening polymerisation of ϵ -CL using $\text{Sn}(\text{oct})_2$ as a catalyst and hydroxyl compound as an initiator

3.4 The structural characterisation of SPCL-HPG amphiphilic copolymers

The SPCL polymers (hydrophobic segment) and SPCL-b-HPG copolymers (hydrophobic-hydrophilic copolymer) were characterized using ^1H and ^{13}C NMR spectroscopies and GPC. The ^1H NMR spectrum of the SPCL in CDCl_3 is shown in figure 3.2 and confirms the presence of the methylene protons of poly (ϵ -caprolactone) at 1.39, 1.66 and 2.32 ppm, respectively, for γ , $\beta+\delta$, and α position respectively. In addition, peaks appeared at 0.83 ppm was assigned to the methyl protons of the core (TMP) suggesting the incorporation of the core within the PCL structure. The average length of each arm is calculated from the integration ratio of the monomer $\text{CH}_2\text{-O}$ and terminal $\text{CH}_2\text{-OH}$ peaks at 4.15 ppm and at 3.6 ppm, respectively.

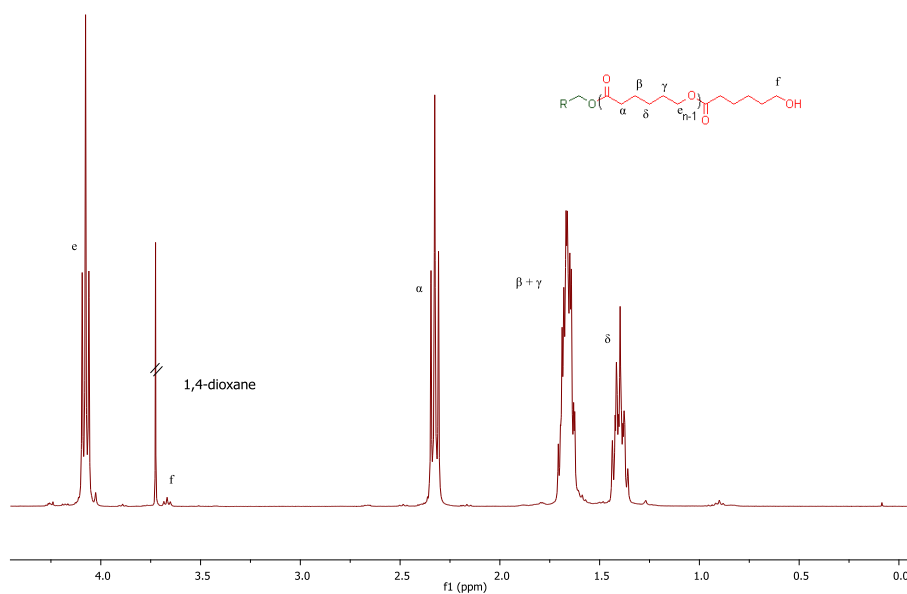


Figure 3.2: ^1H NMR spectra of $\text{SPCL}_{60}\text{-HPG}_{90}$ in CDCl_3

In the ^1H NMR spectrum of SPCL-b-HPG shown in figure 3.3, in addition to the peaks correspond to PCL, a multiplet at 3.60 ppm, was assigned to the CH and CH_2 protons of HPG.

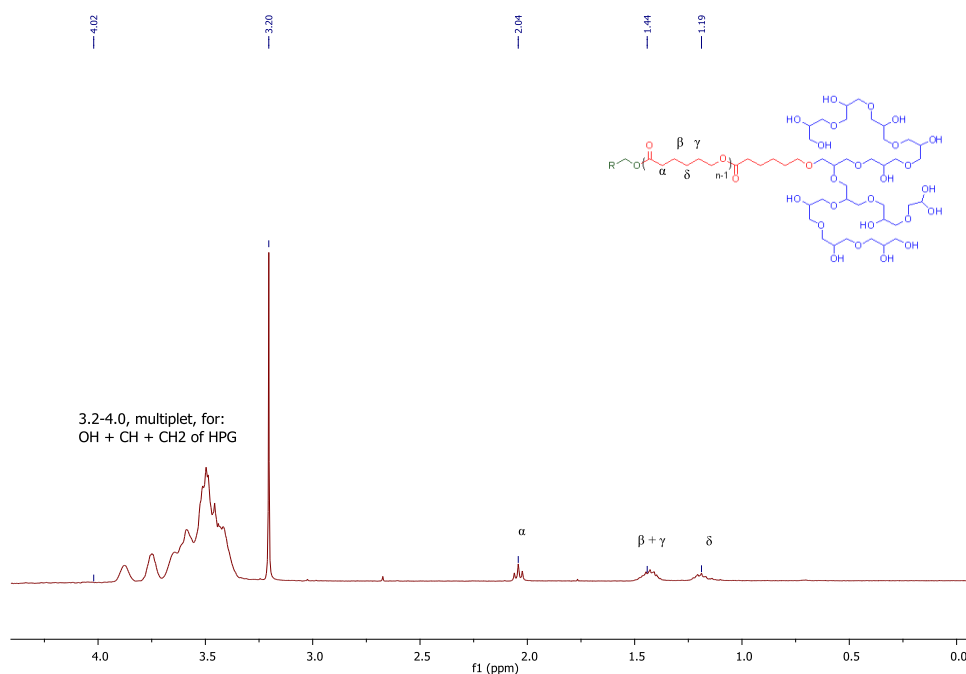


Figure 3.3: ^1H NMR spectra of $\text{SPCL}_{60}\text{-HPG}_{90}$ in D_2O

The molecular weights of polycaprolactone (SPCLs) were determined by ^1H NMR spectroscopy and GPC analysis were very similar. Their values were almost identical to the theoretical values based on the core to monomer ratio, indicating a high level of control. Polydispersity indexes were relatively low and measured within the range of 1.28 to 1.47.

Table 3.1: Summary of the estimated M_n values by GPC and ^1H NMR spectroscopy, and the expected M_n of the hydroponic segment of star polymers (SPCL)

SPCL _n	$M_n/\text{g mol}^{-1}$			Đ
	Theoretical ^a	^1H NMR ^b	GPC ^c	
SPCL ₁₅	5270	5000	7000	1.21
SPCL ₃₅	12118	12500	14000	1.6
SPCL ₆₀	20679	20000	21000	1.5

Note: Numbers in subscript represents the number of repeat units (caprolactone) per polymer chain
a. Calculation based on feed ratio of the monomer units to core
b. As determined by integration of ^1H NMR in CDCl_3
c. As determined by GPC (using tetrahydrofuran as the eluent)
Đ: polydispersity index

The molecular weight characteristics of the amphiphilic star copolymers (SPCL-HPG) were also determined by ^1H NMR spectroscopy and GPC analysis. On this occasion they appear to be large error based on the theoretical values.

The GPC results were estimated using water as solvent/eluent and the values obtained were very low. The M_n values were smaller than the M_n calculated for the hydrophobic star block. This could indicate that the hydrophobic arms are constructed in water (not well solvated as the case was for PCL in THF solvent). So these M_n values are a guide only because of the method used (GPC calibrated with linear polyglycol and these polymers is branched

polyglycidol). For the same reason, in the ^1H NMR spectra, integration of the hydrophilic region based on the constructed hydrophobic arms caused an overestimation in the molecular weights of the polymers.

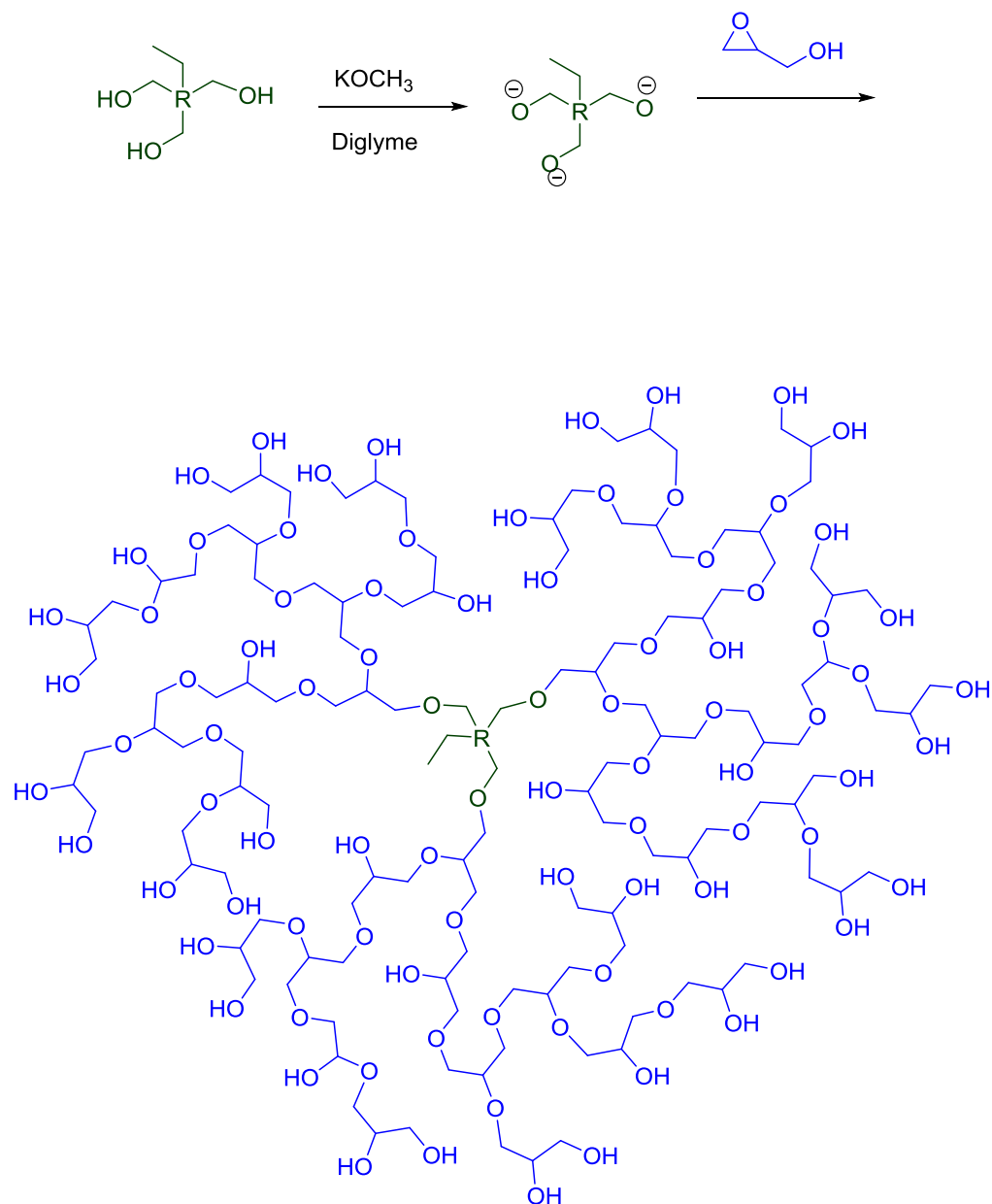
Table 3.2: Summary of the estimated M_n values by GPC and ^1H NMR, and the expected M_n of the star co-polymers (SPCL-HPG)

PyPCL $_n$ -HPG $_m$	Theoretical ^a	^1H NMR ^b	GPC ^c	\bar{D}
SPCL $_{15}$ -HPG $_{90}$	11930	25000	4800	1.9
SPCL $_{35}$ -HPG $_{90}$	18778	32000	4500	2.2
SPCL $_{60}$ -HPG $_{90}$	27339	45000	4800	1.6
n is the number of the caprolactone units while m is the units of glycidol according to theoretical assumption.				

3.5 One-pot Synthesis of hyperbranched polyglycerols (HPG)

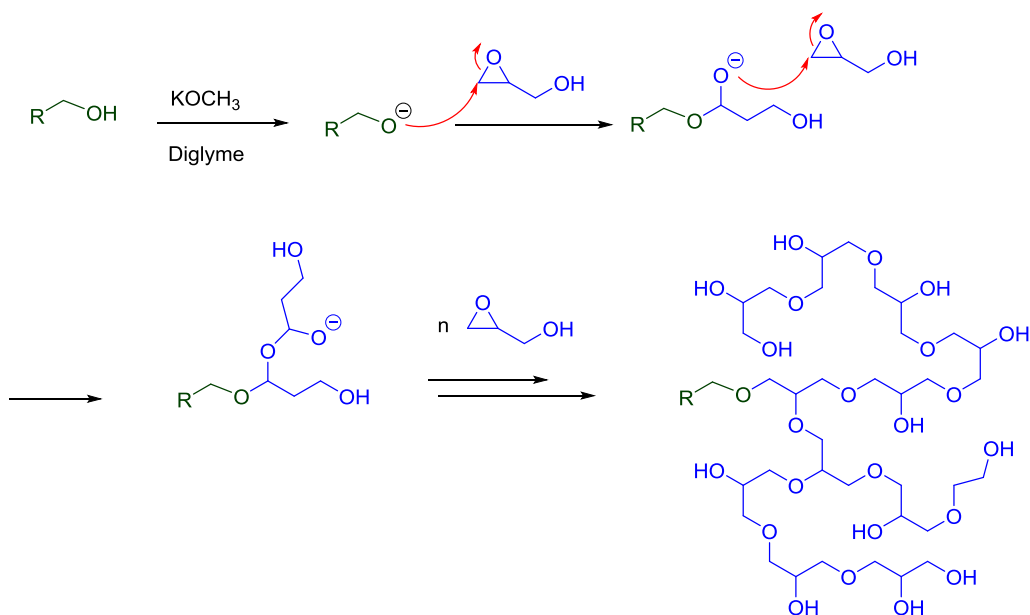
HPG polymers **6** are synthesized by adding strong base (potassium methoxide) to the core **1** and propagation of the monomer **3** (glycidol) at 90 °C (Scheme 3.4).

Initially, the reaction is initiated by deprotonating the hydroxyl groups of the core with potassium methoxide followed by slow addition of glycidol. The deprotonated species goes on to ring open the epoxide ring and form an alkoxide. This alkoxide then reacts with another glycidol monomer to form the desired HPG polymers, Scheme 3.5. However, non-cored HPG may also form if the glycidol monomer being deprotonated by any excess base or by the deprotonated core and act as an alternative core (Scheme 2.6).

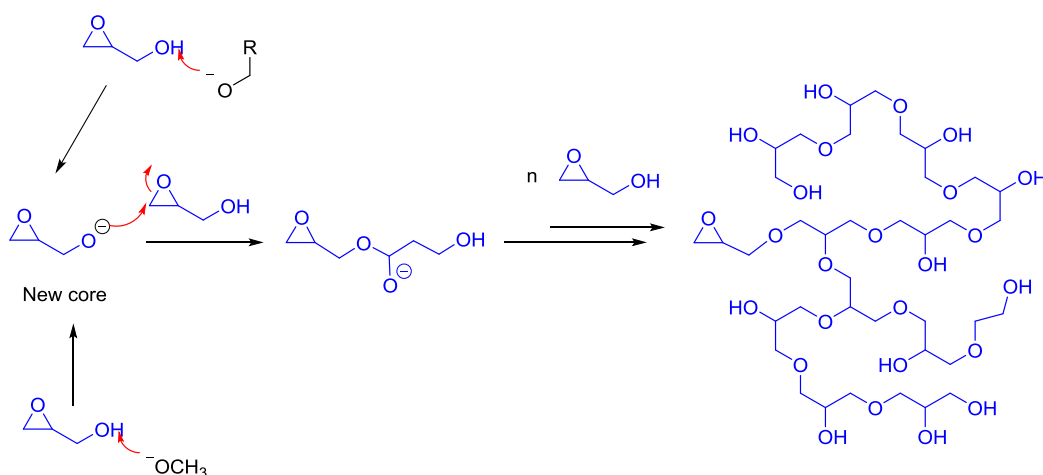


6

Scheme 3.4: Synthesis of hyperbranched polyglycerols 6



Scheme 3.5: Reaction mechanism of the anionic ring opening polymerisation of polyglycerols



Scheme 3.6: homo-polymerisation phenomena of polyglycerols

3.6 Characterisation of hyperbranched polyglycerols

The structure of HPG was characterized by 1H NMR, ^{13}C NMR, FTIR spectroscopies and GPC. In the 1H NMR spectra, a broad multiplet at 3.70 ppm corresponding to the numerous different CH and CH_2 protons in the polymer. In addition, there was broad multiplet observed at 0.75 ppm which was assigned to the methyl end group for the core suggesting incorporation of TMP into the polyglycidol. The molecular weight of the polymer was estimated by comparing the

integration of the CH/CH₂ resonance to those from the core and found to be 37K Da. In the ¹³C NMR spectra, resonances from the polyglycerol, at 58–75 ppm, were observed in the HPG polymer. The IR spectra of HPG had a broad peak between 3260 and 3370 cm⁻¹ in the spectra, assigned to the terminal OH groups in the polymer. The average molecular weight (Mn) of the HPG polymer obtained using aqueous GPC and ¹H NMR spectroscopy are summarized in Table 3.3. Estimating Mn by ¹H NMR spectroscopy assumes every monomer unit has a core. If this is not the case, and the polymer contains significant amount of homopolymer, the Mn will be overestimated. When comparing this to the Mn via GPC, it could appear that there is the case as the Mn value obtained from GPC analysis closer to the expected value based on core to monomer ratio.

Table 3.3: Molecular weight characterization of HPG polymers

Polymers	Theoretical ^I	NMR ^{II}	GPC ^{III}	PDI ^{III}
TMP ₁ -HPG ₉₀	20	37	18	3.6
I: based on the core to monomer ratio II: as determined by integration of ¹ H NMR resonance in D ₂ O III: As determined by GPC analysis (aqueous)				

The degree of branching (DB) of grafted glycidols could not be calculated from ¹³C NMR resonances because the resonance of linear (L) and terminal (T) carbons were indistinguishable.

3.7 Aggregation of star copolymers

During the synthesis of the amphiphilic star copolymers and HPG polymers, Luo et al described a similar synthesis of the star polymer targeted in this study. [46] However, this method involved a two-pot procedure but also reported a micellar structure that self-assembled in water. [46] Therefore, it was decided to study and maintain the self-assembly of the polymers. Critical micelle concentrations (CMCs) were assessed by fluorescence spectrophotometers

using pyrene as solvatochromic probe. In the presence of micelles, pyrene can move from the bulk aqueous phase (polar region) to the hydrophobic interior of the micelle. This accompanied by a red shift in the excitation spectrum of pyrene. A plot of the polymer concentrations vs. the shift in the pyrene emission is shown in figure 3.4. In this study, the CMC of SPCL60-HPG90 was found to be 10-20 $\mu\text{g/mL}$.

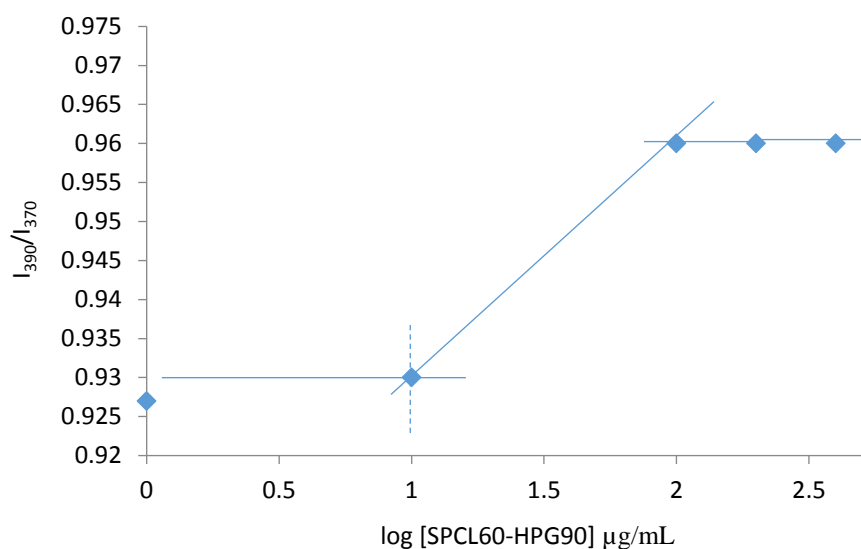


Figure 3.4: CMC determination of SPCL₆₀-HPH₉₀

Having shown that the star copolymers could aggregate, the aggregation of the HPG (control) was also studied. The CMC of TMP-HPG₉₀ was determined to be 150 $\mu\text{g/mL}$, (figure 3.5), which was higher than the star copolymer. This is expected as the star copolymer has significant hydrophobic region leading to a lower CMC.

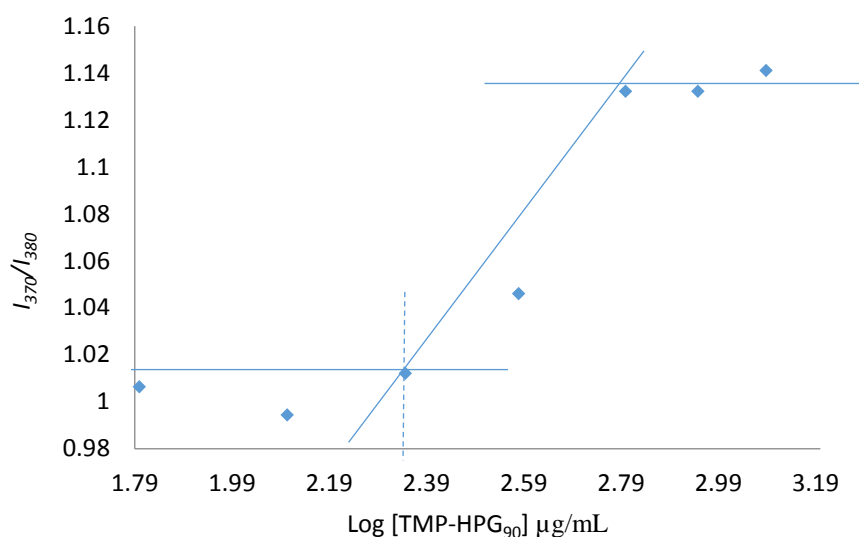


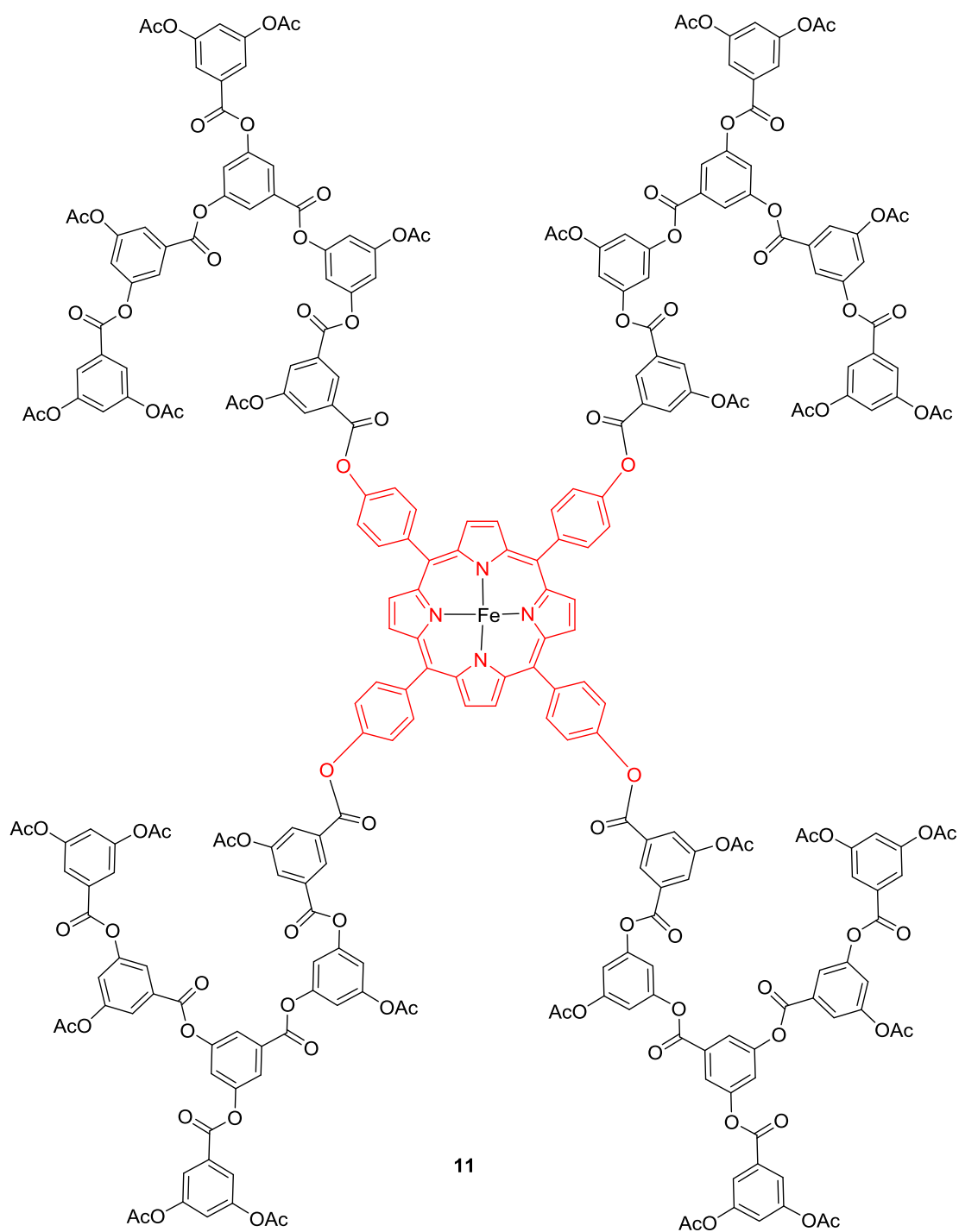
Figure 3.5: CMC level of TMP-HPG₉₀

The hydrodynamic diameter of the star copolymer (SPCL60-HPG90) and the TMP-HPG90 at the micelle concentration was measured using dynamic light scattering and found to be 170 and 100 nm, respectively. This data confirms that both polymers do aggregate in water into certain size and shape.

3.8 Selection of a suitable macromolecular guest

The main aim of this study was to investigate the ability of the star copolymers to host large drug molecules. These guests can be peptides, DNA, proteins, etc.. In our group, a synthetic mimic of a hemoglobin.^[47] This molecule is shown in figure 3.6.

Although this molecule could reversibly bind oxygen over a number of cycles, it was not water soluble. Before this molecule could be applied as an artificial blood product it must be solubilizing in water. Attempts to make a water soluble version were successful, but the new molecule failed to bind to oxygen due to a water promoted oxidation of the Fe metal. Therefore, it was proposed that encapsulation of the original synthetic model (shown in scheme 3.7) within a hydrophobic environment. As such proposed to encapsulate the hemoglobin model within the core of the star copolymers.

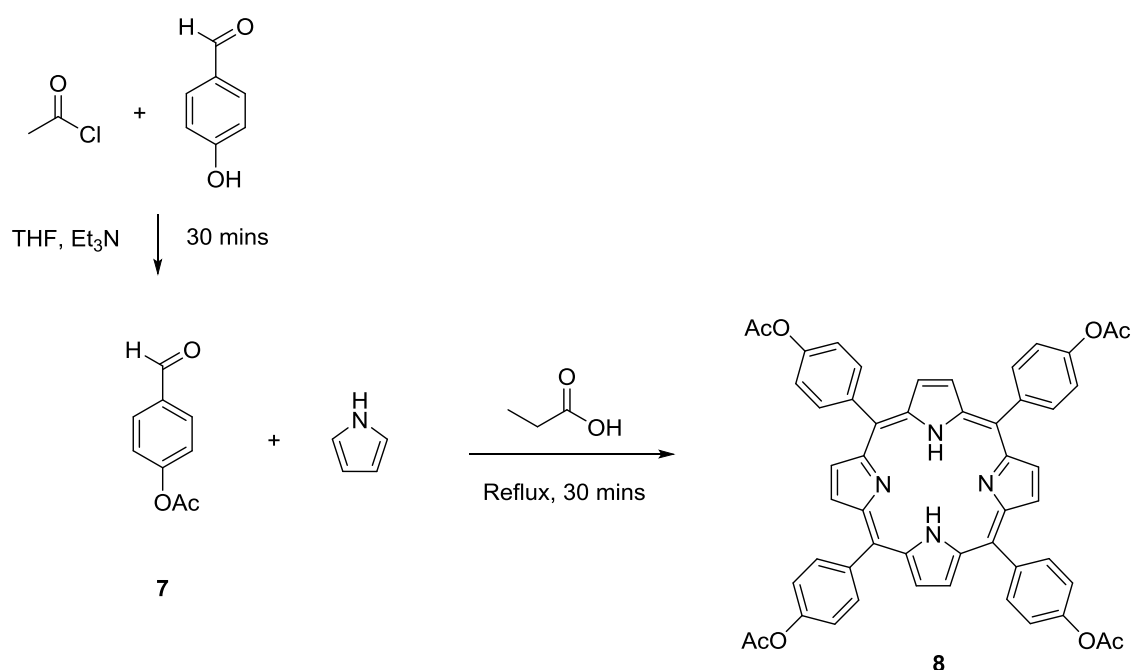


Scheme 3.7: The structure of the organic soluble artificial blood polymer

3.9 The synthesis of a porphyrin cored functionalized HBP (large molecule)

The synthesis of the porphyrin cored HBP (the hemoglobin mimic) has been reported ^[92] and started for the synthesis of the porphyrin core. Tetrakis-(4-acetoxyphenyl) porphyrin, TAPP **8**,

was synthesized from equimolar amounts of pyrrole and 4-acetoxybenzaldehyde **7**, which was synthesized via acetylating 4-hydroxy benzaldehyde using acetyl chloride. The synthesis is shown in scheme 3.8.

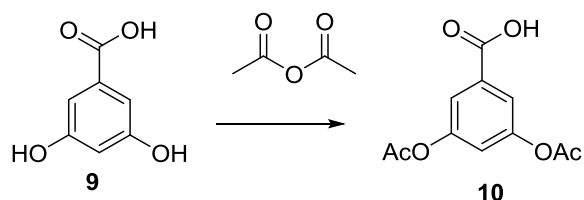


Scheme 3.8: Synthesis of tetrakis (4-acetoxyphenyl) porphyrin **8**

The successful synthesis of TAPP **8** was confirmed by ¹H NMR spectroscopy, which had doublets at 8.30 ppm and 7.52 ppm, corresponding to the *ortho* and *meta*-phenylic protons respectively. In addition, the β-pyrrolic protons of the porphyrin were observed as a singlet at 8.85 ppm, while the two highly shielded inner porphyrin protons were characterized by a singlet at -2.87 ppm. Moreover, the successful synthesis of a porphyrin was further proved by UV/Vis spectroscopy. The distinct, sharp and intense Soret band was observed at 418 nm, together with four weaker Q-bands at 515 nm, 549 nm, 590 nm and 643 nm respectively.

The monomer required for the porphyrin cored HBP was synthesized via the reaction of 3,5-dihydroxybenzoic acid **9** and acetic anhydride, using sulfuric acid as an acid catalyst, scheme 3.9. This yielded the desired 3,5-diacetoxybenzoic acid **10** in a yield of 80%.

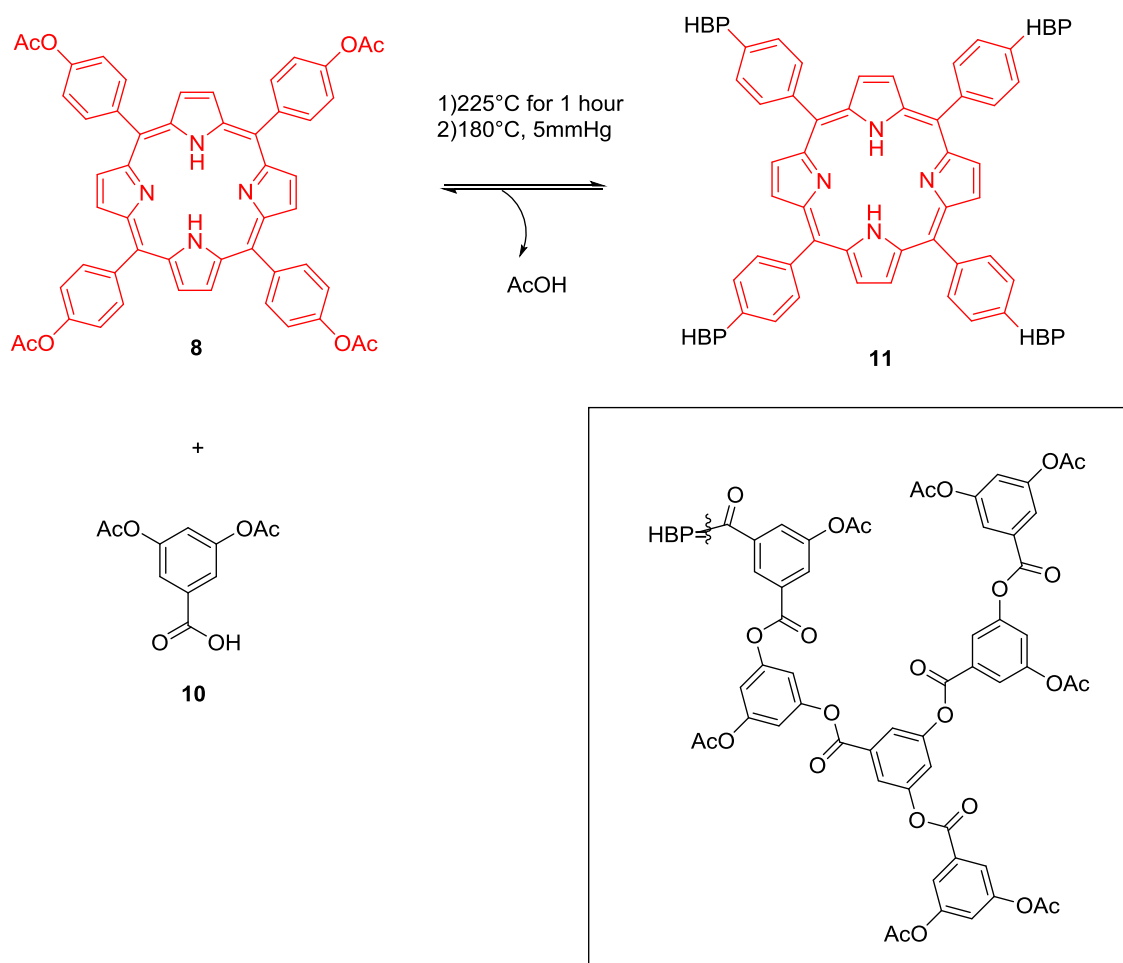
The formation of 3,5-diacetoxybenzoic acid was confirmed by ^1H NMR spectroscopy. The spectrum showed a proton resonance at 2.35 ppm, which corresponds to the six CH_3 protons of the two acetoxy groups. In addition, a molecular ion peak at 237 g mol^{-1} was observed in the mass spectrum.



*Scheme 3.9: synthesis of monomer **13** from benzoic acid **14***

The hydrophobic HBP **11** could then be obtained, scheme 3.10. TAPP **8** was reacted with 3,5-dihydroxybenzoic acid **11** in a molar ratio of 1:20, respectively. Specifically, firstly, the mixture was heated to $225 \text{ }^\circ\text{C}$ for 45 minutes before reducing the temperature to $180 \text{ }^\circ\text{C}$ and placing the reaction under reduced pressure for 4 hours. The hydrophobic HBP **11** was then precipitated from hot THF and cold methanol in a yield of 50%.

The GPC analysis of TAPP-HBP **11** showed an M_n value of 18100 g mol^{-1} with a PDI value of 2.07. The low PDI indicated involvement of the core during that the polymerisation. The GPC trace showed only a broad peak for the hydrophobic HBP, free, non-functionalised porphyrin was not visible. The ^1H NMR spectrum showed a proton resonance for the inner shielded porphyrin protons at -2.81 ppm and the pyrrolic β -hydrogens at 8.92 ppm . Furthermore, the success of the polymerisation was confirmed further through an observation of the characteristic singlets of the dendritic, linear and terminal proton resonance between $7.91\text{-}8.05 \text{ ppm}$.



Scheme 3.10: Reaction synthesis of the artificial blood polymer from acetoxyporphyrin **8** as the core and acetoxymonomer **11**

3.10 Encapsulation of a large hydrophobic macromolecular

Having successfully synthesised the macromolecular (SPCL-HPG **5**) and the macromolecular guest (TAPP-HBP **11**), encapsulation of the large guest within the host was studied. UV/vis spectroscopy was utilised to quantify the concentration of the encapsulated guest (HBP **11**) using the Beer Lambert equation. The first was to determine the molar extinction coefficient of TAPP-HBP **11** using acetone as the solvent. A linear plot of HBP **11** in organic solvent (acetone) was obtained and a ϵ value of $4.6 \times 10^5 \text{ M}^{-1}$ was determined.

Encapsulation of the hydrophobic TAPP-HBP **11** was conducted using star copolymers with different chain length for the PCL arms, but the same size of HBP capping units (fixed at DP

=90). Complexes were formed using 10 mg/mL of each host polymer and excess of the guest TAPP-HBP **11**. A methanol solution of the polymer was then mixed with an acetone solution of the hydrophobic. The solvents were evaporated to yield a purple/brown solid, which was dissolved in distilled water. Insolubilized hydrophobic, guest TAPP-HBP **15** was removed by filtration, and the absorbance measured by UV/Vis spectroscopy. Similarly, the control (hydrophilic hyperbranched polymer) was complexed with the hydrophobic HBP guest molecule.

The Soret band for guest TAPP-HBP **11** shifted from 417 to around 424 nm upon encapsulation for all of the polymers, indicating that solubilisation was successful, see table 2.4. A steady increase in the amount of guest encapsulated HBP **11** was observed as the length of the polymer arms increased. For example, the star copolymer which has 60 caprolactone units per arm (SPCL₆₀-HPG) has encapsulated two times more of the guest TAPP-HBP **15** than the SPCL₁₅-HPG with 15 caprolactone units.

Table 3.4: Table showing the encapsulation of TAPP-HBP **15** within the host polymers at 10mg/mL

Polymers 10mg/mL	ⁱ DP _{CL}	ⁱⁱ D _{gly}	ⁱⁱⁱ A	Loaded [HBP 15] M	λ_{\max}	
					Before	After
TMP1-HPG90	0	90	0.56	3.61E-06	417	424
SPCL15-HPG90	15	90	0.26	1.73E-05	417	424
SPCL35-HPG90	35	90	0.38	2.53E-05	417	424
SPCL60-HPG90	60	90	0.49	3.26E-05	417	426
ⁱ degree of polymerization of caprolactone per arm ⁱⁱ degree of polymerization of glycidol per arm ⁱⁱⁱ absorption after dilution by 31 factor for all the star copolymers and by 3 factors for the control (TMP-HPG)						

The control HPG could solubilise some of the guest TAPP-HBP **11** but the amount was very small, figure 3.9. This is surprising as the host HPG does not have space, however, it does aggregate (as it was approved earlier using pyrene as probe). Thus, it was proposed that the host HPG aggregate around the hydrophobic guest and hence offered solubilisation to the guest, figure 2.11, *a*. The encapsulation of the macromolecular guest with the star copolymers also happen due to aggregation, but since the star copolymers have great hydrophobic segment it could aggregate into certain shape to offer greater solubilisation for the guest, figure 3.11, *b*.

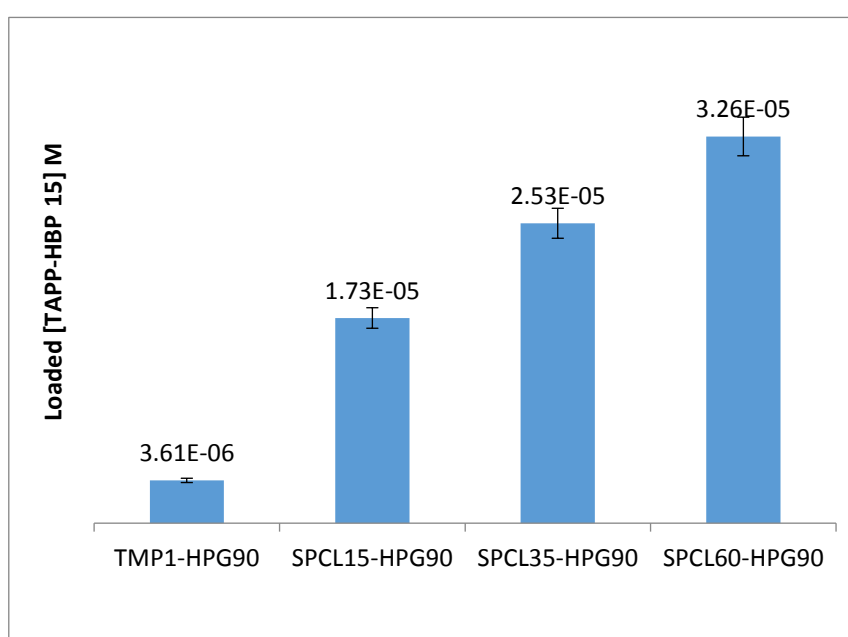


Figure 3.6: Trend to show the increase in the concentration of the encapsulated HBP **11** within different size of star copolymers and one control

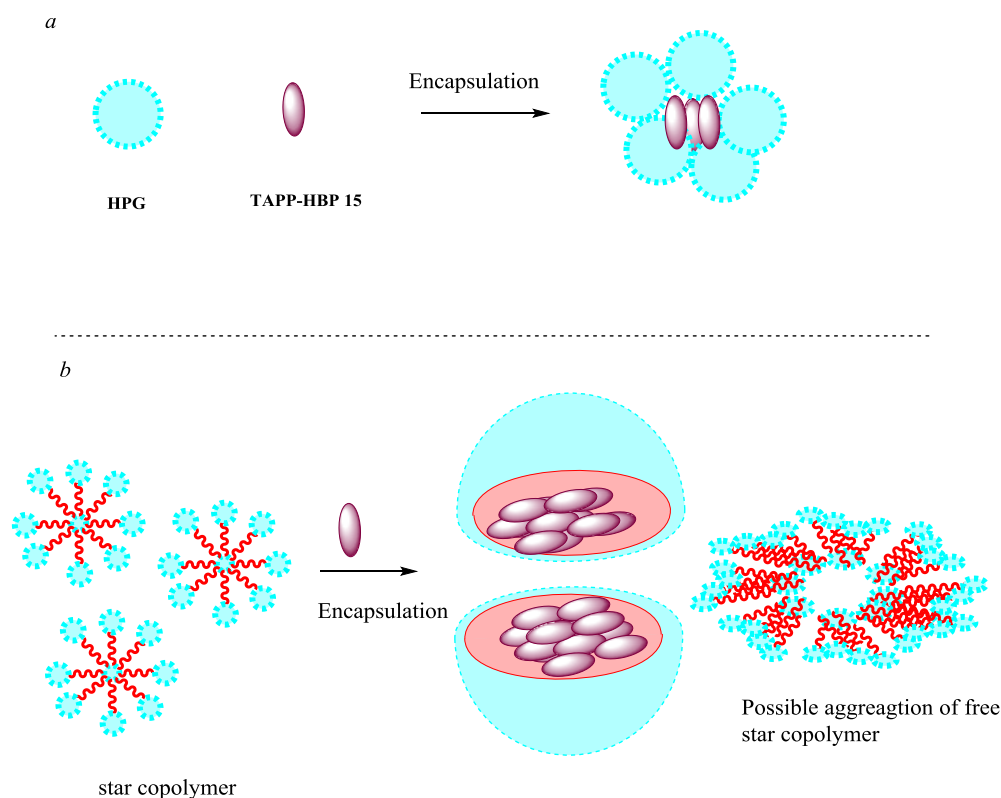


Figure 3.7: schematic representation showing where the encapsulation of the macromolecular guest (TAPP-HBP 15) with a) HPG and b) star copolymer happen

3.11 Summary

In summary, star copolymers based on polycaprolactone and polyglycidol (SPCL-HPG) were synthesised successfully via one-pot procedure using ring opening polymerisation. Three star copolymers (SPCL-HPGs) were prepared with different chain length and similar size of the capping group (SPCL15-HPG90, SPCL35-HPG90 and SPCL60-HPG90) in order to study the effect of the chain length upon encapsulating large molecule. The structures of the star polymers were confirmed by NMR spectroscopy and GPC. Hydrophilic HPG polymer was synthesised via ring opening polymerisation as the only control system of the proposed drug delivery system. The aggregation of the star copolymers and the control was approved by fluorescence technique using pyrene as a probe. The hydrodynamic diameter size for the star copolymers and the control was determined at their respective critical micelle concentration

(CMC) via DLS which was in the range of 100 to 200 nm. A model macromolecular guest, a synthetic mimic of hemoglobin (TAPP-HBP **11**), was synthesised successfully and has been encapsulated within the star copolymers and the control system. Significant amount of the guest was loaded within the star copolymers than it was for the control system. The poor encapsulation of the guest within the control (HPG) thought to be related to the aggregated structure of the polymer; HPG does not have hydrophobic segment that can form micelle structure with large hydrophobic domain to encapsulate great amount of the guest as it was seen for the star copolymers. So, the star copolymers was deemed to be a solution for improving the aqueous solubility of large molecule. This delivery system could be a suitable carrier for peptide or other large biomolecules only if the chain of its hydrophobic segments been functionalised. This could be achieved by synthesising a functionalised caprolactone monomer and then synthesising the star copolymer in the same manner as our delivery system.



Chapter 3

Porphyrin cored star copolymers for photodynamic therapy

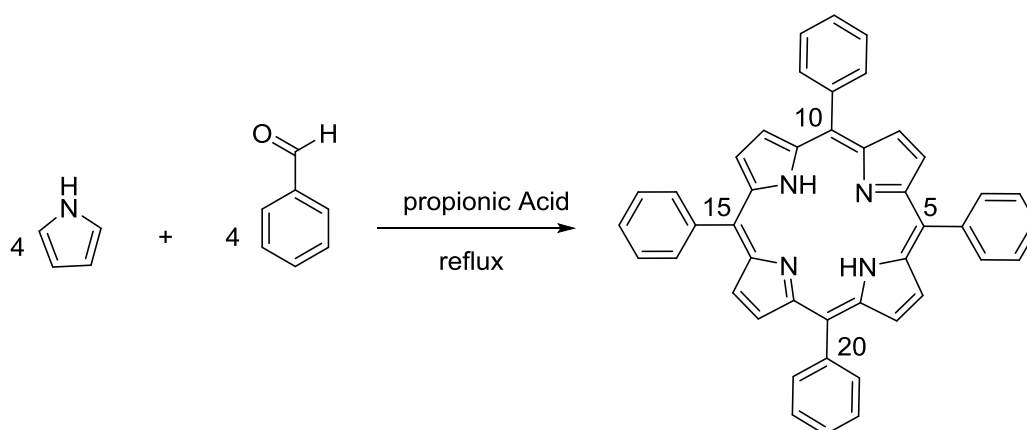


4. Porphyrin cored star copolymers for photodynamic therapy

Result and Discussuio

4.1 Synthesis and characterisation of porphyrin photosensitizers

The synthetic methods for generating porphyrins are generally result in low yielding. However, their synthesis can be achieved using inexpensive starting materials and is generally straightforward. In commonly, the synthesis of porphyrins typically requires the reaction of stoichiometric amounts of pyrrole and an aldehyde of choice to give the appropriate substitution at the *meso* positions, which are labelled with the numbers 5, 10, 15 and 20 in Scheme 4.1.



Scheme 4.1: Synthesis of tetraphenylporphyrin TPP

Porphyrins are UV-active molecules characterised by a very intense Soret emission band at about 410 nm and four lower energy Q-bands. The lowest energy Q-band at about 650 nm, which is associated with absorptivities in the infrared to the thousands, is the transition of interest for PDT. In addition, porphyrins have been linked with highly efficient formation of reactive oxygen species (ROS) and affinity for tumour sites. [69]

In this chapter, two porphyrin molecules were chosen to fulfil the aim of developing a polymer-based system for PDT. The selected porphyrins were tetrakis(4-hydroxyphenyl)-porphyrin

(THPP) **12** and tetrakis(3,5-dihydroxyphenyl)-porphyrin (TDHPP) **13**, as shown in Figure 4.2; these porphyrins contain hydroxyl groups, which facilitate the polymerisation. According to the literature, [70] THPP and TDHPP molecules have a low phototoxicity D_{37} (dose required to reduce cell survival by 37%) of 0.02 and 7.2 μM , respectively and a dark toxicity of 3.1 and 15 μM , respectively, using the HeLa cell line. Constructing appropriate polymeric delivery systems from these porphyrins will allow the investigation of the effectiveness of their nature as a dual system for PDT and chemotherapy. Using these porphyrins as initiators/cores for amphiphilic star polymers, different arms will be obtained and hence the effect of arm length upon the aggregations will be highlighted.

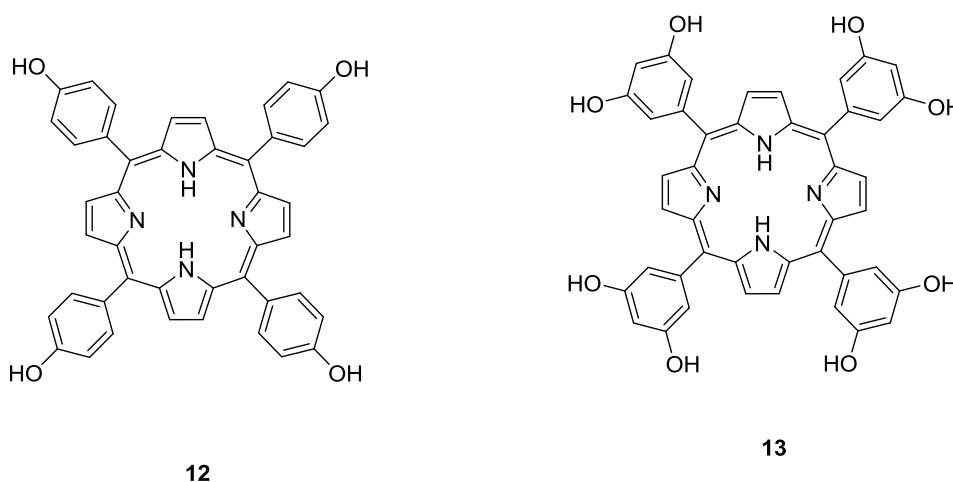
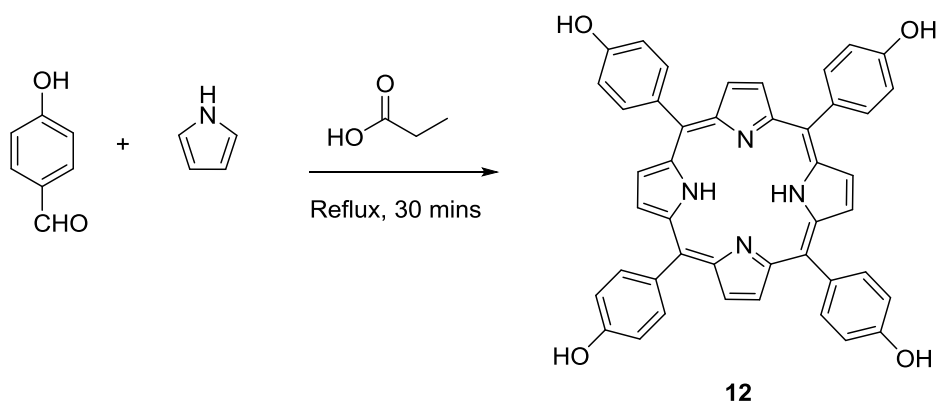


Figure 4.1: Potential porphyrin derivative to be used as a core in drug delivery systems for PDT applications THPP **12** and TDHPP **13**

4.1.1 Tetrakis(4-hydroxyphenyl)-porphyrin (THPP **12**)

THPP **12** was successfully synthesised from 4-hydroxybenzaldehyde and pyrrole following the method by Rothermund and Adler–Longo method. [49] The aldehyde and pyrrole were refluxed for half an hour at equal molar quantities, as shown in Scheme 4.2.

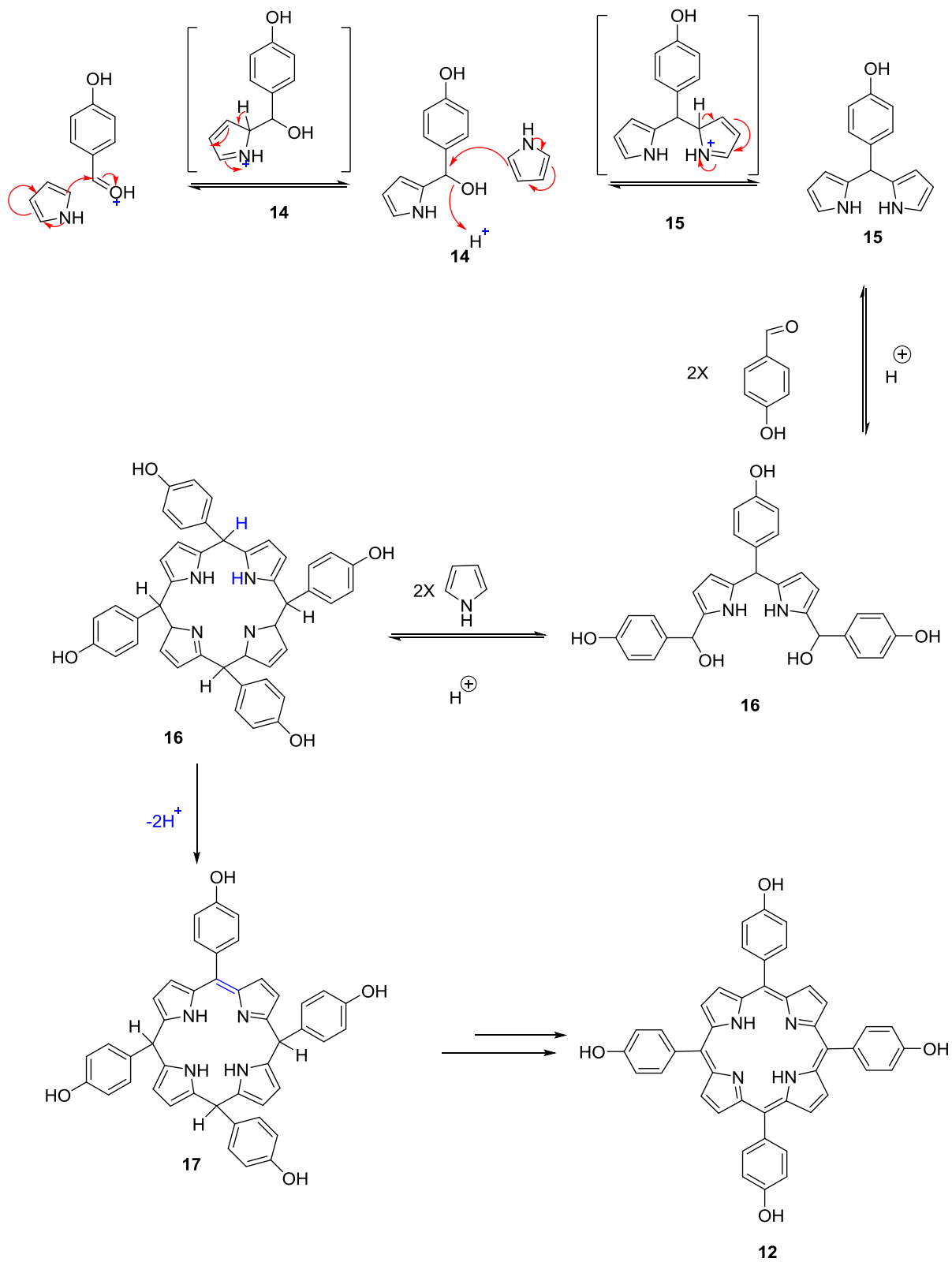


Scheme 4.2: Synthesis of THPP 20

Regarding the ^1H NMR spectrum, the internal N–H proton resonance of THPP were observed in the highest field region (-2.9 ppm) because of the ring current interaction. Resonances corresponding to the O–H and pyrrole or phenyl protons were observed in the low field region of 10.01 ppm (O–H) and 9.1 ppm (β -H–pyrrole), respectively. Resonance at 7.3–8.1 ppm (*ortho* and *meta* H–Ph) were also observed.

The FT-IR spectrum showed an absorption band of strong intensity located at 3420 cm^{-1} , which was attributed to the O–H stretching vibration. The absorption at 3311 cm^{-1} was assigned to the stretching and bending vibrations of N–H, which is a characteristic absorption of free base porphyrins. The UV/vis spectra of THPP in methanol displayed a very intense Soret band at 417 nm and four Q-bands at 512, 550, 585 and 640 nm. The molar extinction coefficient of THPP in methanol was found to be $4 \times 10^6\text{ L mol}^{-1}\text{ cm}^{-1}$.

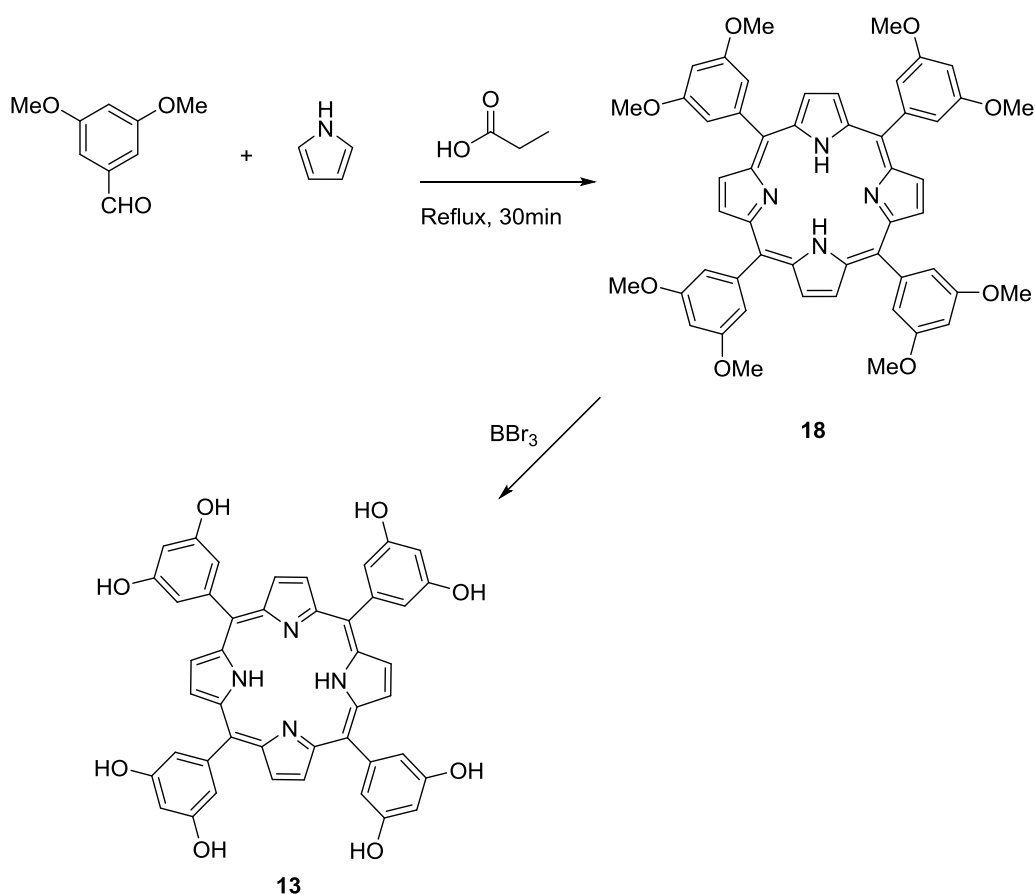
Scheme 4.4 shows the mechanism of synthesis THPP **12**. The electron-dense carbon on the pyrrole attacks the electrophilic carbon on the protonated aldehyde to form the intermediate **14** and then compound **15**. A second equivalent of pyrrole then attacks the sp^3 carbon of compound **15**, resulting in the loss of water and the formation of intermediate **16** and then compound **16**. This is followed by a further electrophilic substitution reaction involving the pyrrole unit and aldehyde until compound **17** is formed; a final oxidation step results in the formation of porphyrin **12**.



Scheme 4.3: Mechanism of synthesis of THPP 12

4.1.2 Tetrakis(3, 5-dihydroxyphenyl)-porphyrin

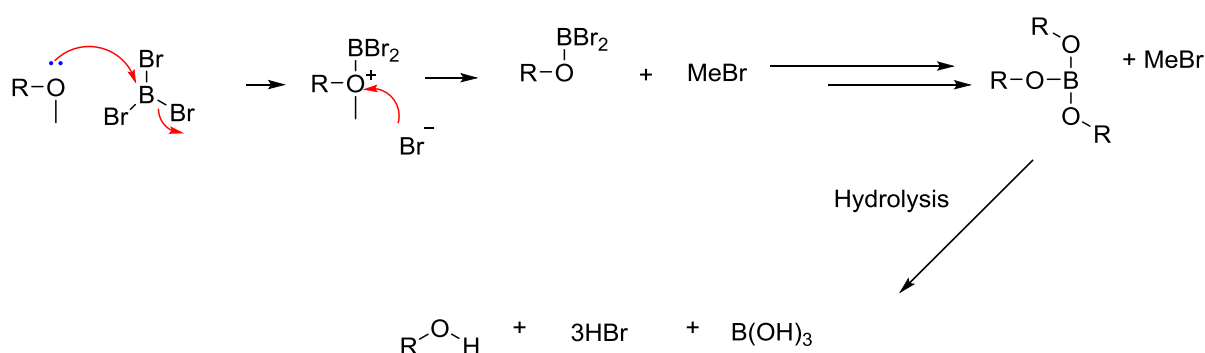
TDHPP **13** was synthesised in a two-pot reaction procedure, as illustrated in Scheme 4.5. The first step involved the synthesis of tetrakis(3,5-dimethoxyphenyl)-porphyrin (TDMPP) **18**, which was achieved by refluxing equimolar quantities of 3,5-methoxybenzaldehyde and pyrrole for 30 minutes. The second step of preparing the desired porphyrin **13** was achieved by the demethylation of TDMPP using boron tribromide as the demethylation agent.



Scheme 4.4: Synthetic method for TDHPP **13**

The UV/vis absorption spectrum of TDMPP **18** confirmed the presence of the porphyrin displaying a Soret band at 420 nm and four Q-bands at 513 nm, 548 nm, 586 nm and 643 nm. The methoxy porphyrin **18** was also confirmed by mass spectrometric analysis, which had a molecular ion peak at 855. Additionally, there was a large singlet at 3.98 ppm from the methoxy protons and a peak at -2.9 ppm for the porphyrin ring N-H protons in the ¹H NMR spectrum.

In the preparation of TDHPP **13** from TDMPP **18**, the methoxy porphyrin was dissolved in anhydrous dichloromethane and stirred under nitrogen for 10 minutes, after which boron tribromide was added dropwise, turning the solution green. Boron tribromide is a strong Lewis acid that interacts with the lone pair of the methoxy oxygen, ejecting a bromide ion that attacks the methyl group, which leaves as methylbromide, as shown in Scheme 4.6. Hydrolysis then occurs, replacing the bromides with hydroxyl groups, and the boron then leaves as boric acid to yield the deprotected product and hydrogen bromide.

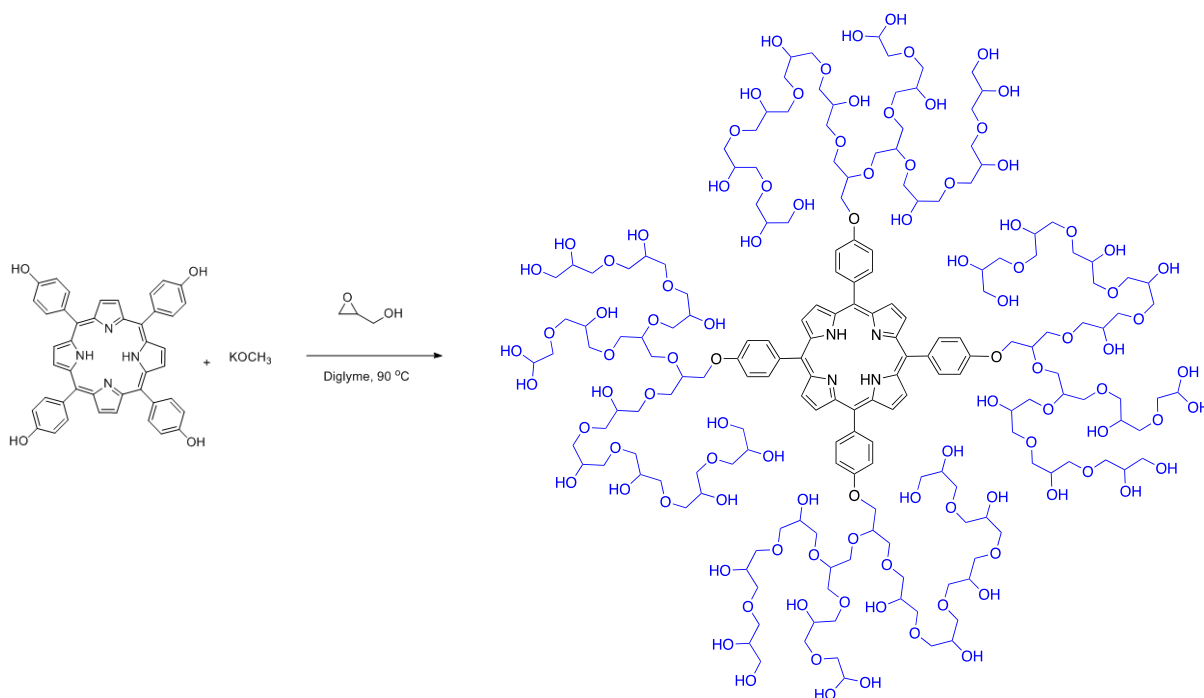


Scheme 4.5: Generic mechanism of demethylation by BBr₃

The reaction was performed at room temperature with stirring for about 5 hours, after which any unreacted boron tribromide was quenched with the slow addition of water. The acidic reaction mixture was neutralised with sodium hydrogen carbonate solution and extracted with ethyl acetate. The crude product indicates initial success by a dramatic change in solubility; the starting material (TDMPP **18**) is soluble in dichloromethane whereas the product was not. The protection was confirmed by ¹H NMR spectroscopic analysis, which showed the loss of the methoxide proton resonance at 3.98 ppm, and by mass spectroscopy, which gave a molecular ion peak at 743. The product was also confirmed by FTIR spectroscopy where a broad peak at 3400 cm⁻¹ indicated the presence of hydroxyl groups.

4.2 Synthesis of porphyrin-cored hyperbranched polyglycerols (HPG)

Having successfully synthesised and characterised the cores/initiators, the control systems, porphyrin-cored polyglycerols, were synthesised next. Porphyrin molecules (THPP **12**, TDHPP **21**) were used for the anionic ring-opening polymerisation of glycidol and produced porphyrin-cored hyperbranched polyglycerol (porphyrin-HBP). The advantage of the covalent incorporation approach is that the porphyrin stays at the central position of the hydrophobic interior and is not retained easily. The synthesis utilised 50 equivalents of glycidol monomer per hydroxyl group of the core to yield HPGs with similar size of HPG per arm in order to determine which Porphyrin-HPG polymer is best for effective PDT. Scheme 4.6 shows the reaction scheme for THPP-cored polyglycerols (THPP-PG).



Scheme 4.6: Reaction scheme of synthesizing THPP-cored polyglycerols; TDHPP-PG was synthesised in the same manner

The core and diethylene glycol dimethyl ether (diglyme) were added to an oven-dried two-neck bottom flask and heated to 90 °C under nitrogen atmosphere until complete dissolution of the porphyrin had occurred. Potassium methoxide was then added and an instant colour change from red purple to green was observed, indicating the deprotonation of the core. A mixture of

glycidol and diglyme (3:1) was slowly injected into the reaction flask with the aid of a syringe pump over a period of several hours. The glycidol was added slowly to prevent explosion. The polymer structure was characterised by ^1H NMR spectroscopy to indicate the successful synthesis of the hyperbranched polymer. Two significant regions were observed in the spectrum. One was in the aromatic region at 7.8–8.4 ppm for the porphyrin (phenolic and pyrrolic protons). The second was at higher field, with a multiplet broad peak at 3.2–4.2 ppm for the CH, CH₂ and OH groups of the polyglycidol backbone.

Fourier transform infrared (FTIR) spectroscopy was also used to confirm the porphyrin–HBP structure. The spectrum displayed a broad peak at 3320 cm⁻¹ for the OH groups and a peak at 2845 cm⁻¹ for the C–H protons and a C–O peak 1630 cm⁻¹.

The molecular weight of the hyperbranched polymer was characterised by gel permeation chromatography (GPC) and compared to the theoretical values and ^1H NMR spectroscopy data, as shown in Table 4.1

Table 4.1: Summary of the average molecular weight of porphyrin-cored polyglycerols using different techniques

Core of HPG	Theoretical	NMR ^a	GPC ^b	Đ ^c
THPP	15479	39000	14000	1.5
TDHPP	30343	61000	42000	2.3
^a As determined by integration of ^1H NMR resonance in D ₂ O ^b As determined by GPC analysis (aqueous) ^c Polydispersity index				

The theoretical molecular weight (M_n) was calculated by multiplying the ratio of the monomer (50) by the number of hydroxyl groups of the cores (four OH groups for THPP and eight for TDHPP) and by the molar mass of the glycidol (74.08 g mol⁻¹) before adding the molar mass of the core (679 g mol⁻¹ for THPP and 743 g mol⁻¹ for TDHPP) to yield 15479 Da for THPP–

PG and 30343 Da for TDHPP–PG. The theoretical Mn would match the Mn obtained by GPC or ¹H NMR only if the polymerisation is highly controlled. However, this is unlikely to occur with the anionic ROP polymerisation of glycidol. Thus, a discrepancy between the theoretical Mn and those obtained by either ¹H NMR or GPC is very likely.

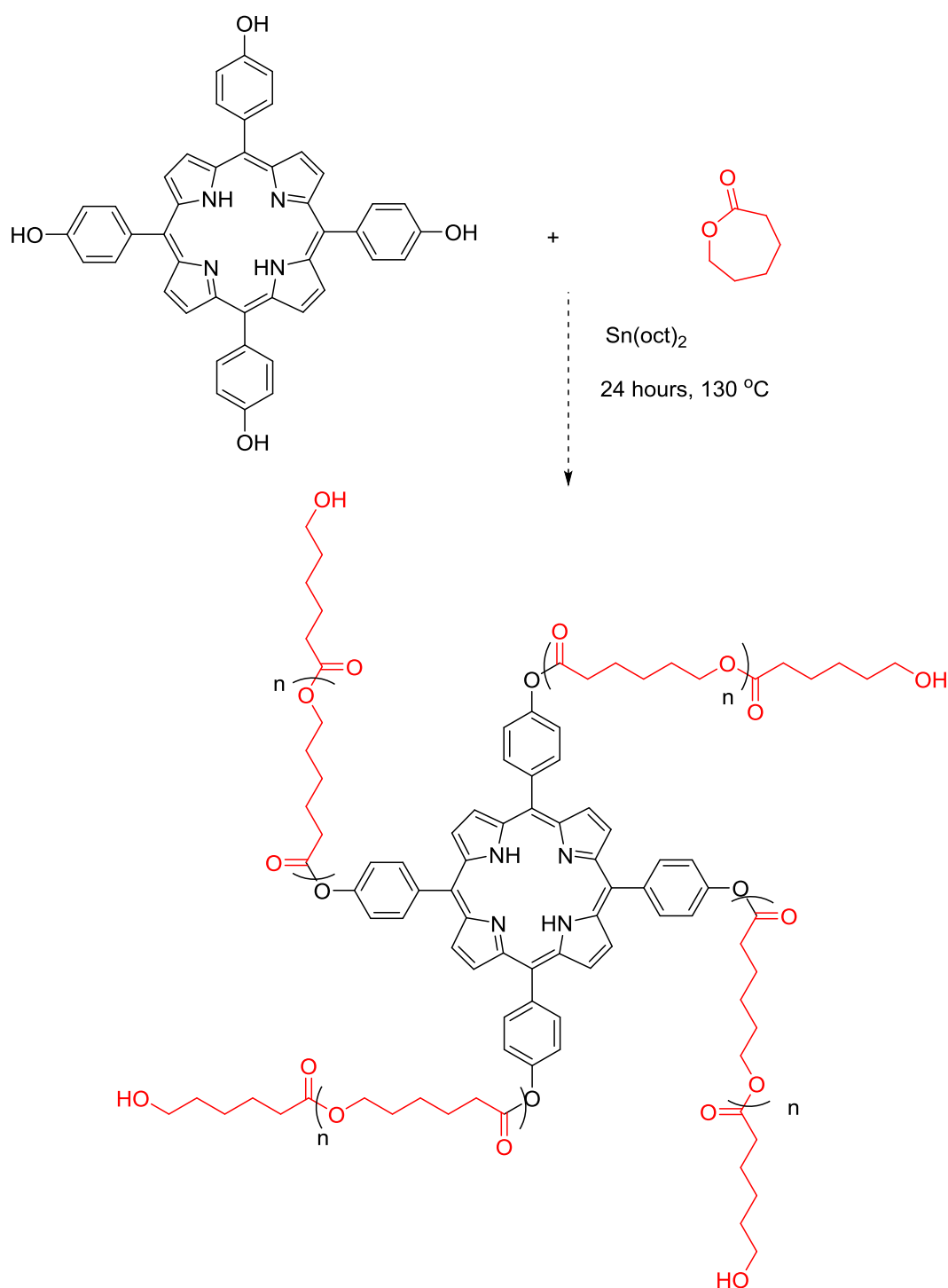
The Mn obtained from GPC (aqueous) was approximately 14 KDa for the THPP–PG and 41 KDa for the TDHPP–PG (relative to linear polyethylene glycol (PEG or PEO) with a polydispersity of 1.5 and 2.3 in aqueous solution), respectively. This was quite close to the theoretical Mn values.

Meanwhile, the Mn obtained by ¹H NMR spectroscopy analysis for both polymers were higher than both the theoretical Mn and the Mn by GPC; this is because ¹H NMR spectroscopy cannot differentiate between polymers with or without a core. Interpretation of the ¹H NMR spectroscopy data overestimates the molecular weight by assuming that every monomer has a core, whereas the GPC underestimates the Mn owing to the error derived from calibrating the instrument with a linear polymer such as PEG or polystyrene.

The Mn obtained by ¹H NMR and UV spectroscopy were closer to the theoretical Mn than that obtained by GPC but, in general, there was no regular trend observed between the Mn obtained using different techniques owing to the uncontrolled polymerisation of glycidol.

4.3 Porphyrin star poly(ϵ -caprolactone)-polyglycerol copolymers

The synthesis involved a two-step one-pot reaction as was employed for the non-porphyrin-cored star copolymers. First, the porphyrin core and the catalyst ($\text{Sn}(\text{oct})_2$) were reacted with the ϵ -CL monomer via a ring-opening polymerisation at 130 °C for 24 hours, as shown in Scheme 4.8.



Scheme 4.7: Ring-opening polymerisation of porphyrin initiator with ϵ -caprolactone monomer

A small sample was withdrawn and analysed by ^1H NMR spectroscopy to ensure that the photoactive porphyrin initiator was incorporated into the star polymer before proceeding to the second step. The ^1H NMR spectra showed the typical signals of PCL whereas the porphyrin protons were not observed. This confirmed that the porphyrin did not get incorporated during

the polymerisation procedure. This could be owing to conjugation of the oxygen lone pair in to the porphyrin making it unreactive (Figure 4.2). Therefore, a spacer was attached between oxygen and the porphyrin; this would break the conjugation and hence allow the polymerisation of ϵ -caprolactone.

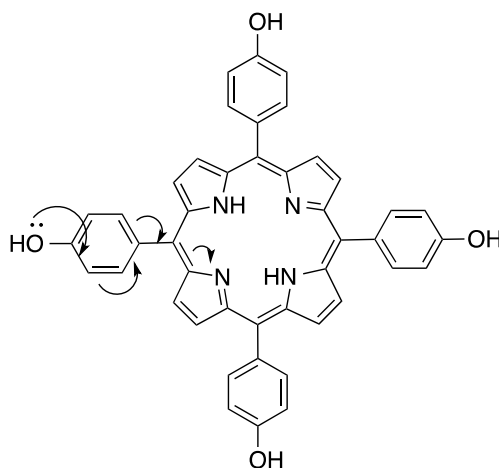


Figure 4.2: delocalization of the hydroxyl lone pair with the aromaticity of the porphyrin ring

4.4 Synthesis

of

porphyrin initiators

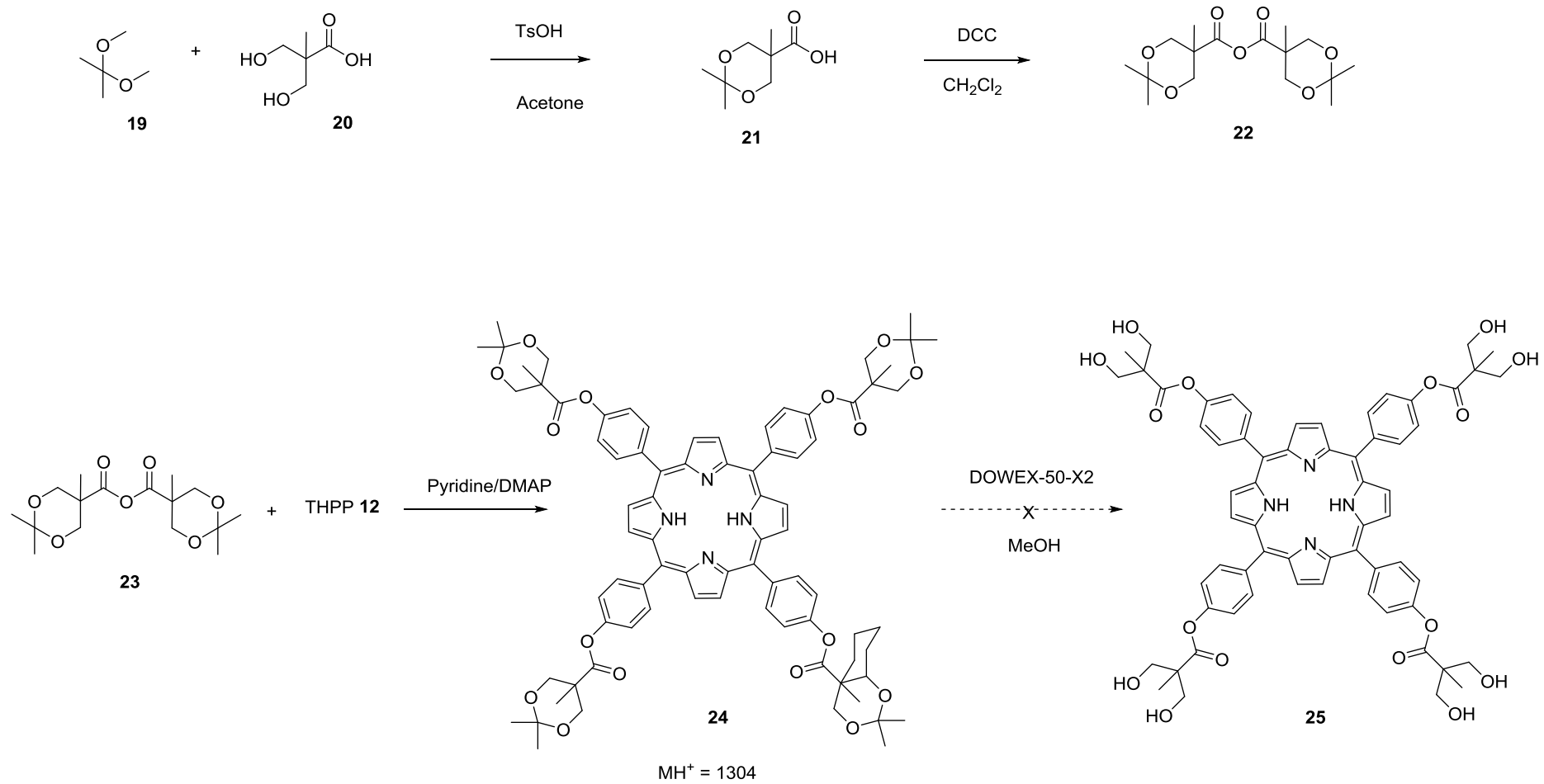
Porphyrins are known to be highly conjugated molecules; consequently, delocalisation reduces the reactivity of the lone pair of the hydroxyl group, preventing it from reacting with some monomers. For this reason, the anionic polymerisation of caprolactone initiated by porphyrin was not feasible and hence increasing the reactivity of porphyrin molecules was crucial for polymerisation to occur. Attaching a spacer between the oxygen and the porphyrin could break the conjugation and hence allow the polymerisation of ϵ -caprolactone to occur.

4.4.1 Acetonide–porphyrin

Our initial idea for breaking the conjugation of porphyrin was to add bis-MPA (2,2-bis(methylol)propionic acid) **20**, scheme 4.9. Adding a spacer with two active sites will also

increase the number of arms of the star polymer, which is a desired feature in terms of maximising the number of branching arms.

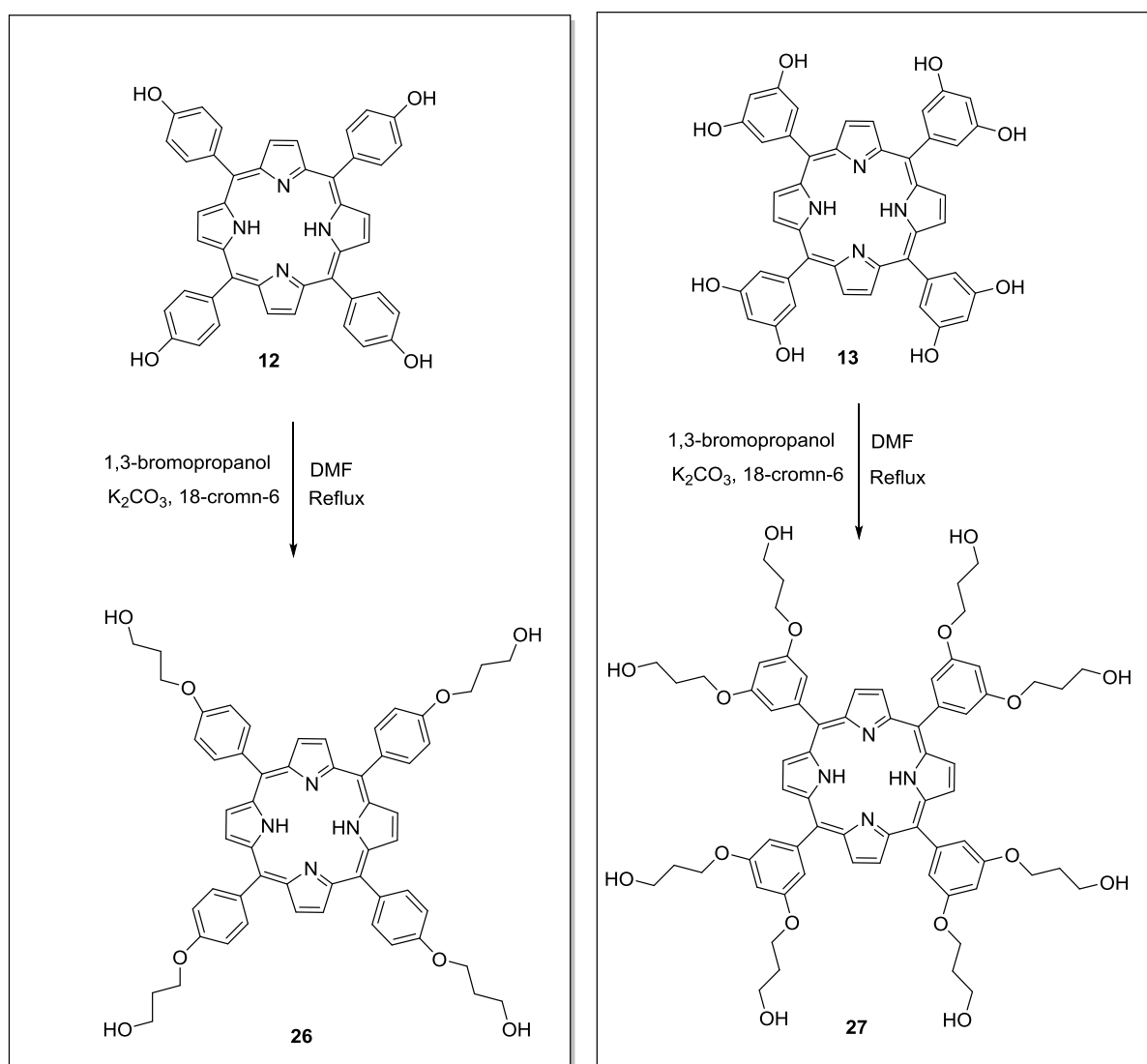
The preparation of diol **25** is shown in Scheme 3.8 and starts with the protection of the diol group of 2,2-bis(hydroxymethyl)propionic acid **20** by reaction with 2,2-dimethoxypropane **19** and a catalytic amount of *p*-toluenesulfonic acid monohydrate (TsOH) in dry acetone to afford **21**. Anhydride **22** was then synthesised by self-condensation of **21** in chloroform using *N,N'*-dicyclohexylcarbodiimide (DCC). The crude anhydride **22** was purified from excess DCC and the *N,N'*-dicyclohexylurea (DCU) byproduct by precipitation into hexane to afford an essentially pure product. Coupling of **21** with the phenolic groups of THPP **12** was successfully accomplished, as confirmed by mass spectrometry with an MH⁺ of 1304, using 1.5 equivalents of **22** per hydroxyl group to obtain a 90% yield of **24**. The esterification reaction was carried out in a 1:3 mixture of pyridine and chloroform using DMAP (4-(dimethylamino) pyridine) as the acylation catalyst. However, there was a problem with the deprotection step using DOWEX-50-X2 resin or sulfuric acid; the phenolic ester linkage between the porphyrin and the acetonide was hydrolysed instead of the dimethoxy end group. The reaction of the final step to obtain compound **25** was time consuming and requires further exploration using different concentrations of DOWEX or different agents. Therefore, another spacer with a straightforward reaction was required.



Scheme 4.8: Reaction scheme for the synthesis of acetone-porphyrin

4.4.2 Spacer–porphyrin (S-porphyrin)

The syntheses of S-THPP **26** and S-TDHPP **27** were achieved easily through the reaction of porphyrin and 1,3-bromopropanol with K_2CO_3 and 18-crown-6 in dry DMF (Scheme 4.10). The reaction was vigorously stirred under reflux overnight and the completion of the reaction was monitored by TLC. The identity of the porphyrin initiator was confirmed via mass spectrometry (M^+H^+ of 911 and 1215 for S-THPP **26** and S-TDHPP **27**, respectively). The 1H NMR spectrum also confirms the formation of the S-porphyrin initiator, with the notable presence of the spacer proton resonance.



Scheme 4.9: Reaction schemes for S-THPP **26** and S-TDHPP **27**

4.4.3 Synthesis of spacer–porphyrin-cored hyperbranched polyglycerols

Following the successful synthesis of spacer–porphyrin molecules, hyperbranched polyglycerols S-THPP-HPG **28** and S-TDHPP-HPG **29** (Figure 4.3) were synthesised in the same manner as THPP-HPG.

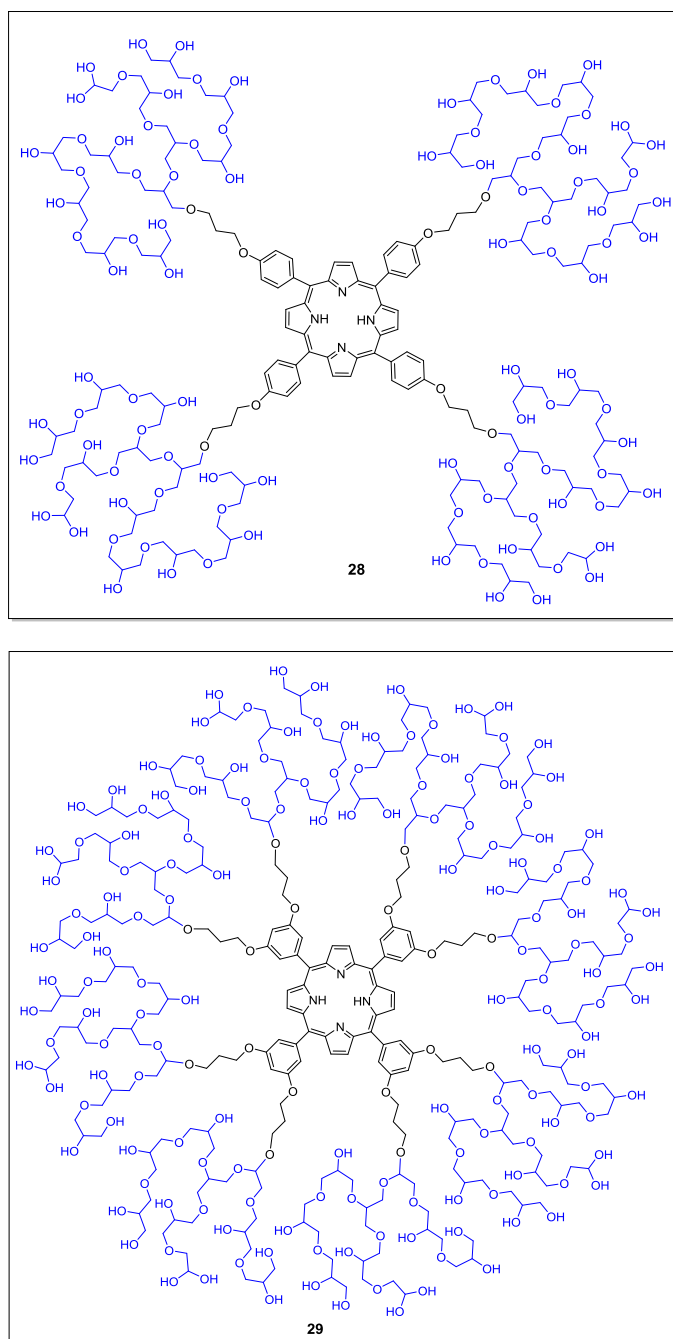


Figure 4.3: Structures of S-THPP-HPG **28** and S-TDHPP-HPG **29**

The molecular weight of the hyperbranched polymer was characterised by gel chromatography (GPC)

and compared to the theoretical and ^1H NMR data, as shown in Table 4.2.

Table 4.2: Summary of the average molecular weight of porphyrin-cored polyglycerols using different techniques

	Theoretical	NMR ^a	GPC ^b	PDI
S-THPP ₁ -HPG ₅₀ 28	15711	50000	19000	1.5
S-TDHPP ₁ -HPG ₅₀ 29	30806	15000	8500	2.3
^a As determined by integration of ^1H NMR resonance in D ₂ O				
^b As determined by GPC analysis (aqueous)				

4.5 Synthesis of porphyrin star poly(ϵ -caprolactone)-polyglycidol copolymers (SPPCL-HPG)

The synthesis of SPPCL-HPG involved a two-step one-pot reaction, as shown in Scheme 4.11. First, the spacer–porphyrin core and Sn(oct)₂ as the catalyst were reacted with ϵ -CL monomer via a ring-opening polymerisation at 130 °C for 24 hours. The molar ratio of the core to the monomer was varied to make a family of star polymers. Before proceeding to the second step, a small sample was withdrawn for analysis. Table 4.3 shows the molecular weight of the initial star polymers obtained via different analytical techniques.

Table 4.3: Molecular weight of the initial star polymers determined by different techniques

1 st step crude	(Core : monomer) / arm	Mn ^a	Mn ^b	Mn ^c	PDI
S-TDHPP ₁ -PCL ₁₀ 32	1:10	10337	23000	19000	1.2
S-TDHPP ₁ -PCL ₃₅ 32	1:35	33165	70000	40000	1.1
S-THPP ₁ -PCL ₄₀ 30	1:40	19173	22000	22000	1.0
^a Theoretical Mn ^b As determined by integration of ¹ H NMR resonance in CDCl ₃ ^c As determined by GPC analysis (THF)					

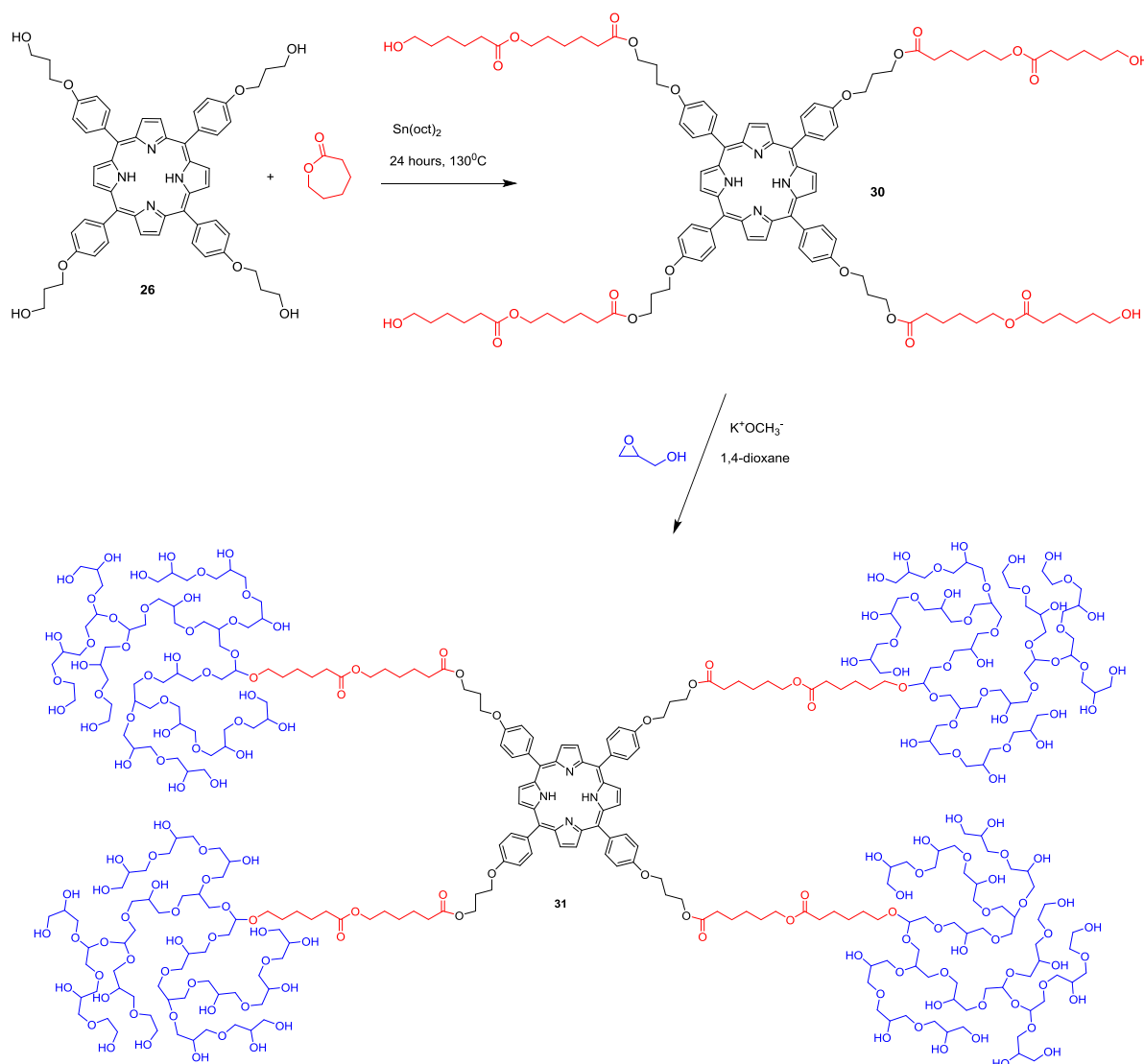
The second step in the synthesis of the star copolymers SPPCL-HPG (**31** and **33**) involved the addition of the HPG units. This was done by using the SPPCL (**30** or **32**) as a core unit for the anionic ring-opening polymerisation of glycidol. The polymer was precipitated from methanol into cold acetone and dialysed (with a 12 KDa molecular weight cut off) against water for 48 hours. The material obtained was dried and characterised to determine the molecular weight and structure of the final star polymers.

The ¹H NMR spectra of the star copolymers showed the presence of both blocks, suggesting the success of the reaction. However, the protons of the hydrophobic core (SPPCL) were collapsed in water and hence integrating the hydrophilic protons per hydrophobic block did not afford a reliable estimation of the Mn values. Aqueous GPC for the star copolymers could not be used to estimate the Mn because of the nature of the polymer in aqueous media, which forms aggregates (diameter of less than 200 nm), and the size obtained will be underestimated.

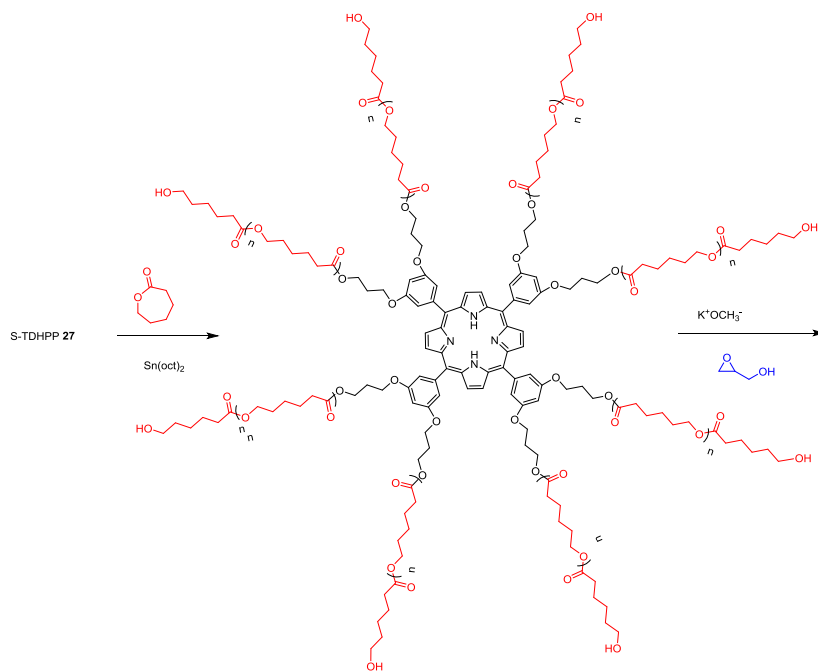
Table 4.4: Molecular weight of the star copolymers determined by different techniques

2 nd step crude	(Core : glycidol) / arm	Mn ^a	Mn ^b	Mn ^c	PDI
S-TDHPP ₁ -PCL ₁₀ -HPG ₃₅ 33	1:35	31057	35000	27000	1.4
S-TDHPP ₁ -PCL ₃₅ -HPG ₃₅ 33	1:35	53885	40000	50000	2.2

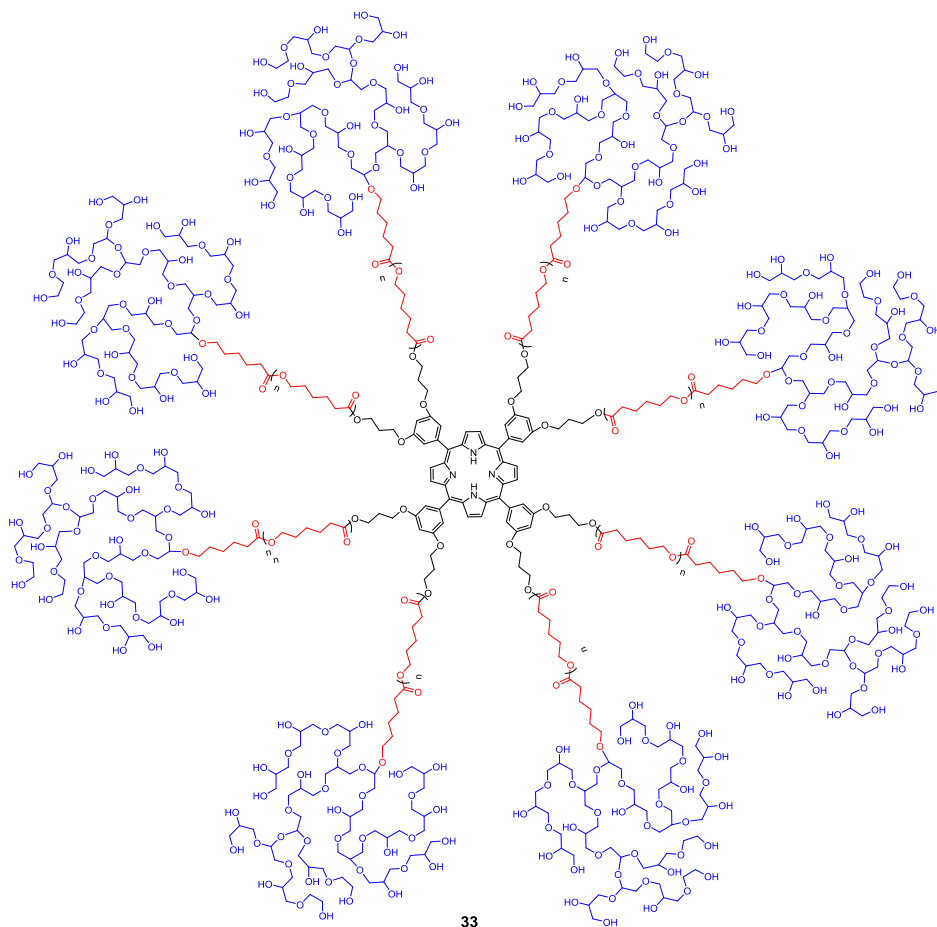
S-THPP₁-PCL₄₀-HPG₆₀ 31	1:60	36933	90000	51000	1.0
^a Therortical Mn ^b As determined by integration of ¹ H NMR resonance in D ₂ O ^c As determined by GPC analysis (aqueous)					



Scheme 4.10: Synthesis of S-THPP-cored star copolymer (SPPCL-HPG 31)



32



Scheme 4.11: Synthesis of *S*-THPP- cored star copolymer (SPPCL-HPG 33)

4.6 Micelle formulation

Polymeric micelles made from amphiphilic copolymers can spontaneously form in aqueous media. This thermodynamically favoured aggregation occurs above the so-called critical micelle concentration (CMC). Micelles with a low CMC are preferred as they have a high level of thermodynamic stability. Micelles with a low CMC can be obtained by increasing the hydrophobic segment of the amphiphilic copolymer. Therefore, the amphiphilic star copolymers described are composed of many hydrophobic segments and are thus expected to form micelles at a lower CMC compared to hyperbranched polyglycerols (porphyrin-HBPs), which do not have very large hydrophobic segments and which have been proven to aggregate in the previous chapter. In this project, the CMCs of the star copolymers and HPG were examined using dynamic light scattering (DLS) and fluorescence to give an indication of the different aggregated structures.

4.6.1 Dynamic light scattering

DLS has been found to be just as sensitive as fluorescence spectroscopy in the determination of the CMC. Simultaneously, DLS can determine the hydrodynamic diameter of the aggregated structures. To determine the CMC of the polymers, aqueous solutions within the concentration range of $1 \times 10^{-2} \text{ mg mL}^{-1}$ and 1 mg mL^{-1} were prepared.

The CMC of the star copolymer (S-THPP₁-PCL₄₀-HPG₆₀ **31**, 51 KDa) was determined in the first instance as $125 \text{ } \mu\text{g/mL}$ ($5.8 \text{ } \mu\text{M}$), which is in agreement with the CMCs reported for other amphiphilic polymeric micelles. At low concentrations reading of 0.0 was observed because aggregated structures were not formed. At higher concentrations of polymer, two different aggregated structures were found, first at $125 \text{ } \mu\text{g/mL}$ and the second at $300 \text{ } \mu\text{g/mL}$ with hydrodynamic diameters of 250 and 360 nm, respectively. The smaller hydrodynamic diameter has been assigned as micelles but the molecules with a diameter greater than 200 nm are

thought to be vesicles or rod structures. Interestingly, the porphyrin-cored hyperbranched polymer (S-THPP-HPG **28**, 20 KDa) has a smaller hydrodynamic diameter but a similar CMC level (125 $\mu\text{g}/\text{mL}$) to the star copolymer (S-THPP₁-PCL₄₀-HPG₆₀ **31**, Figure 4.4 b). HBP (THPP-HPG, 14 KDa) has a higher CMC level at around 1.3 mg/mL (93 μM , Figure 4.4 c), as expected. The star copolymers behaved differently to the HPG polymers; two different aggregated structures were observed for the star copolymers while there was only one for the HPG polymers.

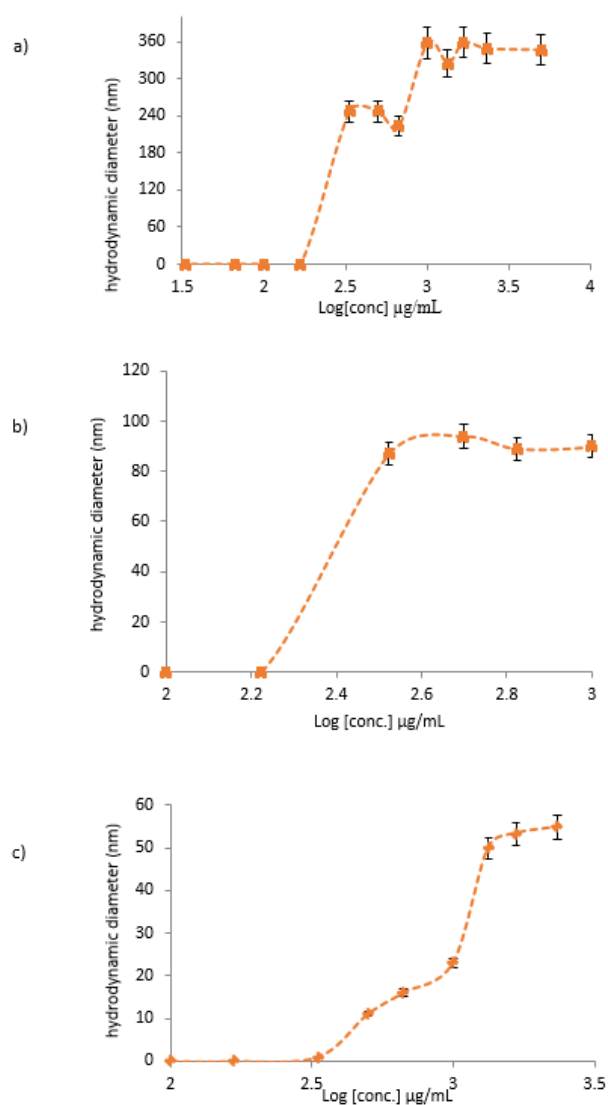


Figure 4.4: Plots of the hydrodynamic diameter obtained for various concentrations of a) S-THPP₁-PCL₄₀-HPG₆₀ **31**, b) S-THPP-HPG **28** and c) THPP-HPG in deionised water.

4.6.2 Fluorescence technique

CMCs were also determined by fluorescence measurement using pyrene as a probe. [12] Pyrene inside micelles is in a hydrophobic microdomain. This is different to the aqueous environment. Consequently, a red shift of pyrene's emission is observed in the excitation spectrum when the aggregation occurs the pyrene enters the hydrophobic micelle.

The CMC of S-THPP1-PCL40-HPG60 **31** as determined by fluorescence (67 $\mu\text{g/mL}$) was slightly lower than that obtained by DLS (120 nm). As with DLS, another structure was observed at a higher concentration of 300 $\mu\text{g/mL}$, Figure 4.5 a. There was no significant difference between the CMC level obtained for the two different techniques, suggesting reliable data. Table 4.5 show a summary of the CMC level obtained for all the polymers along with their respective hydrodynamic diameters as obtained by DLS. The results showed that all the HPG polymers have higher CMC level than star copolymers because the lack of hydrophobic segment within their structure.

Table 4.5: Summary of CMC levels obtained for polymers and their diameter at the CMC level

Polymers	Fluorescence $\mu\text{g/mL}$	Hydrodynamic diameter nm
S-THPP ₁ -PCL ₄₀ -HPG ₆₀ 31	70	200
S-THPP-HPG 28	150	90
THPP-HPG	300	50
S-TDHPP ₁ -PCL ₁₀ -HPG ₃₅ 33	200	200
S-TDHPP ₁ -PCL ₃₅ -HPG ₃₅ 33	170	200
S-TDHPP-HPG 29	350	100
TDHPP-HPG	80	60

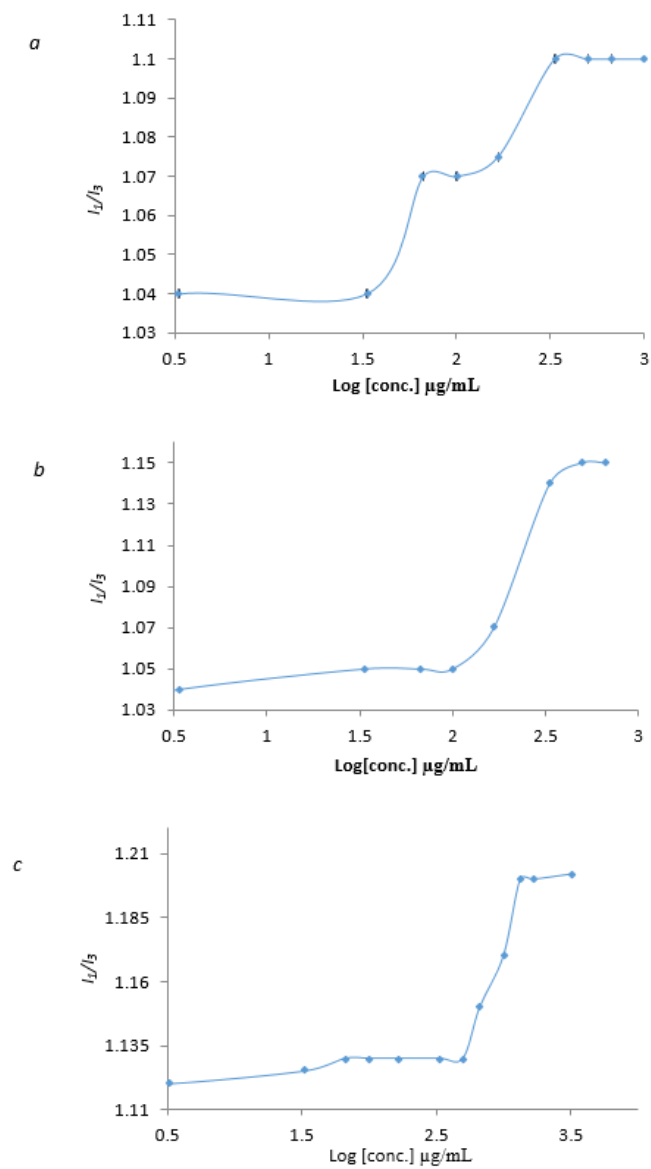


Figure 4.5: Plots of the intensity ratio of I_1/I_3 against log concentration of a) SPPCL-HPG 41, b) S-THPP-HPG 31 and c) THPP-HPG in deionised water.

4.7 In vitro study (cytotoxicity and phototoxicity)

Having successfully synthesised and characterised porphyrin star copolymers and control polymers, the cell viability, including cytotoxicity and phototoxicity, was evaluated in human breast adenocarcinoma MCF-7 and EJ bladder cells.

4.8 Cell work using MCF-7

The human cancer cell line MCF-7 was maintained in tissue culture in a Petri dish at 37 °C in a 5% CO₂ atmosphere in a biosafety cabinet. Compounds that were considered for the PDT first were: S-THPP1-PCL40-HPG60 **31** and S-TDHPP1-PCL10-HPG35 **33**. For effective PDT, a low concentration of the PSs and a low dose of light are desirable. Concentrations were calculated with respect to the porphyrin using Beer–Lambert analysis. Therefore, concentrations started at 150 μM for compound **31** and 140 μM for compound **33** in terms of porphyrin concentrations. For the phototoxicity studies, two light doses were used: 5 and 10 mW cm⁻².

As discussed in the introduction, the ideal PS should not harm healthy cells (when not exposed to light). Therefore, the cells treated with the PSs at their highest concentration should exhibit complete death when exposed to the specific light. As desired, both compounds exhibited little dark toxicity (cell viability > 90%) at their highest concentrations. However, phototoxicity was not as expected: 60% of cells were still viable at a high concentration of compound **31** whereas the other compounds had at least 80% viability at their highest concentration, see figure 4.6.

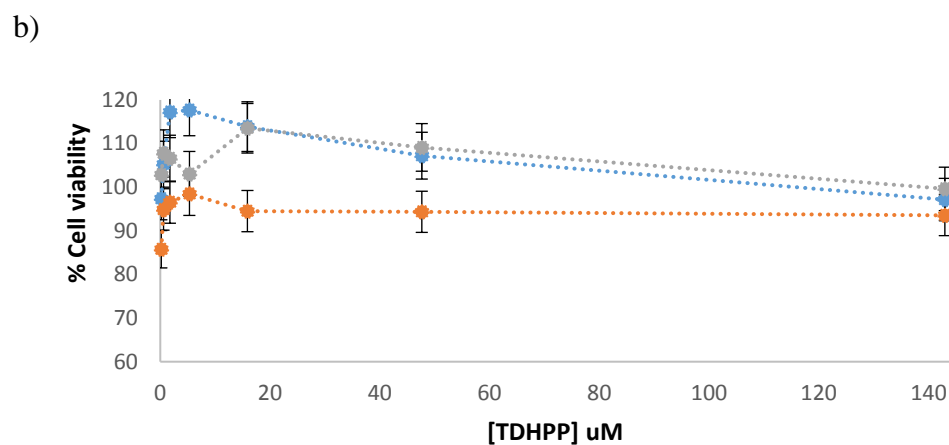
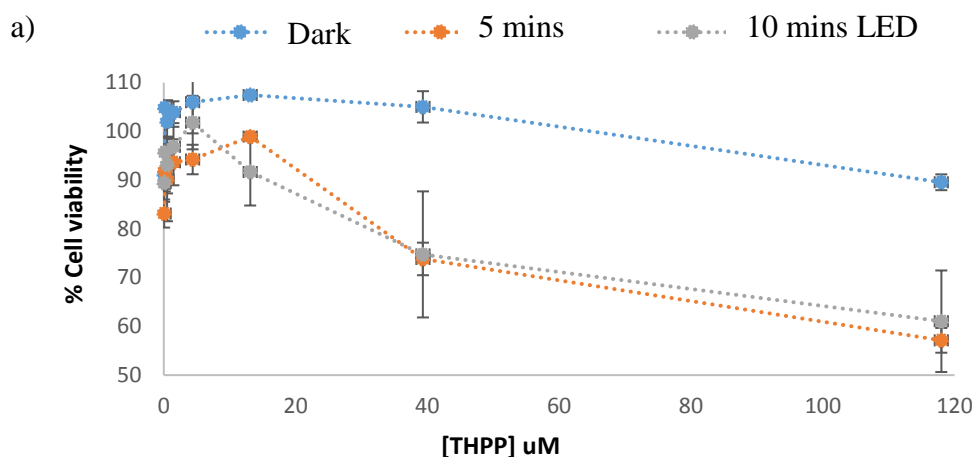


Figure 4.6: % Cell viability of the phototoxicity SRB assay of MCF-7 cells treated with different concentrations of a) compound **41** and b) compound **33** at different LED doses of zero (dark), 5 minutes LED (0.84 J/cm^2) and 10 minutes LED (1.65 J/cm^2).

One reason for the poor phototoxicity is that the PS did not absorb the light and failed to produce ROP; this could be due to the media. Therefore, the experiment was repeated without media prior to light treatment. However, removing the media from the cells for a short period (5 or 10 minutes) may affect the growth of the cells so a control experiment was carried out to determine whether removing the media from the non-treated cells (10 minutes) affects the cell growth. The results obtained from this control experiment indicated that removing the media do not affect cell growth (Figure 4.7).

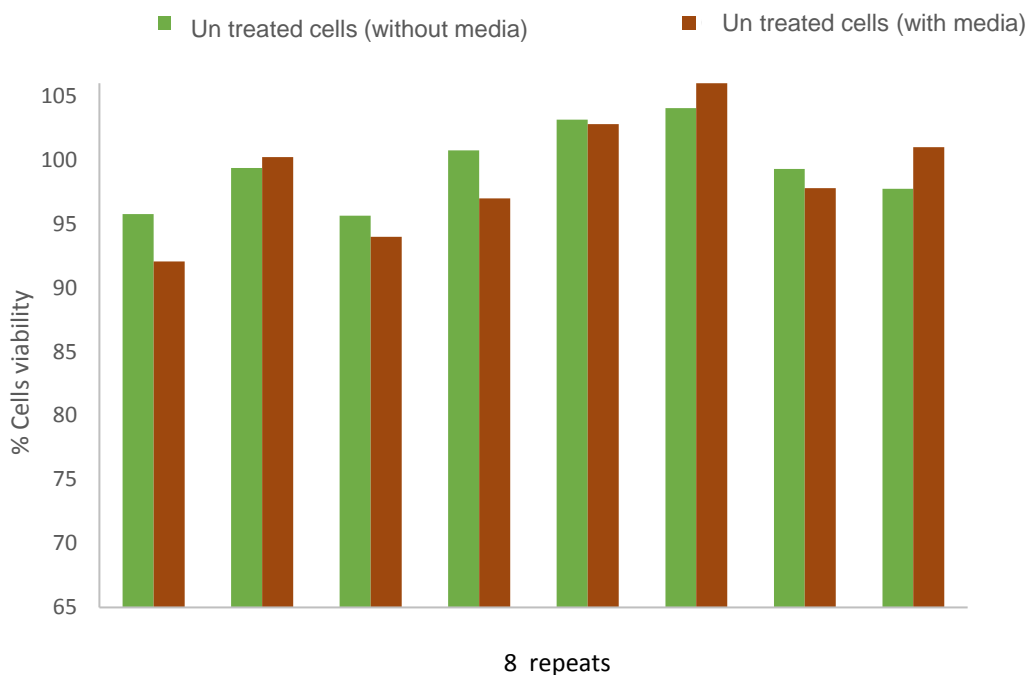


Figure 4.7: % Cell viability of the dark toxicity SRB for of MCF-7 cells with and without removal of the media for 10 minutes

The dark toxicity of the compounds was studied again at different concentrations. The results showed that all the compounds are considered safe (Figure 4.8). Without any light irradiation, the toxicity of compound **31** and compound **33** at high concentrations (900 and 400 μM , respectively) was negligible; the overall cell viability was higher than 80%.

The phototoxicity was then studied at two different light doses (5 minutes LED and 10 minutes LED) for both compounds. The results for the 10 min LED light dose (Figure 4.9) show significant phototoxicity (LD_{50}) for compound **31** and compound **33** at 14 and 50 μM , respectively. However, the phototoxicity of these concentrations was poor with 5 minutes of LED treatment.

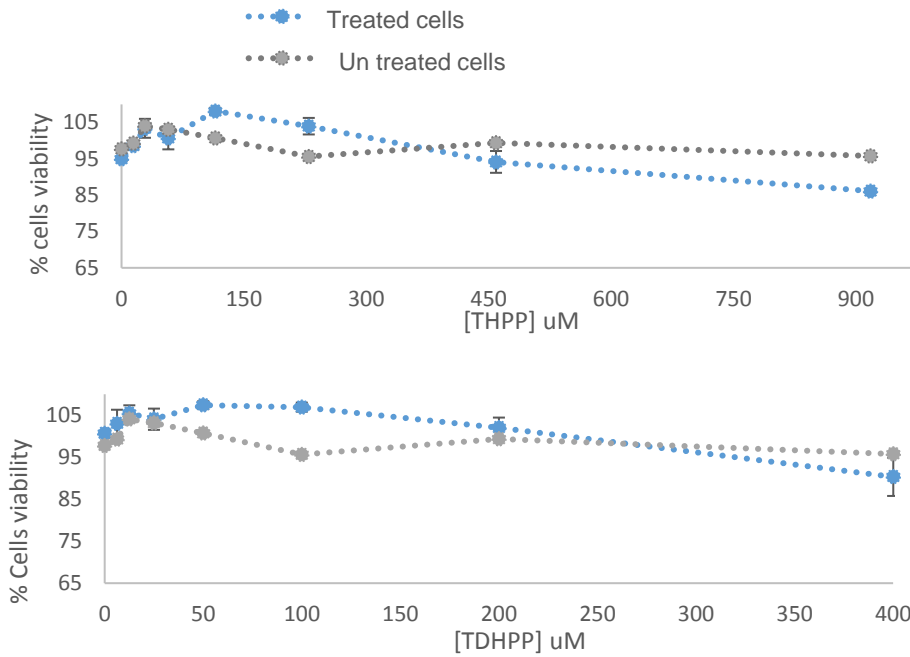


Figure 4.8: % Cell viability of the dark toxicity SRB assay of MCF-7 cells treated with different concentrations of a) compound **31** and b) compound **33**

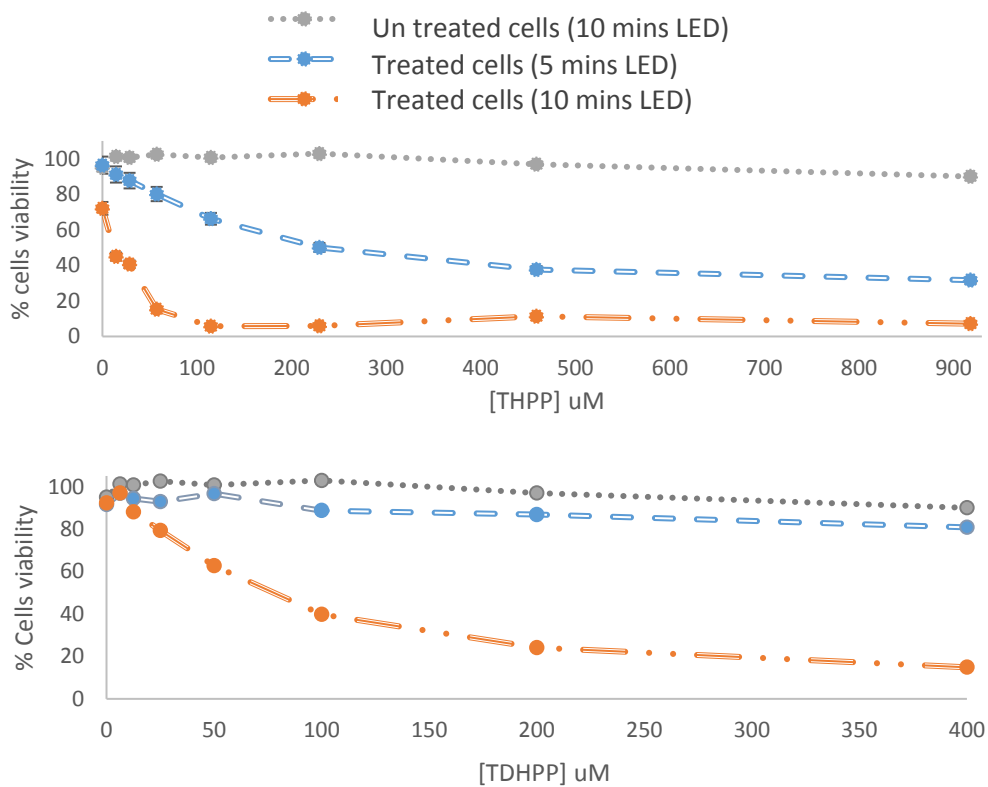


Figure 4.9: Phototoxicity of MCF-7 cells treated with different concentrations of a) compound **31** and b) Compound **33**

4.9 MTT assay using EJ cell lines

Initially, compounds were divided into two groups based on the core used; Table 3.5 provides details of the labelling used. THPP **12** and TDHPP **13** were labelled as *th* and *td*, respectively, the polymers cored with THPP were labelled with odd italic numbers while polymers cored with TDHPP were labelled with even italic numbers, as shown in Table 4.6.

Table 4.6: Compounds labelling

THPP-set	THPP (<i>th</i>)	THPP-HPG (<i>1</i>)	S-THPP-HPG 28 (<i>3</i>)	S-THPP-PCL ₄₀ -HPG ₆₀ 31 (<i>5</i>)
TDHPP-set	TDHPP (<i>td</i>)	TDHPP-HPG (<i>2</i>)	S-TDHPP-HPG 29 (<i>4</i>)	S-TDHPP-PCL ₁₀ -HPG ₃₅ 31 (<i>6</i>)

The dark toxicity of each set was initially studied by MTT assay (a colorimetric assay that assesses cellular metabolic activity) and a bladder cell line (EJ). From the graph shown in Figure 4.11, it clear that THPP and THPP-HPG have significant dark toxicity. Interestingly, the toxicity is markedly decreased if a spacer (S-THPP-HPG) or a polymer (S-THPP-PCL₄₀-HPG₆₀ **31**) is added between the porphyrin and the hyperbranched polyglycerol HPG.

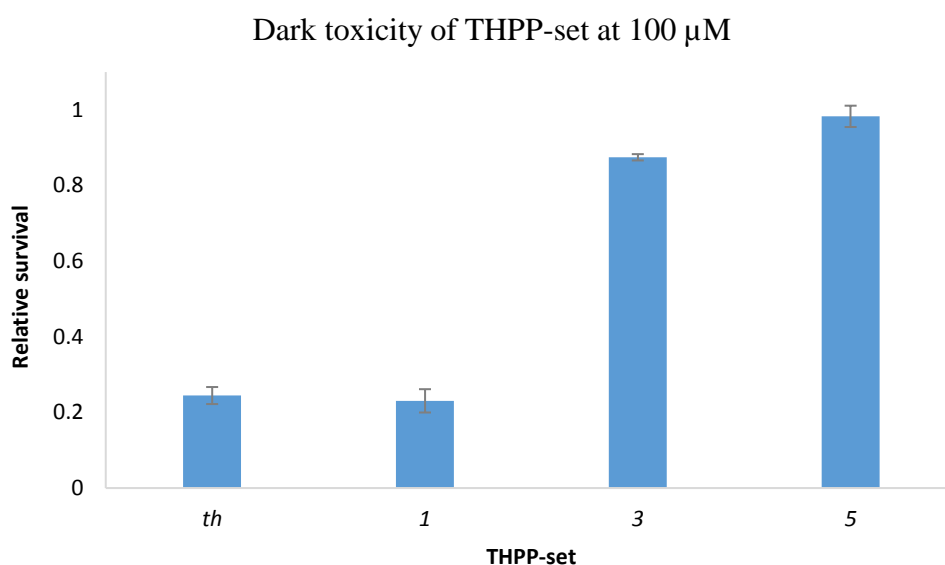


Figure 4.10: Graph showing the dark toxicity of the THPP-set compounds in EJ cells at 100 μ M

The dark toxicity of the THPP was further investigated over a range of concentrations (0.1–100 μM). The results showed that THPP killed around 70% of the cells at concentrations higher than 10 μM , as shown in Figure 4.11.

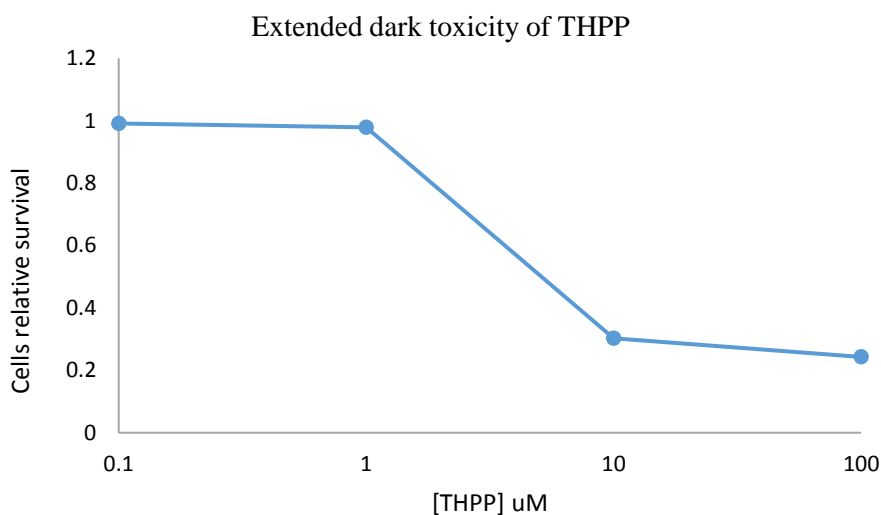


Figure 4.11: Dark toxicity of THPP at different concentrations in EJ cell line

In contrast, none of the molecules possessing the porphyrin with eight hydroxyl groups (TDHPP) exhibited any dark toxicity at 100 μM , figure 4.12. Comparing these results to those reported in the literature, THPP had a D_{37} (dark toxicity where 37 refers to the dose required to reduce cell survival to 37%) of 0.3 μM using a human tumour cell line (HeLa) whereas TDHPP had a C_{37} of 15 μM .^[83]

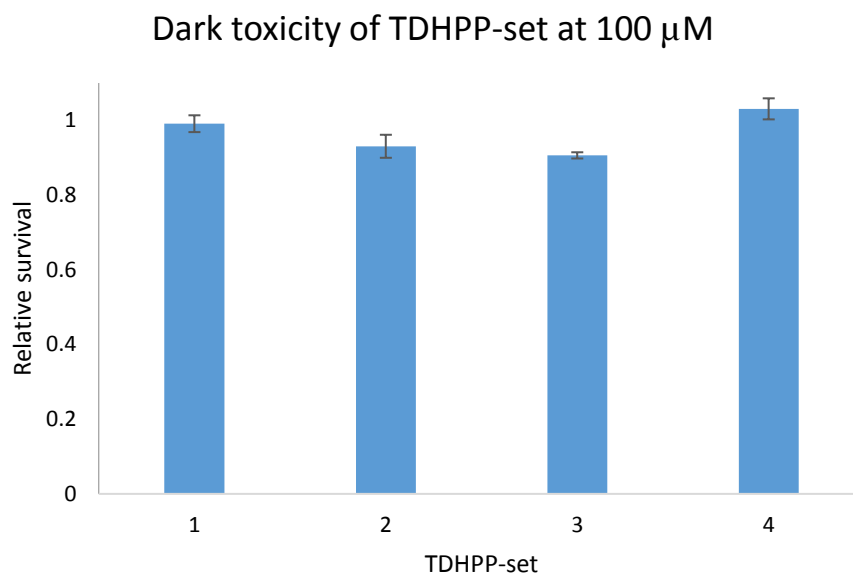


Figure 4.12: Dark toxicity of TDHPP molecule and TDHPP-cored polymer at 100 μM

For use in PDT, the phototoxicity of both sets was studied at various concentrations (TH-set: 0.1–10 μM , TD-set: 0.1–100 μM). It was decided to study the light toxicity of the TH-set at low concentrations (0.1–10 μM) because it has dark toxicity at very low concentrations. The results revealed that compounds 1 and 3 have a light toxicity LD₅₀ (dose required to reduce cell survival to 50%) of 1 μM and 5 μM , respectively, figure 4.13. Both compounds killed the cells completely at 10 μM . In contrast, compound 5 exhibited little light toxicity at 10 μM and a higher concentration might be effective for PDT.

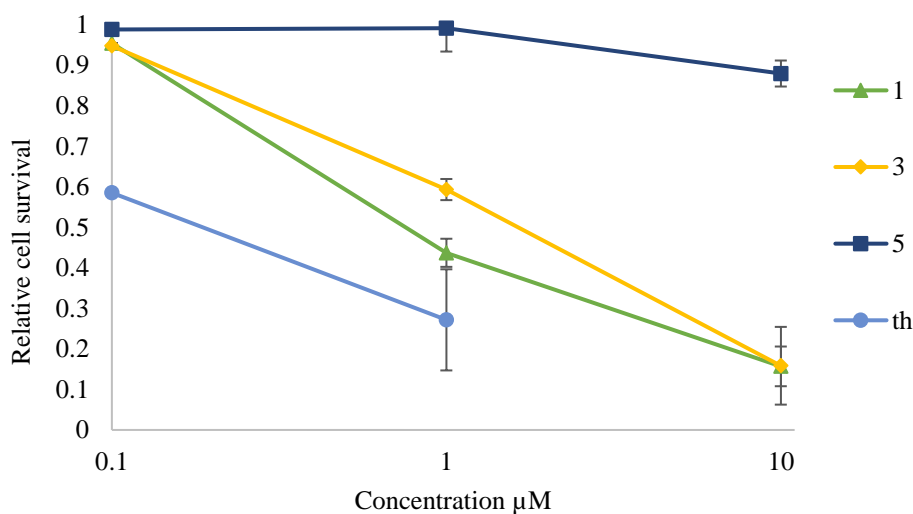


Figure 4.13: Phototoxicity of THPP-set compounds using EJ cell line at a light dose of 10 mW/cm^2

However, the TD-set showed no significant phototoxicity at 10 μM . The only exception was the control (TDHPP), which had an LD₅₀ of 8.5 μM , as shown in Figure 3.14. With increasing concentration, recorded LD₅₀ values were concentration of 40 μM and 100 μM for S-TDHPP-HPG and TDHPP-HPG, respectively.

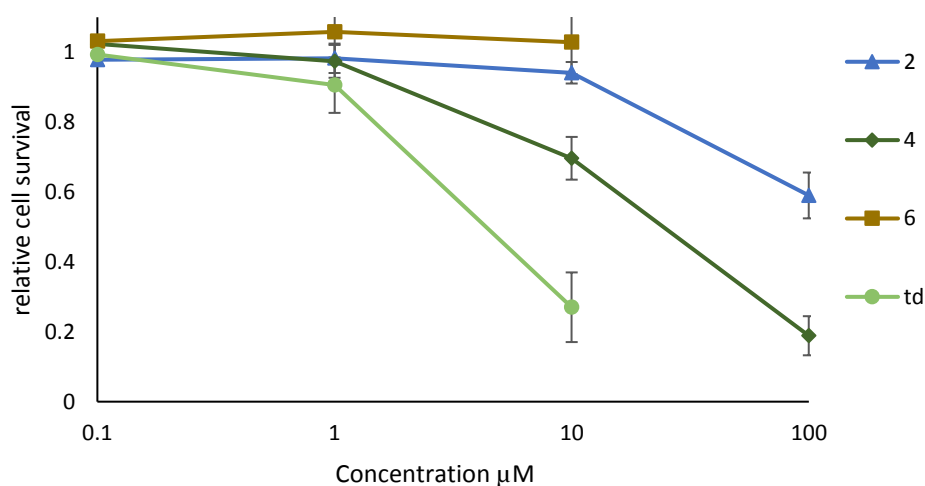


Figure 4.14: Phototoxicity of TDHPP-set compounds using EJ cell line at a light dose of 10 mW/cm²

4.9.1 Intracellular localisation

The intracellular localisation of the molecules (THPP-set and TDHPP-set) into EJ (bladder carcinoma) cells was imaged by confocal microscopy, table 3.5 and 3.6. Both THPP and TDHPP molecules (naked porphyrin) diffused within the cell. Porphyrin-HPGs (compounds 1, 2, 3 and 4) also diffused within the cells but as the spacer was added the diffused fluorescence decreases. The porphyrin-PCL-HPGs star copolymers (compounds 5 and 6) showed no diffusion into the cells at 10 μM . Higher concentration of the star copolymers is required for the diffusion to occur and due to funding problem this could not be investigated further.

Table 4.7: Table to show the confocal images for naked porphyrin (THPP (*th*)), compound 1 (THPP-HPG), Compound 3 (S-THPP-HPG **33**) and compound 5 (SPPCL₄₀-HPG₆₀ **41**)

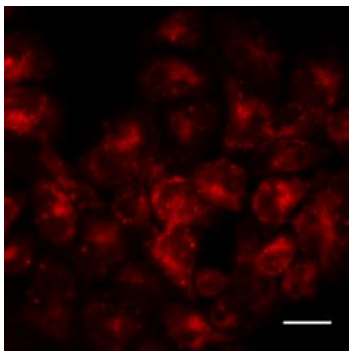
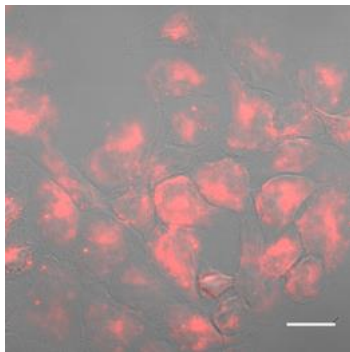
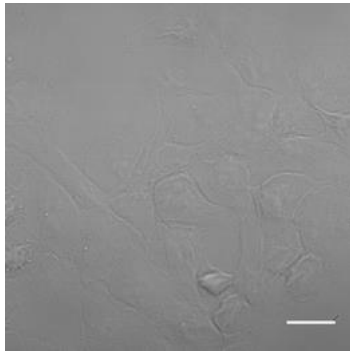
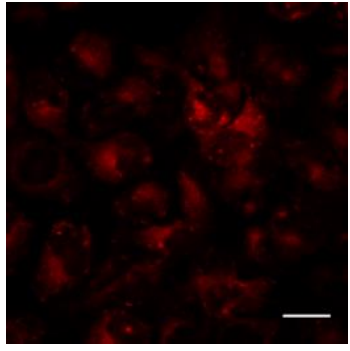
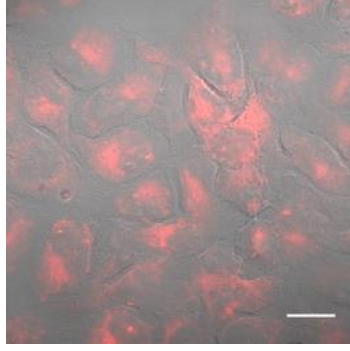
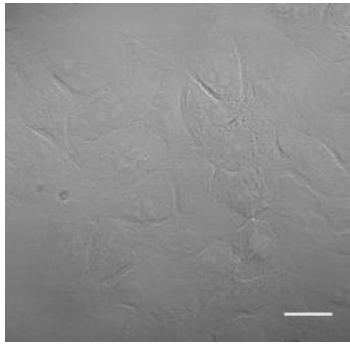
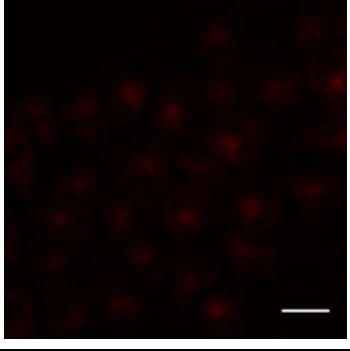
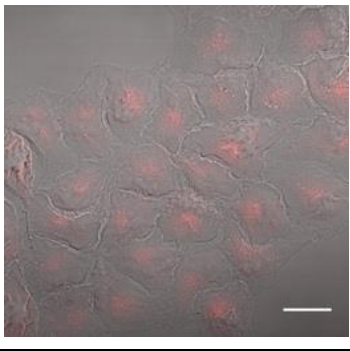
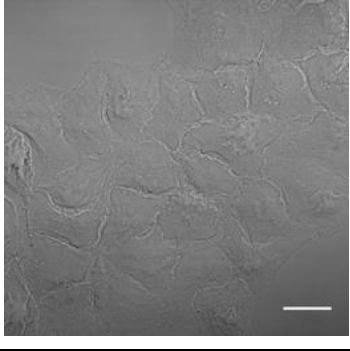
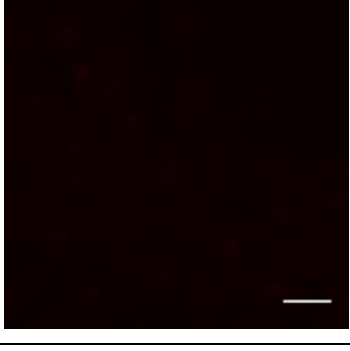
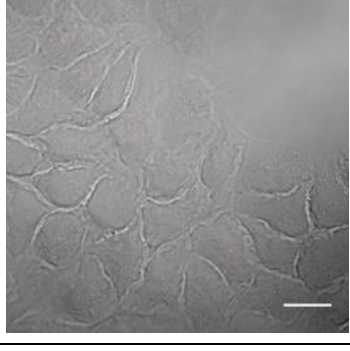
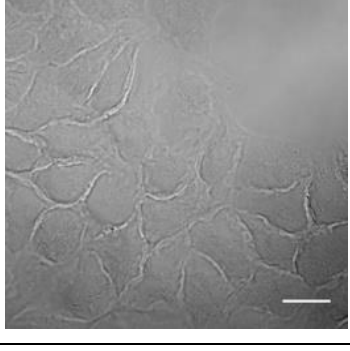
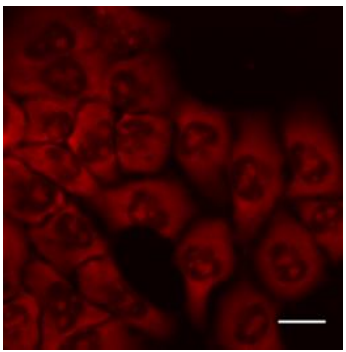
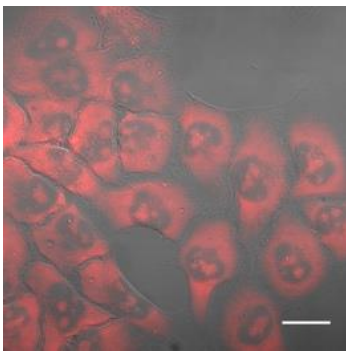
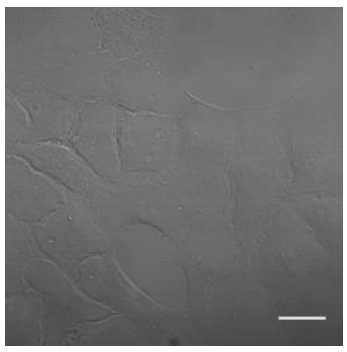
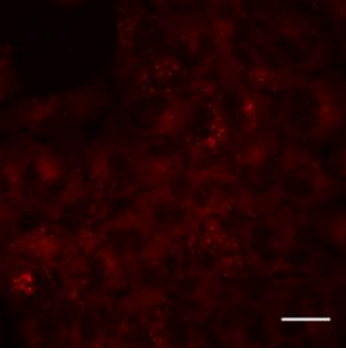
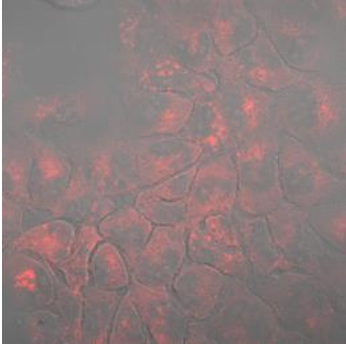
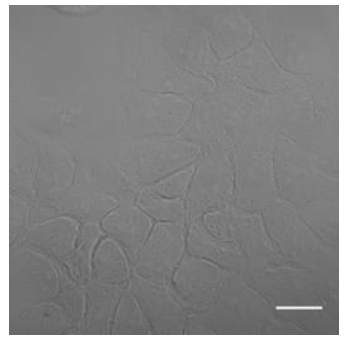
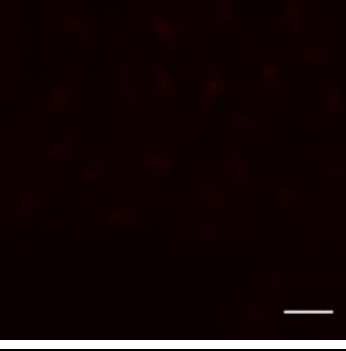
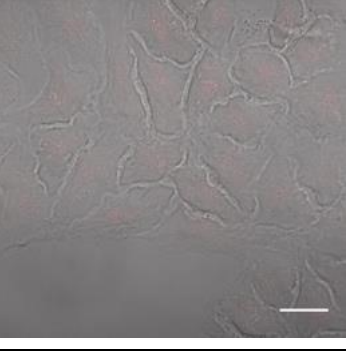
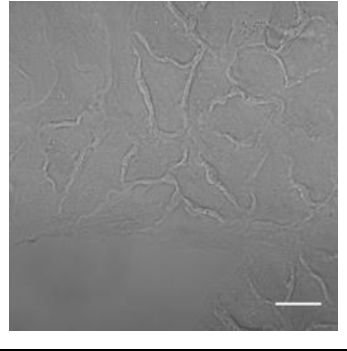
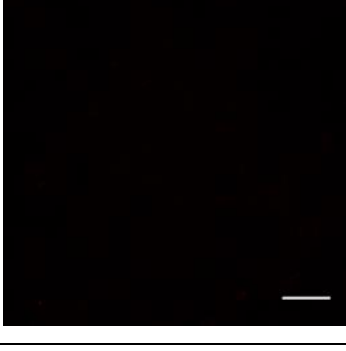
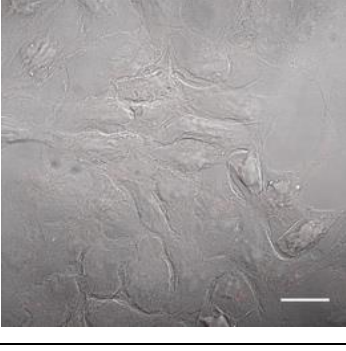
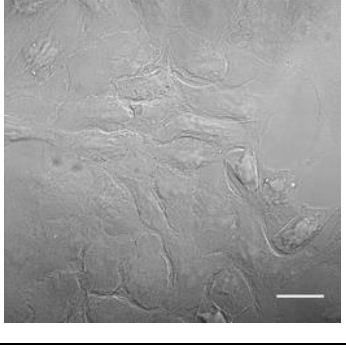
	red	overlay	bright
<i>th</i>			
<i>1</i>			
<i>3</i>			
<i>5</i>			

Table 4.8: Table to show the confocal images for naked porphyrin (TDHPP (td)), compound 2 (TDHPP-HPG), Compound 4 (S-TDHPP-HPG **34**) and compound 5 (SPPCL₁₀-HPG₃₅ **43**)

	red	overlay	bright
td			
2			
4			
6			

4.10 Summary

In this chapter, star copolymers based on polycaprolactone and polyglycidol with porphyrin core were synthesised successfully for photodynamic therapy (PDT) application. Thus, the solubility of porphyrins in aqueous solution was enhanced significantly via covalent incorporation within aggregated water-soluble polymers. Two porphyrin molecules with hydroxyl end group were selected as a core these are: tetrakis(3,5-dihydroxyphenyl) porphyrin (TDHPP), and tetrakis(4-(hydroxyphenyl)porphyrin (THPP). However, the reactivity of TDHPP and THPP was not good for the ring opening polymerization of caprolactone until a spacer was added. Thus, two star copolymers were synthesised from spacer-porphyrin (S-THPP-PCL-HPG) and S-TDHPP-PCL-HPG). The control (porphyrin-HPG) were synthesised from porphyrins with and without spacer units. The particle size of all the aggregated polymers was then determined via DLS and found to be between 100-200 nm. The cytotoxicity and phototoxicity of the star copolymers (compound **31** and **33**) were tested initially via SRB assay using MCF-7 cell line. The result showed that both of the polymers, compound **31** and **33**, exhibited negligible toxicity at concentration of 400 and 900 μM . The phototoxicity of these compounds were obvious at 14 and 50 μM , respectively. The cytotoxicity and phototoxicity of all the porphyrin cored polymers were investigated further for their PDT behaviour via a simple MTT assay, using the EJ (bladder carcinoma) cancer cell line. The relative viability of the polymers and its controls in the dark were higher than 0.8 at 100 μM except the THPP-HPG polymer which had a viability 0.2. Under light irradiation (10 mW/cm^2), significant toxicity was observed at 1 μM for the free THPP and at 10 μM for the free TDHPP porphyrin. While phototoxicity of the polymers, considerable cell death was obvious at polymers concentration of 10 μM for the THPP cored polymers except the star copolymer, which did not show any significant toxicity at this concentration. The phototoxicity of TDHPP cored polymers were significant for TDHPP-HPG and S-TDHPP-HPG at 100 μM for and poor for the star copolymer

at same concentration. The intracellular localisation of the molecules porphyrin cored polymers into EJ cells was imaged by confocal microscopy. Both of the free porphyrin (THPP and TDHPP) molecules diffused within the cell at a concentration of 10 μ M. Porphyrin cored HPG polymers also diffused within the cells but as the spacer was added the diffused fluorescence decreases. The porphyrin-PCL-HPGs star copolymers showed no diffusion into the cells. Thus, porphyrin-cored HPG polymers were deemed to be promising photosensitizers for photodynamic therapy (PDT) rather than the star copolymers. Other photosensitizers (such as phthalocyanine and chlorine) could be functionalised with nucleophilic end group and used as core for ROP of glycidol for effective PDT. These compounds as effective photosensitizer could then be investigated further using different cell lines and assay. *In vivo* study would be needed to confirm the compounds effectiveness in PDT.



Chapter 5

Dual Chemo-photodynamic therapy



5.0 Chemo-Photodynamic Combination Therapy

Paclitaxel (PTX) is an anti-microtubule agent extracted from the trunk bark of the Pacific Yew tree, considered as one of the most effective chemotherapeutic drugs ever developed used against a variety of human cancers, such as ovarian, lung, and breast cancers. The active mechanism of PTX is to encourage and stabilise microtubule polymer and blocks cells in G2/M phases of the cell cycle and hence cause cell death. However, the major drawback of PXT is its low water solubility ($\sim 0.46 \mu\text{M}$). Therefore, it is formulated in a mixture of polyoxyethylated castor oil (Cremophor EL) and dehydrated ethanol (50/50, v/v) under the trademark "Taxol". However, Taxol has serious side effects, such as hypersensitivity reactions related to Cremophor EL [2]. Therefore, there is an urgent need for an alternative formulation of PTX that offers a prolonged infusion time, pre-treatments, and which has minimum or no side effects.

Biodegradable and non-toxic nano-delivery systems are promising vehicles in drug delivery because they can protect the drug from degradation during circulation and, in turn, lower the drug toxicity, exhibiting improved pharmacokinetic profiles, and providing better patient compliance. Secondly, nanoparticle-based delivery systems enable preferential delivery of PTX into the target site due to the enhanced permeability and retention (EPR) effect.

In this study, the targeted drug delivery systems porphyrin cored hyperbranched polymers and porphyrin cored star copolymers, are used to enhance the solubility of the hydrophobic drug PTX via hydrophobic interaction. Therefore, the potential of the porphyrin-delivery systems for the synergistic combination of PDT and chemotherapy for cancer treatments is investigated. PTX has a distinct absorbance band at 230 nm attributed to the three benzene rings within its structure (Figure 5.1) which is observed by UV/vis spectroscopic techniques using different organic solvents such as DCM, acetone, DMSO, and others. Therefore, UV/Vis spectroscopy

was chosen to quantify the amount of the loaded PTX and hence the molar extension coefficient of PTX.

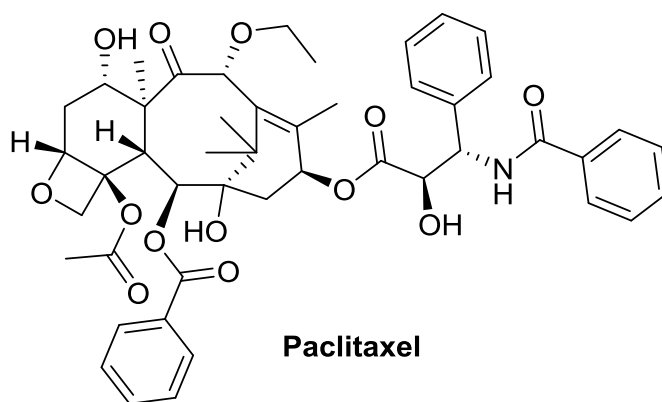


Figure 5.1: The Chemical structure of paclitaxel

PTX is insoluble in PBS 7.4 but is readily soluble in methanol, hence a combination was used containing methanol and PBS in a 3:7 ratio. PTX showed a very good linear response with absorbance and concentration over the rang of 0-20 $\mu\text{g/ml}$ (Table 5.1).

Table 5.1: Characterisation of PTX in MeOH: PBS (3:7)

Parameters	PTX
λ_{max} (nm)	230
<i>Lambert-Beer's law range</i> ($\mu\text{g/mL}$)	0-20
<i>Correlation coefficient</i> (R^2)	0.997
<i>Equation of line</i>	$29749x + 0.0069$ (M)

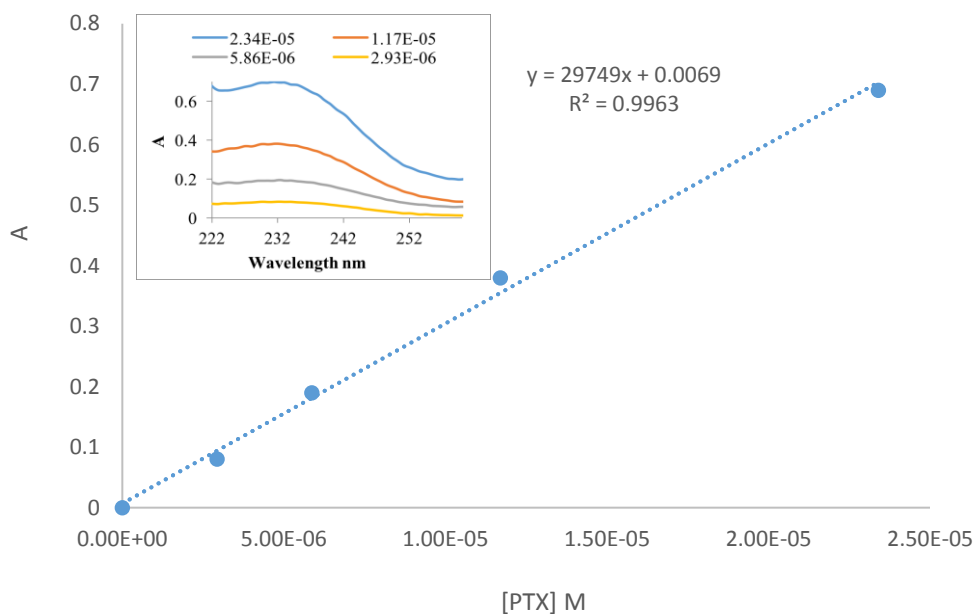


Figure 5.2: Beer Lambert Plot of PTX in MeOH: PBS (3:7)

5.1 Kinetic/Thermodynamic Solubility of PTX in water

Solubility is a key parameter in pharmaceutical research and development and is related to pharmacokinetics, pharmacodynamics, and toxicodynamics. PTX is composed of several hydrophobic substituents, which make it a highly lipophilic compound with an aqueous solubility of less than 0.01 mg/mL (11.7 μ M).^[13–15]

In this part of the study, the water solubility of PTX was determined using different approaches: solid PTX dissolved directly in water (method *a*), and solid PTX dissolved in organic solvent (method *b*), in which upon solvent evaporation water is added. While the Kinetic Solubility of PTX was determined by dissolving PTX in 100% DMSO and, from that, 1% of DMSO solution was extracted.

In both cases, the aqueous solubility of PTX was determined by UV/vis after filtration with a 0.2 μ m syringe filter to remove the insoluble PTX. The results obtained for the water solubility of PTX using different approaches are summarized in Table 5.3. The water solubility of PTX by the thermodynamic method *a* and kinetic approach was very low and with good agreement

to the literature value. In contrast, the PTX aqueous solubility obtained by the thermodynamic method *b* was higher than the literature ranges. ^[13-15] Initially, it was thought that the higher solubility could be explained as the PTX lattice is broken completely in methanol and upon solvent evaporation, PTX forms a new allotrope that is more easily dissolved in water. Therefore, the encapsulation of PTX in the polymeric micelles was studied using the solvent evaporation method (thermodynamic-b) where both the polymer and PTX were dissolved in methanol and upon removing the solvent the crude complex was dissolved in water. This technique was preferred and continued to be used to ensure higher encapsulation efficiency based on the positive result obtained for the aqueous solubility of free PTX.

Table 5.2: Thermodynamic and Kinetic Solubility of PTX in water

Method		Absorption	Wavelength nm	[PTX] μ M
Thermodynamic	<i>a</i>	0.20	230	6.7
	<i>b</i>	0.75	230	25.2
Kinetic 1% DMSO		0.1	237	3.34

5.2 Encapsulation of PTX in the polymeric micelles

As discussed earlier in this chapter, the main aim of this study is to enhance the aqueous solubility of paclitaxel (PTX) within the self-assembled polymer structures. If successful, the system can then be studied as dual chemo and photodynamic anticancer therapy.

It is expected that higher PTX loading will happen when there is enough hydrophobic space within the aggregated structures of each polymer; in other words, the loading capacity of PTX in each aggregated polymer is dependent on the space of their hydrophobic domain. Therefore,

the star copolymers are expected to aggregate at a higher loading of PTX when compared with the simpler HPGs.

There are different methods commonly used for physical drug encapsulation in polymeric micelles such as dialysis, oil-water emulsion, and solvent evaporation, among others. In this study, the solvent evaporation method was used to evaluate the encapsulation of PTX within the polymeric micelles. The encapsulation procedure involved the dissolution of both the polymeric micelle and a large molar excess of the PTX in methanol. The two solutions were combined, and the solvent evaporated, resulting in a polymer-PTX co-precipitate. Water was added to the co-precipitate, to mimic physiological conditions, and the solution was filtered to remove any excess PTX loaded by the polymer by UV/Vis spectroscopy.

5.3 Encapsulation results

To be able to quantify the improvement in solubility of PTX when complexed to the polymeric micelles, it was important to record the UV/vis spectrum of the maximum concentration of PTX used for the encapsulation studies in water, without polymer present. From the absorbance at 230nm of PTX-loaded micelles, the concentration of the PTX loaded by each polymer was calculated using Beer-Lambert analysis and was compared to the maximum concentration of PTX determined for water (e.g. with no polymer present). The results showed that there was a slight increase in the solubility of PTX when encapsulated with different polymers, Table 5.4. The concentration of PTX loaded in the micelles of the star copolymers was slightly higher than its respective hyperbranched polymer as shown in Table 5.5. In addition, there was no noticeable difference in terms of increasing the solubility of PTX, between star copolymers and HPG polymers. Since the potency of PTX toward carcinoma cells is effective at a very low

concentration (in nM), the complexes (PTX loaded in polymer) were taken forward for toxicity studies.

Table 5.3: Encapsulation result of PTX with star copolymers and HPGs

PTX	[PTX] loaded in micelle μM
S-TDHPP-HPG	40
S-TDHPP-PCL ₁₀ -HPG ₃₅	43
S-THPP-HPG	50
S-THPP-PCL ₄₀ -HPG ₆₀	60
[PTX] in water: 25 μM Polymer concentration: 0.5 mg/mL PTX concentration used for encapsulation: 70.5 μM	

5.4 In vitro study

5.4.1 Control experiment to determine PTX toxicity to bladder cell line

The cytotoxicity measurements were carried out by MTT assay in a bladder cell line (EJ) to evaluate the pharmacological efficiency of PTX and its nano-formulation. After 24 hours for the 24 nM and higher concentrations of PTX, the cell viability was less than 0.1%. After 48 and 72 hours, cell viability was 0% for PTX concentration above 24 nM. This result confirms that PTX has a very high pharmacological potency. As such, only very low concentrations of PTX are needed for the micelle-encapsulated study.

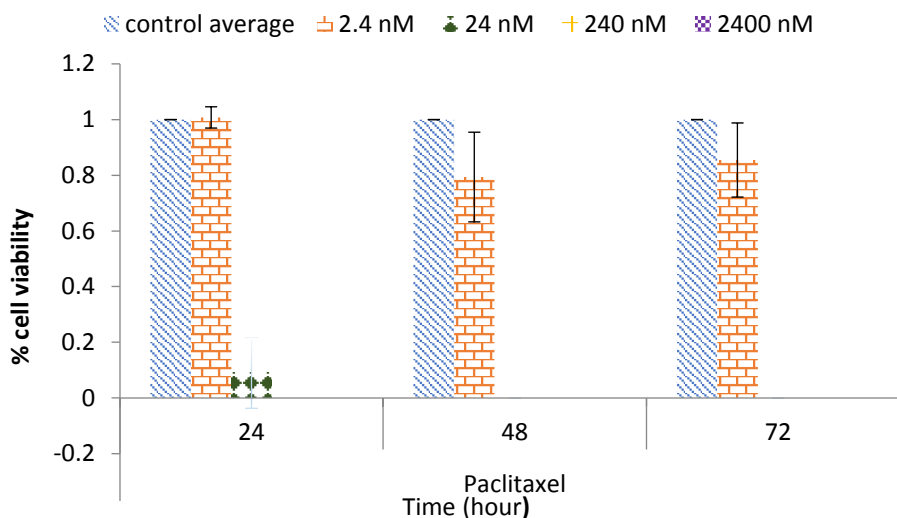


Figure 5.3: PTX toxicity to bladder cell line at different incubation times.

5.4.2 Polymer toxicity to bladder cell line

Initially, the star copolymer (*S*-THPP₁-PCL₄₀-HPG₆₀ **31**) was chosen to evaluate the polymer cytotoxicity in MTT assay using the bladder cell line. Different concentrations of the polymer, ranging from 2.4 to 2400 nM, were used but were shown not to be toxic (Figure 5.5).

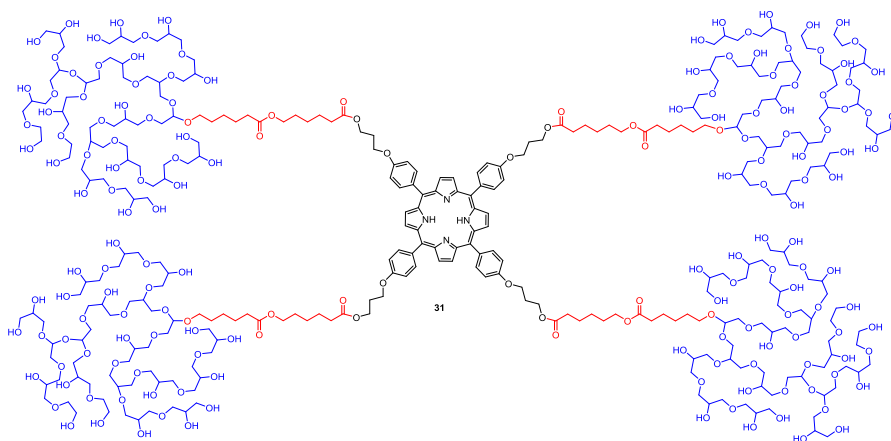


Figure 5.4: Structure of *S*-THPP₁-PCL₄₀-HPG₆₀ **31**

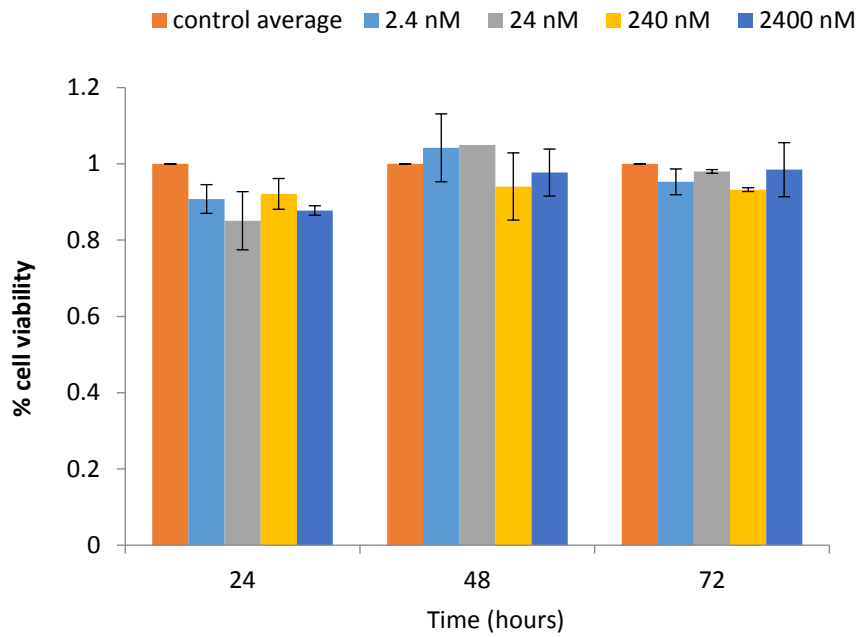


Figure 5.5: Toxicity of different concentrations of the star copolymer to bladder cell line (No PTX encapsulation)

Unfortunately, the cytotoxicity measurement of PTX-loaded star copolymers revealed no toxicity to the bladder cell line, indicating the PTX loaded in the micelle does not have potential to inhibit the cells anymore.

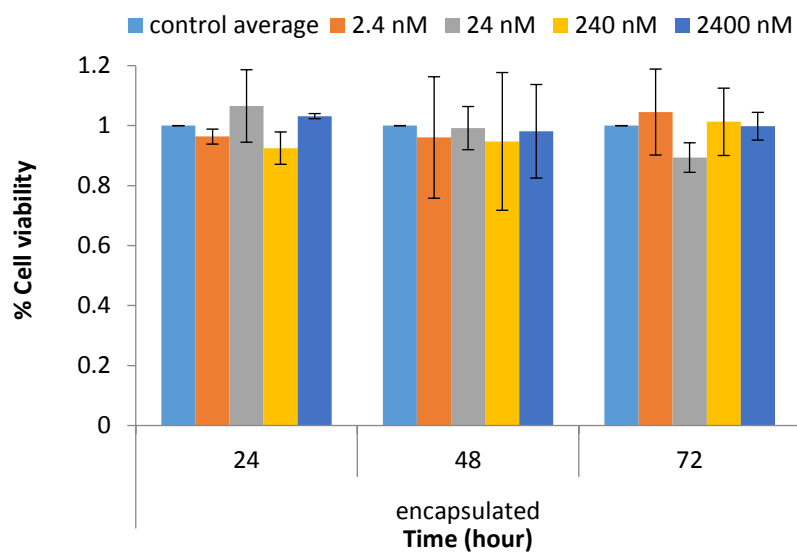


Figure 5.6: Cytotoxicity of PTX encapsulated with star copolymer

The main reason as to why the PTX-loaded-polymeric systems did not show any toxicity could be either of the following; the release of PTX from the micelle is either very slow or it is not happening at all, or the PTX might have reacted with the polymer or with the solvent during encapsulation process, resulting in a loss of formation to its structure and subsequent loss of its pharmacological potency.

To determine which effect was the cause, the release behaviour of PTX loaded in micelle was studied using two different buffer solutions (PH 7.4 and PH 5.0) at 37 °C. A relatively rapid release rate was observed using UV/vis spectroscopy (following the signal at 230 nm) after 24 hours. Although this experiment confirmed that the PTX was not trapped in the micelle, it does not prove that the structure of the PTX had not been changed (it only confirmed that aromatic rings were present) and hence the first reason is not valid.

The PTX exhibited a lot of weak electrophile sites (indicated with red arrows in Figure 5.7), which could be attacked easily with mild nucleophilic molecules. If this was the case, the PTX structure would be changed and could be the reason why the toxicity of PTX-loaded-polymer had been lost.

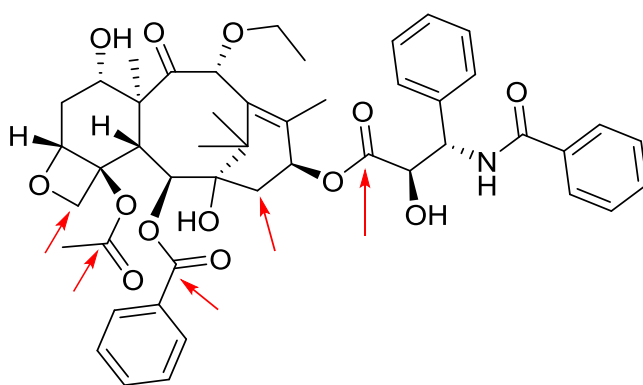


Figure 5.7: Structure of PTX indicating the electrophilic sites

The nucleophilic attack could happen via one of two possibilities; PTX could react with the OH groups of the polymers, or with the methanol used to encapsulate the drug within the polymer.

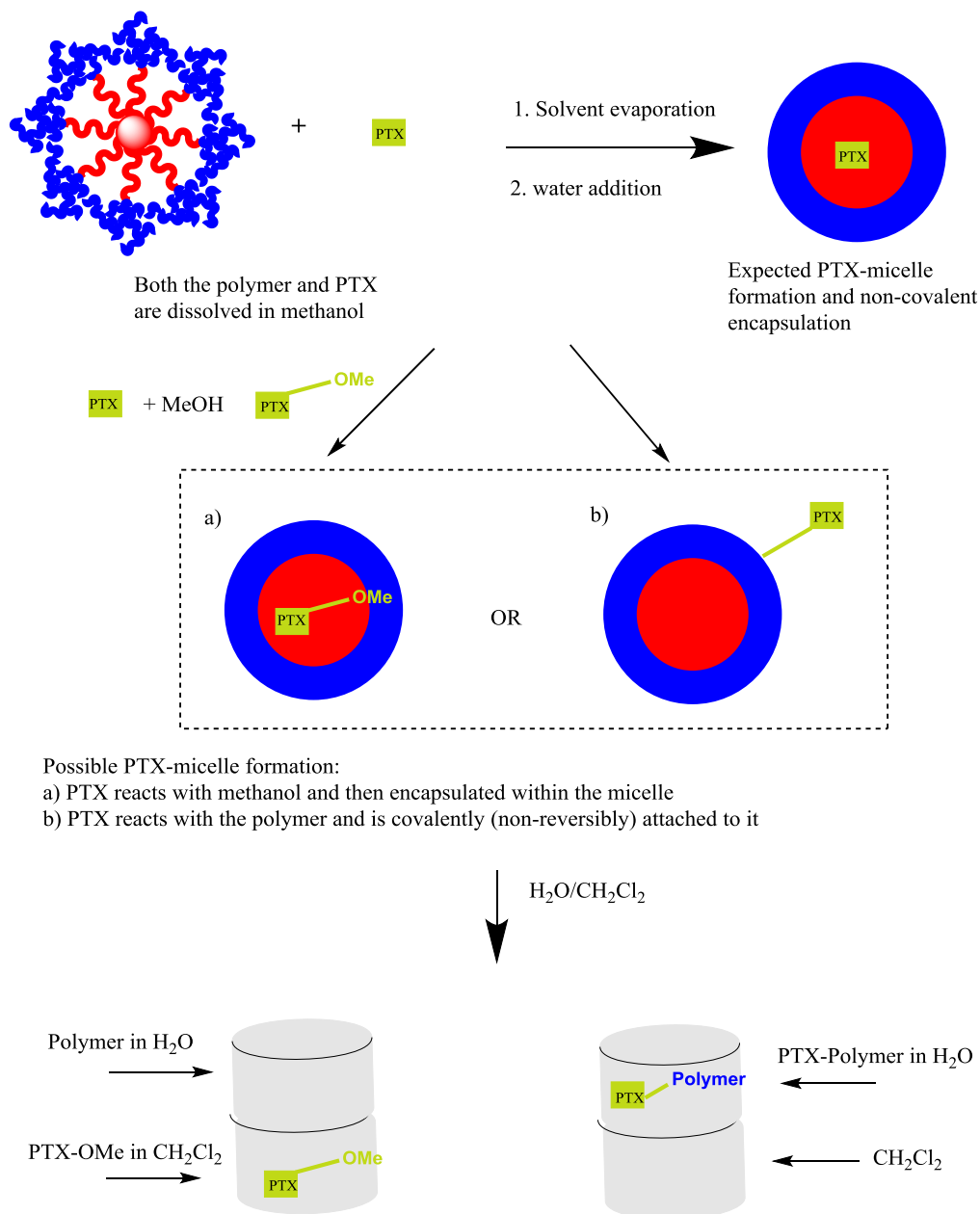


Figure 5.8: Possible PTX-micelle formation

Although the quantification of the PTX loaded in micelles was calculated using UV/Vis, this technique was not useful in determining the degradation of PTX. The reason could be because the degradation of PTX occurs in the non-UV/vis sensitive sites which will not change the λ_{max}

of PTX at 230 nm. However, this technique can be useful to validate one of the possibilities, that PTX had reacted with the micelle, by recording the UV/vis spectra of the extracted organic layer from the PTX-loaded micelle. Interestingly, the UV/vis spectra of the extracted organic layer confirmed the presence of aromatic resonances via the observation of an absorption maximum at 230 nm, indicating that the PTX was extracted in the organic layer.

Another possibility that would explain this is that the PTX had reacted with the methanol during the encapsulation process and was extracted. In an attempt to prove this, a mass spectrum of the extracted PTX from the micelle was measured. The resulting spectra did not show the m/z peak for PTX at 877($M^+ Na^+$) but showed a molecular ion peak at 609 m/z instead. Also, there were some fragments below 609 m/z. Although the structure was unidentified, the results suggested that the PTX had degraded during the encapsulation process.

Earlier, the high aqueous solubility of PTX using the solvent evaporation method was interpreted as methanol breaking the lattice of PTX and upon evaporation being converted to a more soluble allotrope. However, the true explanation may be due to methanol degradation of PTX, which could increase the polarity of the PTX compound. Therefore, the mass spectrum of PTX in methanol was measured for different reaction times to investigate the decomposition of PTX by the methanol, which can act as a nucleophile to attack any weak electrophile site in the PTX. The m/z obtained for PTX in methanol exhibited peaks for PTX at 875.6 and another peak at 907. These peaks are interpreted as follows:

- $907.7 - 875.6 = 32.1$ which is one methanol molecule attached to the PTX
- $875.6 - 22.9 (Na^+) = 852.7$ which is one proton less of the PTX. A proton loss would happen when a bond is broken by a nucleophile attack which would bond to the PTX.

After leaving the PTX in methanol for a longer period, the mass spectrum showed a peak at 907.7 and nothing observed at 875.6, inducing the covalent attachment of methanol to the PTX.

In addition, the PTX water solubility in methanol that has been stored for a long time was very high. The mass spectrum of PTX in DCM showed a peak at 876, for the PTX plus sodium ion, and another at 892, for the PTX plus potassium ion. This result confirms the fact that solvent which acts as a nucleophile can deform the PTX and reduce its potency as a chemotherapeutic drug.

5.5 Encapsulation of PTX using kinetic method

The solvent evaporation method caused degradation of the PTX. Therefore, PTX was encapsulated within the polymeric micelle using a kinetic encapsulation approach. PTX was dissolved in 100% DMSO to 16.4 mg/mL, then 10 μ L was diluted further into 1 mL DMSO to give a PTX stock solution of concentration 164 μ g/mL. The PTX stock solution was further diluted to give concentrations from 0 to 40 μ M and UV/vis spectroscopy analysis was used to give a Beer-Lambert Plot for PTX. In DMSO, PTX showed very good linearity with absorbance over the concentration range 0-40 μ g/ml (Table 5.2). The absorption maximum (λ_{max}) of PTX in 10% DMSO was observed at 242 nm which is 12 nm higher than the λ_{max} observed for PTX in methanol (Figure 5.3).

Table 5.2: Characterisation of PTX in Water: DMSO	
Parameters	PTX
$\lambda_{max} (nm)$	242
<i>Lambert-Beer's law range (μM)</i>	0.0 - 0.05
<i>Correlation coefficient (R^2)</i>	0.999
<i>Equation of line</i>	20000X + 0.0048

The kinetic encapsulation method was performed as follows: a polymer was dissolved directly in water to make the desired concentration (0.5 μ g/mL), to the polymer solution PTX (DMSO

solution) was added making 0.1% DMSO. The drug loading polymer solution was left stirring for a few hours to ensure the complete encapsulation, and then excess PTX was removed by filtration with a 0.2 μm syringe filter. UV/vis was used to evaluate the loading of PTX by observing the absorption of λ_{max} at 230 nm, using water with 0.1% DMSO as the reference.

Initially, the aqueous solubility of PTX in water using 0.1% DMSO was calculated from its absorbance in the UV/vis spectra and the extinction coefficient determined via Beer-Lambert. Low concentrations of hyperbranched polymers (HPGs) could increase the aqueous solubility of PTX according to their CMCs. The largest HPG, which aggregated at low concentration, increased the solubility of PTX by 429% (Table 5.3), whilst HPGs with Mn ranging from 10-20 K Da encapsulated a similar amount of PTX.

Table 5.3: Summary of PTX loaded in HPG polymers

Polymers 20 μM	Mn Da	CMC $\mu\text{g/mL}$	¹ A	² Corrected encapsulated [PTX] μM	³ % increase of PTX
Water	-	-	0.1	7	0
<i>S-TDHPP-HPG 29</i>	10K	350	0.31	21	200
<i>THPP-HPG</i>	15K	300	0.35	24	243
<i>S-THPP-HPG 28</i>	20K	150	0.34	23	229
<i>TDHPP-HPG</i>	40K	80	0.54	37	429
¹ Absorption of encapsulated PTX, dilution was required to get absorption below 1 ² Corrected concentration was determined by subtracting the concentration of PTX in water from the encapsulated PTX concentration ³ The increase in solubility was calculated					

The encapsulation of PTX within the star copolymer micelles could help determine where in the polymer the PTX is encapsulated. Star copolymers which had hydrophobic segments of

similar size but different sized hydrophilic segments (SPPCL₃₅-HPG₃₅ and SPPCL₄₀-HPG₆₀) were used to encapsulate excess PTX at a polymer concentration of 30 µg/mL. The star copolymer which had a higher size of hydrophilic segments (SPPCL₄₀-HPG₆₀) had lower CMC and, hence, enhanced the solubility of PTX the most.

Polymers 10 µM	CMC µg/mL	A	Conc. µM	% increase of PTX
SPPCL10-HBP ₃₅	200	0.22	15	113
SPPCL35-HBP ₃₅	170	0.24	16	132
SPPCL40-HBP ₆₀	50	0.66	30	328

Copolymers which had a similar size of hydrophilic segments and different sized hydrophobic segments had encapsulated roughly similar amounts of PTX because they have similar CMC. This means that the encapsulation of the PTX occurs within the aggregated form of the star copolymer and is dependent on the CMC, rather than occurring in a specific segment of the polymer.

5.6 Summary

In this project, the chemotherapeutic molecule, paclitaxel, was encapsulated within the porphyrin cored polymers via hydrophobic interaction. During the encapsulation process, where the drug molecule was dissolved in methanol and mixed with methanol solution of the polymer to form the complex, the potency of the drug molecule was lost when it was tested in MTT assay using MCF-7 cell line. After further investigation, it turns out that there are a lot of electrophilic sites in the drug that could be reacted with a nucleophilic solvent and hence using methanol was not a good option. Therefore, 0.1% of DMSO was used to aid the encapsulation of the paclitaxel

within the polymer without harming the drug. However, the potency of the complexes could not be analysed due to lack of time and funding.



Chapter 6

Conclusion and further work



6.0 Conclusion and Further-work

In this project, we synthesised successfully macromolecular carriers with the ability to host macromolecular guest via one pot procedure. The synthesis of the macromolecule host started from using trimethylol propane as a multifunctional core followed by two subsequent ring opening polymerization steps of caprolactone and glycidol, respectively. Three star copolymers (SPCL-HPGs) were prepared with different chain length and similar size of the capping group (SPCL₁₅-HPG₉₀, SPCL₃₅-HPG₉₀ and SPCL₆₀-HPG₉₀) in order to study the effect of the chain length upon encapsulating large molecule. A hydrophilic HPG polymer was synthesised as the only control system of our proposed drug delivery system. The polymers (star copolymer and HPG) do form aggregates in water, this was confirmed using pyrene as probe for determining the CMC and by DLS which showed their hydrodynamic diameter size (100-200 nm). Having synthesised successfully the proposed drug delivery system and the control, a model macromolecular guest, a synthetic mimic of hemoglobin (TAPP-HBP **15**), was synthesised successfully with average molecular weight of 18K Da. Upon encapsulation, significant amount of the guest (1.7×10^{-5} to 3.3×10^{-5} M) was loaded within the star copolymers than it was for the control system (3.6×10^{-6} M). The poor encapsulation of the guest within the control (HPG) was thought to be related to the aggregated structure of the polymer; HPG does not have a hydrophobic segment that can form micelle structure with large hydrophobic domain to encapsulate great amount of the guest as it was seen for the star copolymers. So, the star copolymers was deemed to be a solution for improving the aqueous solubility of large molecule. This delivery system could be a suitable carrier for peptide or other large biomolecules only if the chain of its hydrophobic segments been functionalised. This could be achieved by synthesising a functionalised caprolactone monomer and then synthesising the star copolymer in the same manner as our delivery system.

The second part of the project discussed the synthesis of star copolymers with porphyrin core for Photodynamic therapy (PDT). Porphyrins and their derivatives have been used extensively in PDT. In this study, the solubility of porphyrins in aqueous solution was enhanced significantly via covalent incorporation within aggregated water-soluble polymers (porphyrin cored star copolymers, and porphyrin cored HPG). Two porphyrin molecules with hydroxyl end group were selected as a core these are: tetrakis(3,5-dihydroxyphenyl) porphyrin (TDHPP), and tetrakis(4-(hydroxyphenyl)porphyrin (THPP). However, TDHPP and THPP were very unreactive initiators for ring opening polymerization of caprolactone until a spacer was added. Thus, two star copolymers were synthesised from spacer-porphyrin (S-THPP-PCL-HPG) and S-TDHPP-PCL-HBP). The control (porphyrin-HPG) were synthesised from porphyrins with and without spacer units. The particle size of all the aggregated polymers was between 100-200 nm determined by DLS. The cytotoxicity and phototoxicity of the star copolymers (compound **31** and **33**) were tested initially via SRB assay using MCF-7 cell line. The result showed that both of the polymers, compound **31** and **33**, exhibited negligible toxicity at concentration of 400 and 900 μM . The phototoxicity of these compounds were obvious at 14 and 50 μM , respectively. The cytotoxicity and phototoxicity of all the porphyrin cored polymers were investigated further for their PDT behaviour via a simple MTT assay, using the EJ (bladder carcinoma) cancer cell line. The relative viability of the polymers and its controls in the dark were higher than 0.8 at 100 μM except the THPP-HPG polymer which had a viability 0.2. Under light irradiation (10 mW/cm²), significant toxicity was observed at 1 μM for the free THPP and at 10 μM for the free TDHPP porphyrin. While phototoxicity of the polymers, considerable cell death was obvious at polymers concentration of 10 μM for the THPP cored polymers except the star copolymer, which did not show any significant toxicity at this concentration. The phototoxicity of TDHPP cored polymers were significant for TDHPP-HPG and S-TDHPP-HPG at 100 μM for and poor for the star copolymer at same

concentration. The intracellular localisation of the molecules porphyrin cored polymers into EJ cells was imaged by confocal microscopy. Both of the free porphyrin (THPP and TDHPP) molecules diffused within the cell at a concentration of 10 μ M. Porphyrin cored HPG polymers also diffused within the cells but as the spacer was added the diffused fluorescence decreases. The porphyrin-PCL-HPGs star copolymers showed no diffusion into the cells. Thus, porphyrin-cored HPG polymers were deemed to be promising photosensitizers for photodynamic therapy (PDT) rather than the star copolymers. Other photosensitizers (such as phthalocyanine and chlorine) could be functionalised with nucleophilic end group and used as core for ROP of glycidol for effective PDT. These compounds as effective photosensitizer could then be investigated further using different cell lines and assay. *In vivo* study would be needed to confirm the compounds effectiveness in PDT.

In the final part of this project, porphyrin cored polymers were used to encapsulate chemotherapeutic drug molecule, paclitaxel, via hydrophobic interaction. The encapsulation method used initially were seen to be great but when the potency of the complex (drug-load in polymer) was not observed when it was tested against breast cancer cell line. After further investigation, it turns out that the drug has lost its potency during the encapsulation process (methanol reacted with the paclitaxel). Therefore 0.1% of DMSO was used to aid the encapsulation of the paclitaxel within the polymer without harming the drug. However, the potency of the complexes was not analysed due to lack of time and funding.



Chapter 7

Experimental



7.0 Experimental

7.1 General consideration

7.1.1 Reagents, solvents and general equipment

All reagents and solvents were obtained from commercial sources (primarily Sigma- Aldrich) and were used without further purification unless otherwise. Dry solvents were obtained from the University of Sheffield Chemistry Department Grubbs solvent dispensing system. All glassware was cleaned and flame-dried under ambient conditions.

7.1.2 Nuclear magnetic resonance spectroscopy

¹H NMR spectra were performed at 400 MHz using a Bruker 'AV3HD-400' spectrometer equipped with a 5mm probe. ¹³C NMR was performed at 100 MHz using a Bruker 'AV-400' spectrometer equipped with a 5mm BBO BB-1H probe. Chemical shifts are reported in parts per million (ppm) from trimethylsilane. All samples were prepared using deuterated solvents supplied by Sigma Aldrich. Resonance were analysed using Bruker TopSpin 3.0 NMR software. Impurities were assigned using 'NMR Chemical Shifts of Common Laboratory Solvents as Trace Impurities'.

7.1.3 UV-Vis Spectroscopy

The ultraviolet absorbance characteristic of materials was recorded on an Analytic Jena AG Specord s600 uv/vis spectrometer and analyzed using its attached Software (WinASPECT). Solutions were made up in an appropriate solvent and the instrument was calibrated with pure solvent before use.

7.1.4 IR Spectroscopy

Infra-Red (IR) spectra were recorded using a Perkin Elmer Paragon Spectrum 100 FT-IR

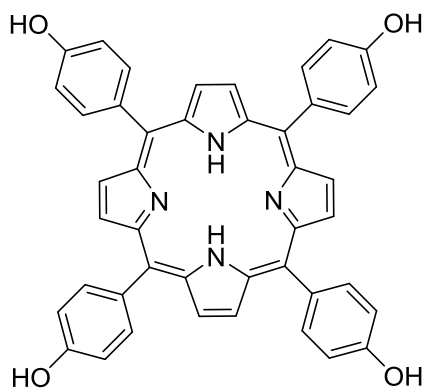
spectrophotometer with ν_{\max} in cm^{-1} . Samples were recorded neat (without using Nujol or KBr) using sodium chloride plates and recorded as a thin film subsequent to solvent evaporation.

7.1.5 Thermal analysis

Melting point characteristic of materials was recorded on

7.2 Synthesis of porphyrin molecules

7.2.1 5,10,15,20-Tetrakis(4-hydroxyphenyl)-21H,23H-porphine (THPP 12)

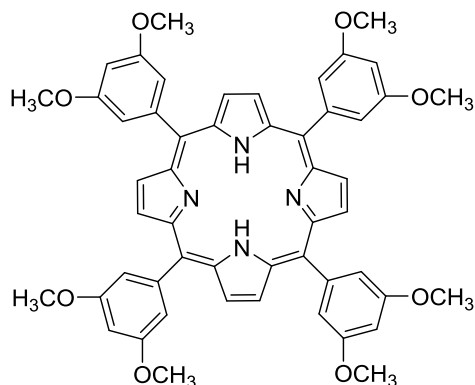


Freshly distilled pyrrole (4.17 ml, 60 mmol) and 4-hydroxy benzaldehyde (7.3 g, 60 mmol) were added to propionic acid (300 ml) that was maintained under reflux. The mixture was refluxed for 1 hour, allowed to cool to room temperature and placed for 1 hour at $-5\text{ }^{\circ}\text{C}$ and the filtered cake was washed thoroughly with the mixture of propionic acid and ethanol (1:1), and CHCl_3 , respectively.

Yield: 1.32 g, 13%. ^1H NMR (400 MHz, $(\text{CD}_3)_2\text{SO}$): δ_{H} 9.99 (s, 4H, phenolic *p*-OH), 8.85 (s, 8H, pyrrolic-CH), 7.97 (d, 8H, phenolic *m*-CH), 7.18 (d, 8H, phenolic *o*-CH), -2.92 (s, 2H, NH-pyrrole); ^{13}C NMR (400 MHz, CD_3OD): δ_{C} 156.5, 143.7, 120.0, 114.4, 101.8; IR (cm^{-1}) 3431 (OH); UV Absorbance (MeOH) λ_{\max} (nm) = 418.5, 516, 554, 649; $(\text{M}+\text{H})^+$ (ESI-MS) =

679 (calculated 679 g mol^{-1}).

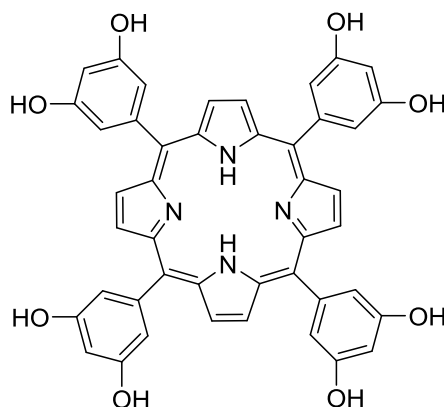
7.2.2 Tetrakis (3, 5-dimethoxyphenyl)-21H, 23H-porphyrin (TDMPP 18)



Freshly distilled pyrrole (4.17 ml, 60 mmol) and 3, 5- dimethoxybenzaldehyde (10.0 g, 60 mmol) were added to propionic acid (300 ml). The mixture was maintained under reflux for 30 minutes, allowed to cool to room temperature and collected via vacuum filtration. The obtained product was washed thoroughly with methanol before being oven dried at 40 $^{\circ}\text{C}$ to give purple crystals.

Yield: 2.9 g 23%, ^1H NMR (400 MHz, CDCl_3): δ_{H} 8.94 (s, 8H, pyrrolic β -H), 7.43 (s, 8H, phenolic *o*-CH), 6.95 (s, 4H, phenolic *p*-CH), 3.99 (s, 24H, phenylic *m*- CH_3), -2.89 (s, 2H, NH); ^{13}C NMR δ_{c} (400 MHz, CDCl_3): δ 158.9, 144.0, 119.8, 113.8, 100.2, 26.9; IR: $\nu_{\text{max}}/\text{cm}^{-1}$ 1150 (OMe); UV Absorbance (CH_2Cl_2) λ_{max} (nm)= 420.5, 513, 548, 585.5, 643.5; ($\text{M}+\text{H}$) $^+$ (ESI-MS) = 855 (calculated 855 g mol^{-1}).

7.2.3 Tetrakis (3, 5-dihydroxyphenyl)-21H, 23H-porphyrin (TDHPP 13)

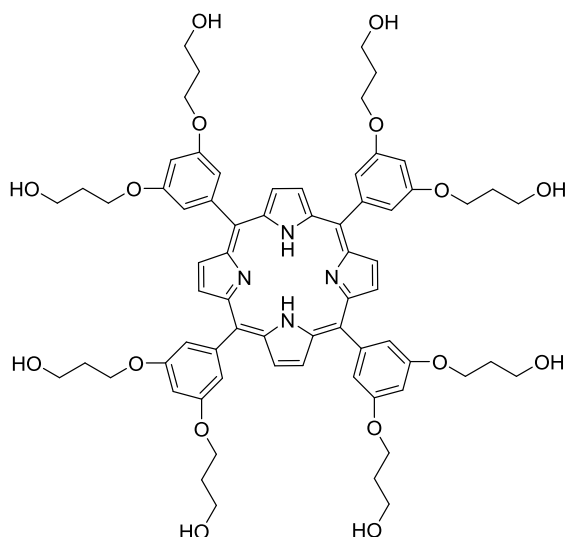


A round bottomed flask was bulls charge with 5, 10, 15, 20- tetrakis (3,5-dimethoxyphenyl)-porphyrin **18** (1g, 1.17 mmol), anhydrous dichloromethane (40 ml) and flashed with nitrogen. BBr_3 (3 ml, 31.6 mmol) was added via syringe and the reaction mixture was stirred gently under nitrogen at room temperature for 5 hours. The reaction was then quenched carefully with distilled water (1.5ml, 0.08mol) and stirred for a further 20 mins. The crude mixture was then neutralised with a saturated solution of sodium hydrogen carbonate and extracted with ethyl acetate.

Yield: 0.9 g, 90%; ^1H NMR (400 MHz, CD_3OD) δ_{H} 9.04 (d, 8H, pyrrolic β -H), 7.52 (d, 8H, phenylic *o*-CH), 6.96 (t, 4H, phenylic *p*-CH), 4.91 (s, 8H, phenylic *m*-OH), -2.89 (s, 2H, NH); ^{13}C NMR (400 MHz, CD_3OD) δ_{C} 156.5, 143.7, 120.0, 114.4, 101.8; IR (cm^{-1}) 3431 (OH); UV Absorbance (MeOH) λ_{max} (nm) = 416.5, 512.5, 547.5, 588, 644.5; $(\text{M}+\text{H})^+$ (ESI-MS) = 743 (calculated 743 gmol^{-1}).

7.3 Synthesis of porphyrin initiator

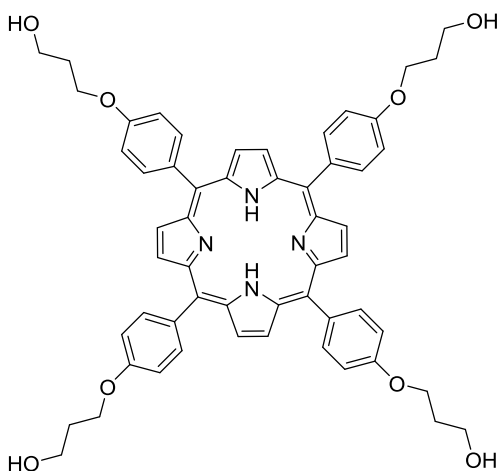
7.3.1 Spacer-porphyrin (S-TDHPP 27)



5,10,15,20-Tetrakis(3,5-dihydroxyphenyl)-21H,23H-porphyrin (200 mg, 0.269 mmol), K₂CO₃ (906 mg, 6.4 mmol, 24 equiv.), and 18-crown-6 (20 mg) were added to 60 mL of dimethylformamide (DMF). 1,3-Bromopropanol (582 mg, 4.18 mmol, 16 equiv) was added and the reaction was stirred vigorously under reflux overnight followed by TLC analysis. The DMF was evaporated under reduced pressure and the reaction mixture was dissolved in 200 mL of THF and extracted three times with water (100 mL) with the addition of brine to obtain phase separation. The solvents were evaporated, and the crude product was dissolved in a small amount of THF, precipitated in cold diethyl ether, filtered, and dried to yield S-TDHPP **27** a purple solid.

Yield: 170 mg, 86%, ¹H NMR (400 MHz, DMSO-d₆): δ_H 8.90 (d, 8H, pyrrolic β-H), 7.32 (d, 8H, phenylic *o*-CH), 6.97 (t, 4H, phenylic *p*-CH), 4.58 (s, 8H, phenylic *m*-OH), 4.22 (t, 8H, -O-CH₂-CH₂), 3.58 (t, 8H, -CH₂-OH), 2.67 (m, 8H, -CH₂-CH₂-CH₂-), -3.01 (s, 2H, NH); ¹³C NMR(400 MHz, DMSO-d₆): δ_C 158.4, 135.5, 135.4, 134.6, 119.5, 112.0, 56.87, 54.01, and 31.62; ESI-MS (M+H)⁺ = 1207 (calculated 1207).

7.3.2 Spacer-porphyrin S-THPP 26

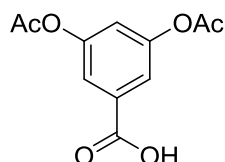


5,10,15,20-Tetrakis(4-hydroxyphenyl)- 21H,23H-porphyrin (177 mg, 0.261 mmol), K_2CO_3 (453 mg, 3.13 mmol, 12 equiv), and 18-crown-6 (10 mg) were added to 30 mL of dimethylformamide (DMF). 1,3-Bromopropanol (291 mg, 2.09 mmol, 8 equiv) was added and the reaction was stirred vigorously under reflux overnight followed by TLC analysis. The DMF was evaporated and the reaction mixture was dissolved in 200 mL of THF and extracted three times with water (100 mL) with the addition of brine (30 mL) to obtain phase separation. The solvents were evaporated, and the crude product was dissolved in a small amount of THF, precipitated in cold diethyl ether, filtered, and dried to yield S-THPP **26** a purple solid.

Yield: 150 mg, 85%, 1H NMR (400 MHz DMSO- d_6): δ_H 8.85(s, 8H, β -Pyrrole), 7.97(d, 8H, phenylic *m*-CH), 7.18(d, 8H, phenylic *o*-CH), 4.58 (s, 4H, phenylic *m*-OH), 4.20 (t, 8H, -O-CH₂-CH₂), 3.63 (t, 8H, -CH₂-OH), 2.47 (m, 8H, -CH₂-CH₂-CH₂-), -3.01 (s, 2H, NH); ^{13}C NMR (400 MHz DMSO- d_6): δ_C 158.4 (ArC- O), 135.5 (p-ArC), 135.4 (m-ArC), 134.6 (pyrrole C), 119.5 (meso-porphyrin C), 112.0 (o-ArC), 56.9 (-O-CH₂-CH₂), 54.0 (-CH₂-OH), and 31.6 (-CH₂-CH₂-CH₂-); (M+H)⁺ (ESI-MS) = 912 (calculated 912).

7.4 Synthesis of TAPP cored poly (3, 5-diacetoxybenzoic acid) 15

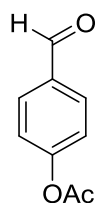
7.4.1 Synthesis of 3, 5-diacetoxybenzoic acid (13)



A round bottomed flask was charged with acetic anhydride (20 ml) and 3, 5- dihydroxybenzoic acid (5.0 g, 50 mmol). The reaction mixture was stirred for 10 minutes and sulfuric acid (50 ml) was added dropwise. The flask was then left to cool for 30 minutes. Distilled water (100 ml) was added into the flask to remove the excess acetic anhydride and acetic acid by-products. The crude product then precipitated a white crystalline solid. After 2 hours of stirring, the product was isolated using gravity filtration and thoroughly washed with distilled water (2 x 30 ml).

Yield 10.5 g, 89 %; $^1\text{H NMR}$ (400 MHz, CDCl_3) δ 10.15 (br, s, 1H, -COOH), 7.75 (d, J 2.2 Hz, 2H, Ar *o*-CH), 7.24 (t, J 2.2 Hz, 1H, Ar-*p*-CH), 2.34 (s, 6H, -CH₃); $^{13}\text{C NMR}$ (400 MHz; CDCl_3) δ 170.2 (COOH), 168.9 (C=O), 151.1 (*m*-Ar), 131.4 (*i*-Ar), 121.3 (*p*-Ar), 120.9 (*o*-Ar), 21.0 (CH₃); IR: $\nu_{\text{max}}/\text{cm}^{-1}$ (thin film, NaCl plates) 2400-3250, 1771 (COOMe), 1692 (COOH), 1597 (Ar C=C); MH^+ (ESI-MS) = 237 (calculated 237); MP 160-164 °C.

7.4.2 Synthesis of 4-acetoxybenzaldehyde (7)

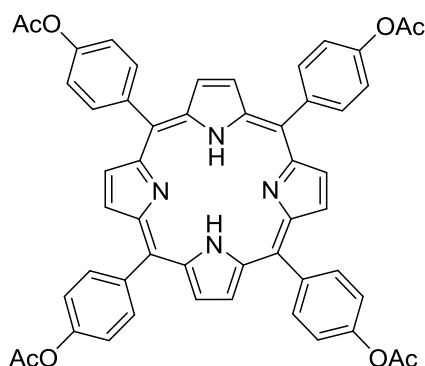


A round bottomed flask was bulls charge with 4-hydroxybenzaldehyde (10 g, 84 mmol), triethylamine (15 ml, 108 mmol) and anhydrous THF (300 ml). The mixture was then stirred

under nitrogen and then acetyl chloride (15 ml, 211 mmol) was added dropwise via a syringe. The mixture was then stirred for a further 30 minutes at ambient temperature. The reaction mixture was then filtered and the brown filtrate was collected and the solvent was reduced via rotary evaporation to form brown oil. The product was dissolved in dichloromethane (200 ml) and washed with a saturated sodium hydrogen carbonate solution (300 mL) and distilled water (200 mL). The organic layer was collected and dried over magnesium sulfate to yield the crude product.

Yield: 8.2 g, 60 %; ^1H NMR (400 MHz, CDCl_3) 9.95 (s, 1H, COH), 7.95 (d, 2H, Ar-H), 7.25 (d, 2H, Ar-H), 2.35 (s, 3H, CH_3); ^{13}C NMR (400 MHz; CDCl_3) 190.9, 168.5, 155.0, 133.9, 131.0, 122.35, 21.0; IR: $\nu_{\text{max}}/\text{cm}^{-1}$ (thin film, NaCl plates) 1756 (C=O), 1280 (C-O); M^+H^+ (ESI-MS) =163 (calculated 164).

7.5 Synthesis of tetrakis (4-diacetoxyphenyl)-21H, 23H-porphyrin (TAPP 12)

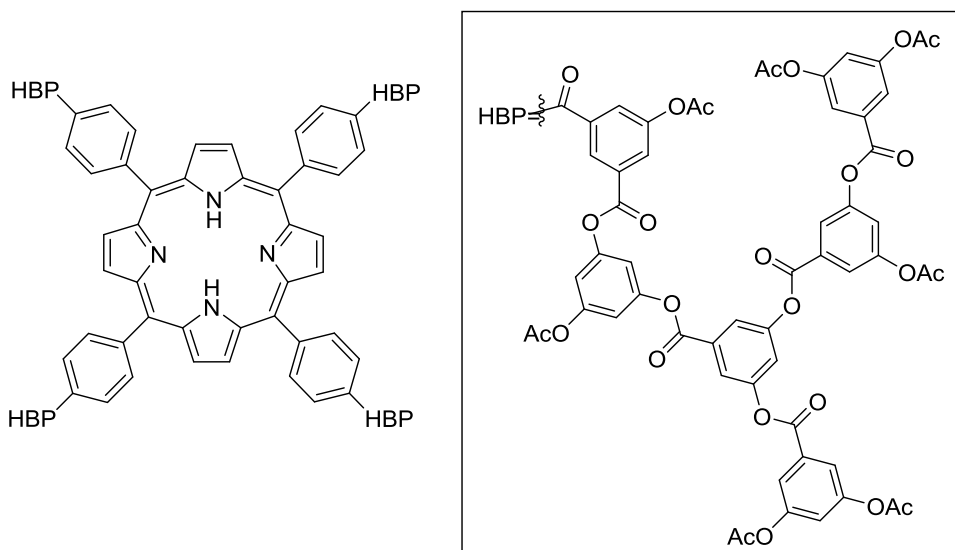


Freshly distilled pyrrole (2.8 mL, 40 mmol) and 4-acetoxybenzaldehyde **7** (6.5 g, 40 mmol) were added to refluxing propionic acid (200 mL). The mixture was maintained under reflux for 30 minutes and then cooled to room temperature. It was then filtered and washed with methanol until colourless.

Yield, 22 %, ^1H NMR (400 MHz, CDCl_3) 8.90 (d, 8H, pyrrolic β -H), 8.25 (d, J 7.8 Hz, 8H, phenolic o -C-H), 7.50 (d, J 7.8Hz, 8H, phenolic m -CH), 2.50 (s, 12H, CH_3), -2.83 (s, 2H, N-

H); ^{13}C NMR (400 MHz; CDCl_3) 169.5, 150.5, 139.5, 135.4, 131.1, 119.7, 119.2, 21.2; IR: $\nu_{\text{max}}/\text{cm}^{-1}$ 1750 (C=O); λ_{max} (CH_2Cl_2) (nm): 418, 515, 549, 590, 643; $\text{M}+\text{H}^+$ (ES-MS) = 847 (calculated 847).

7.6 Synthesis of TAPP cored poly (3, 5-diacetoxybenzoic acid) (15)

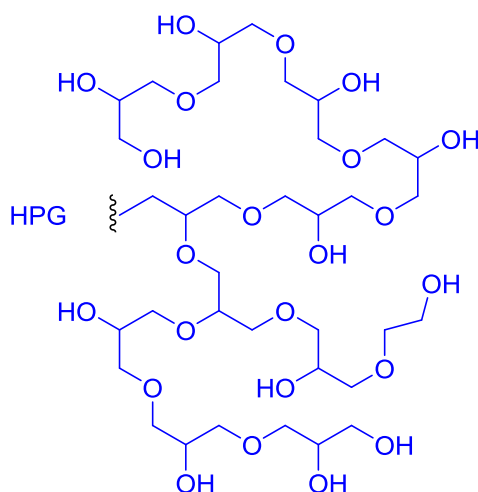


Tetrakis (4-acetoxyphenyl)-porphyrin **12** (0.3 g, 0.35 mol), 3,5-diacetoxybenzoic acid **13** (6.8 g, 28.56 mmol) and diphenyl ether (2.0 g) were added to a round bottomed flask fitted with distillation kit. The reaction mixture was degassed thoroughly and flushed with nitrogen and then heated to 225 °C. After 45 minutes, the temperature was reduced to 180 °C, and the reaction was placed under vacuum for 4 hours. The mixture was then dissolved in THF and precipitated into methanol (600 ml). The brown solid was then filtered and washed using cold methanol. The crude polymer was then loaded onto a Biobead column to remove any unreacted porphyrin.

^1H NMR (400 MHz, CDCl_3) δ 8.95 (s, 8H, pyrrolic β -H), 8.26 (d, J 8.50 Hz, 8H, phenylic o-CH), δ 8.04-7.93 (m, [polymer] Ar-p-CH), 7.52 (d, J 8.50 Hz, 8H, phenylic m-CH), 7.45-7.19

(br, 1H [polymer] Ar-o-CH), 2.36 (s, 24H, CH₃), -2.81 (s, 2H, NH); ¹³C NMR (400 MHz; CDCl₃) 167.7, 163.5, 151.6, 150.4, 132.9, 131.5, 130.2, 129.5, 122.4, 121.9, 120.5, 23.0; λ_{max} (CH₂Cl₂)/nm 418.5, 518, 553, 596, 644; IR: ν_{max}/cm⁻¹ 1752 (C=O); GPC (THF) Mn, 18,600 Da, PDI 2.6.

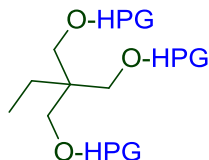
7.7 General procedure for synthesis of hyperbranched polyglycerol



The hydroxyl functional core was added to diethylene glycol dimethyl ether in a round bottom flask fitted with a condenser under nitrogen atmosphere. The solution was stirred at 50 °C until the core was fully dissolved. A base such as potassium methoxide was added to the stirring solution and the temperature was raised to 90 °C for 90 minutes. Glycidol was then added dropwise via a syringe pump and the reaction was left for a further 5 hours. The reaction mixture was cooled to room temperature and the solvent was disposed of. A minimum amount of methanol was added to the product and the mixture left to stir until it had all dissolved. In a separate beaker cold acetone was stirred and then the methanol solution of the product was added to the acetone in a drop wise fashion . Once the addition was complete, the mixture was covered with tin foil and left stirring for 1 hour before disposing of the acetone. Cold acetone was added to the product again before covering with tin foil and stirring for another hour. The acetone was disposed of to yield a yellow product which was dried overnight in a vacuum to

give hyperbranched poly glycerol as a deep yellow extremely viscous liquid.

7.7.1 Synthesis of trimethylolpropane (TMP) core hyperbranched polyglycerol

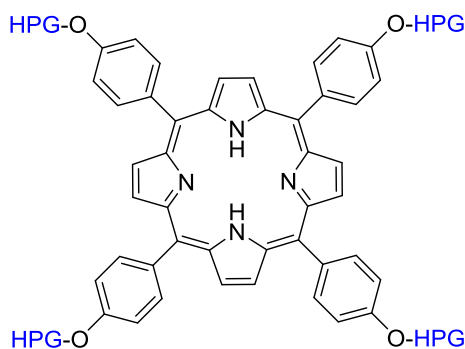


General procedure 6.4.1 was used to synthesize the polymer. The reaction used trimethylolpropane (0.01g, 0.07 mmol), diethylene glycol dimethyl ether (20 ml), potassium methoxide (0.05 g, 0.03 mmol) and glycidol (1.5g, 20.27 mmol).

^1H NMR (400 MHz, D_2O); δ_{H} 4.17-3.22 (br m OH + CH + CH_2), 1.17(m, CH_2); ^{13}C NMR (400 MHz, D_2O) δ_{C} 63.1, 71.2, 78.9; IR (cm^{-1}): 3360 (OH), 2875 (CH_2 , CH), 1335 (C-O-C); GPC (aq.) M_n 18K Da, PDI 3.6.

7.7.2 Synthesis of porphyrin core hyperbranched polyglycerol

7.7.2.1 THPP to glycidol molar ratio per OH group 1:50

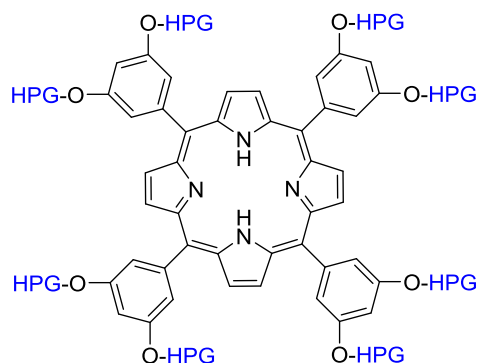


General procedure 6.4.1 was used to synthesize the polymer. The reaction used TDHPP porphyrin (0.1g, 0.15 mmol), diethylene glycol dimethyl ether (20 ml), potassium methoxide (0.041 g, 0.58 mmol) and glycidol (2.22g, 30.0mmol).

^1H NMR (400 MHz, D_2O) δ_{H} : 9.81, 8.45, 4.11-3.20 (br m OH + CH + CH_2); ^{13}C NMR (400

MHz, D₂O) δ_C 62.5, 70.6, 79.1; IR (cm⁻¹): 3270 (OH), 2916 (CH₂, CH), 1636 (C=O), 1327 (C-O-C), 1051 (C-O); Mn 14K Da, PDI 1.5.

7.7.2.2 TDHPP to glycidol molar ratio per OH group 1:50

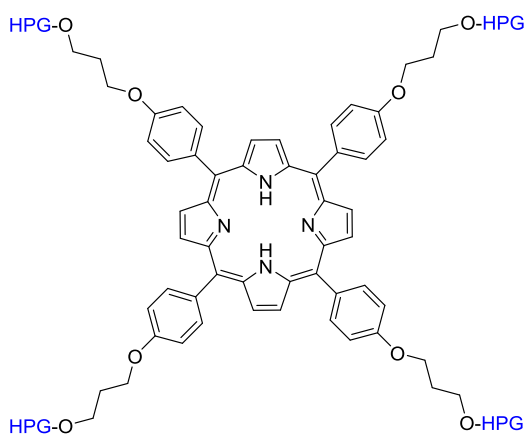


General procedure 6.4.1 was used to synthesize the polymer. The reaction used TDHPP porphyrin (0.1g, 0.13 mmol), diethylene glycol dimethyl ether (20 ml), potassium methoxide (0.08 g, 1.07 mmol) and glycidol (3.84g, 52.0mmol).

¹H NMR (400 MHz, D₂O) δ_H : 9.89, 8.55, 4.08-3.20 (br m OH + CH + CH₂); ¹³C NMR (400 MHz, D₂O) δ_C 62.7, 70.3, 78.1; IR (cm⁻¹): 3342 (OH), 2871 (CH₂, CH), 1626 (C=O), 1330 (C-O-C), 1062 (C-O)); GPC (aq.) Mn 14K Da, PDI 1.5.

7.7.3 Synthesis of (porphyrin with spacer) core hyperbranched polyglycerol

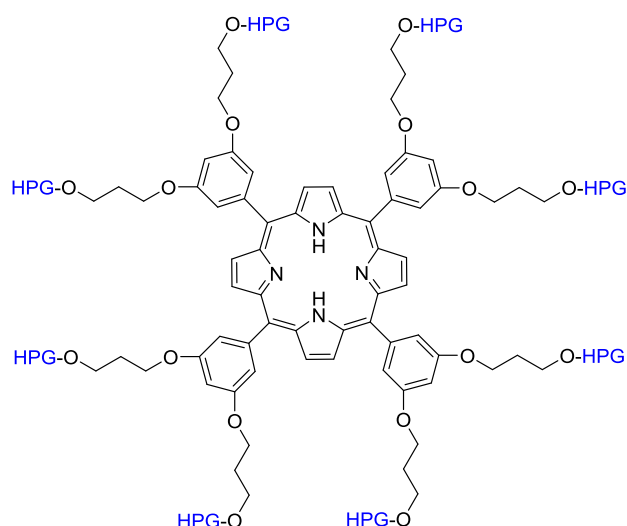
7.7.3.1 S-THPP to glycidol molar ratio per OH group 1:50



General procedure 6.4.1 was used to synthesize the polymer. The reaction used TDHPP porphyrin (0.1g, 0.11 mmol), diethylene glycol dimethyl ether (20 ml), potassium methoxide (0.031 g, 0.43 mmol) and glycidol (1.63g, 22.0mmol).

^1H NMR (400 MHz, D_2O) δ_{H} : 9.87, 8.50, 4.08-3.21 (br m OH + CH + CH_2); ^{13}C NMR (400 MHz, D_2O) δ_{C} 62.3, 70.0, 78.8; IR (cm^{-1}) : 3391 (OH), 2873 (CH_2 , CH), 1641 (C=O), 1327(C-O-C), 1042 (C-O); GPC (aq.) M_n 20K Da, PDI 2.3.

7.7.3.2 S-TDHPP to glycidol molar ratio per OH group 1:50



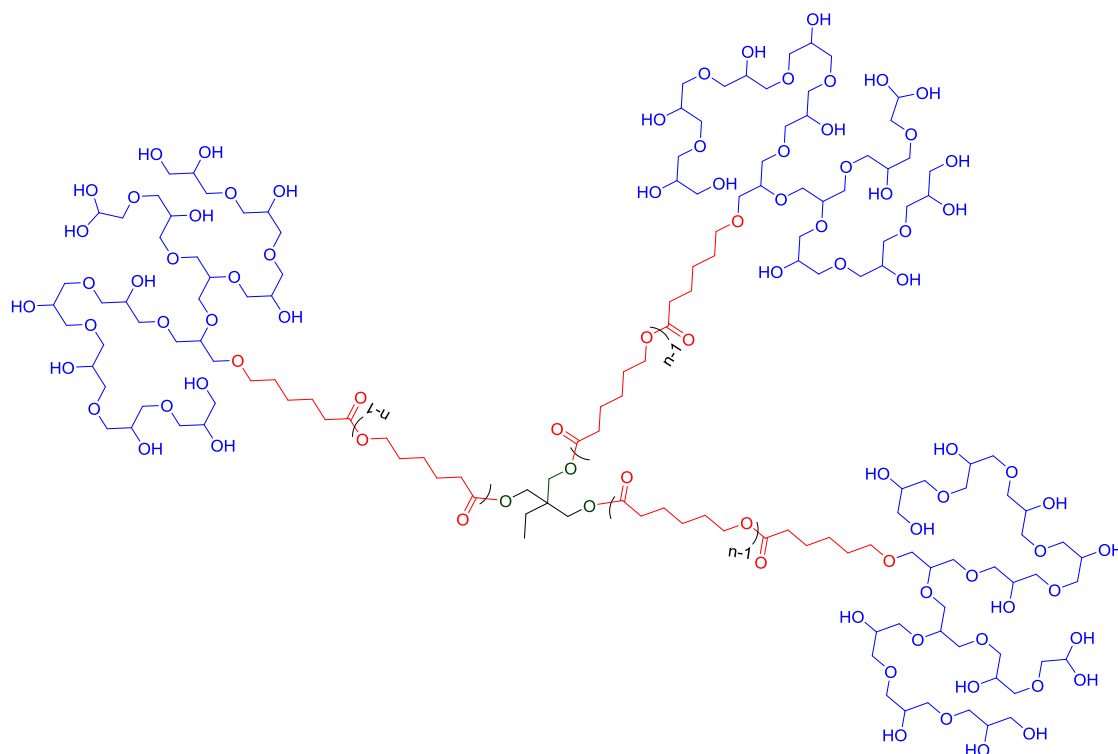
General procedure 6.4.1 was used to synthesize the polymer. The reaction used S-TDHPP porphyrin (0.1g, 0.08 mmol), diethylene glycol dimethyl ether (20 ml), potassium methoxide (0.046 g, 0.6 mmol) and glycidol (2.36g, 32.0mmol).

^1H NMR (400 MHz, D_2O) δ_{H} : 9.83, 8.52, 4.05-3.22 (br m OH + CH + CH_2); ^{13}C NMR (400 MHz, D_2O) δ_{C} 61.3, 70.2, 78.7; IR (cm^{-1}) : 3351 (OH), 2867(CH_2 , CH), 1649 (C=O), 1329 (C-O-C), 1047 (C-O); GPC (aq.) M_n 8.5K Da, PDI 1.5.

7.8 General Procedure for Synthesis of Amphiphilic Copolymers Based On Poly(Caprolactone) and Polyglycerols

Poly (ϵ -caprolactone)-block-polyglycerols (PCL-HPG) copolymers were synthesized in two steps. Initially PCL was synthesized by controlled ring-opening polymerization of ϵ -caprolactone (ϵ -CL) using initiator (such as alcohol), in the presence of stannous octoate (SnOct_2). The molecular weight of PCL depended on the molar ratio of ϵ -CL to hydroxyl group/s in the initiator. The polymerization procedure was described as follows: The core and ϵ -CL were quickly added into a dry polymerization flask under nitrogen atmosphere. Tin (II) 2-ethyl hexanoate (0.05 % w/w) was added to the mixture, then the reaction flask was degassed three times and stirred under nitrogen for 24 hours at 130 °C. The second step was started after the withdrawal of small sample of the reaction flask for GPC analysis. Then, the temperature was decreased to 90 °C followed by the addition of 1,4-dioxane and a base such as potassium methoxide. The reaction flask was then degassed with at least three cycles followed by the slow addition of glycidols. Stirring the reaction mixture for several hours after the complete addition, the mixture was cooled to room temperature and then the solvent was evaporated. The minimum amount of methanol was added to the product and the residue was filtered. The filtrate was then added to a beaker of acetone drop-wise. Once the addition was complete, the mixture was covered with tin foil and left to stir for 1 hour. The solvent was disposed of and the product dried to give star poly (caprolactone) block hyperbranched polyglycerol.

7.8.1 Synthesis of trimethylolpropane (TMP) cored star poly (caprolactone)- block-hyperbranched TMPPCL-b-HPG



TMP₁PCL₁₅-b-HPG₃₀

The general procedure was used to synthesis the polymer. The reaction used TMP (60.0 mg, 0.46 mmol), CL (2.3 g, 20.7 mmol), Sn(Oct)₂ (10mg) and glycidol (3.1 g, 40.4 mmol).

Yield: 3.6 g, 65%; ¹H NMR (400 MHz, D₂O) δ_H 2.33 (H, m, α-CH₂), 1.66 (m, β and δ-CH₂), 1.39 (m, γ-CH₂) 3.20-4.25 (br m OH + CH + CH₂); ¹³C NMR (400 MHz, D₂O) δ_C 173.8, 70.7, 64.2, 34.3, 28.4, 25.4, 24.6; IR (cm⁻¹): 3277 (OH), 2861 (CH sp³), 1724 (C=O stretch), 1644, 1335 (C-O-C stretch), 1060 (C-O stretch); GPC (aq.) Mn 4.8K Da, PDI 1.9.

TMP₁PCL₃₅-HPG₃₀

General procedure was used to synthesis the polymer. The reaction used TMP (0.1g, 0.92 mmol), CL (4.18ml, 36.68mmol), Sn(Oct)₂ (10mg) and glycidol (6.8g, 92.0 mmol).

Yield: 10.3 g, 60%; ¹H NMR (400 MHz, D₂O) δ_H 2.32 (H, m, α-CH₂), 1.66 (m, β and δ-CH₂),

1.38 (m, γ -CH₂) 3.20-4.23 (br m OH + CH + CH₂); ¹³C NMR (400 MHz, D₂O) δ_C 173.4, 70.5, 65.2, 34.3, 28.1, 25.1, 24.7; IR (cm⁻¹): 3279 (OH), 2851 (CH sp³), 1728 (C=O stretch), 1650, 1332 (C-O-C stretch), 1060 (C-O stretch); GPC (aq.) Mn 4.5K Da, PDI 2.2.

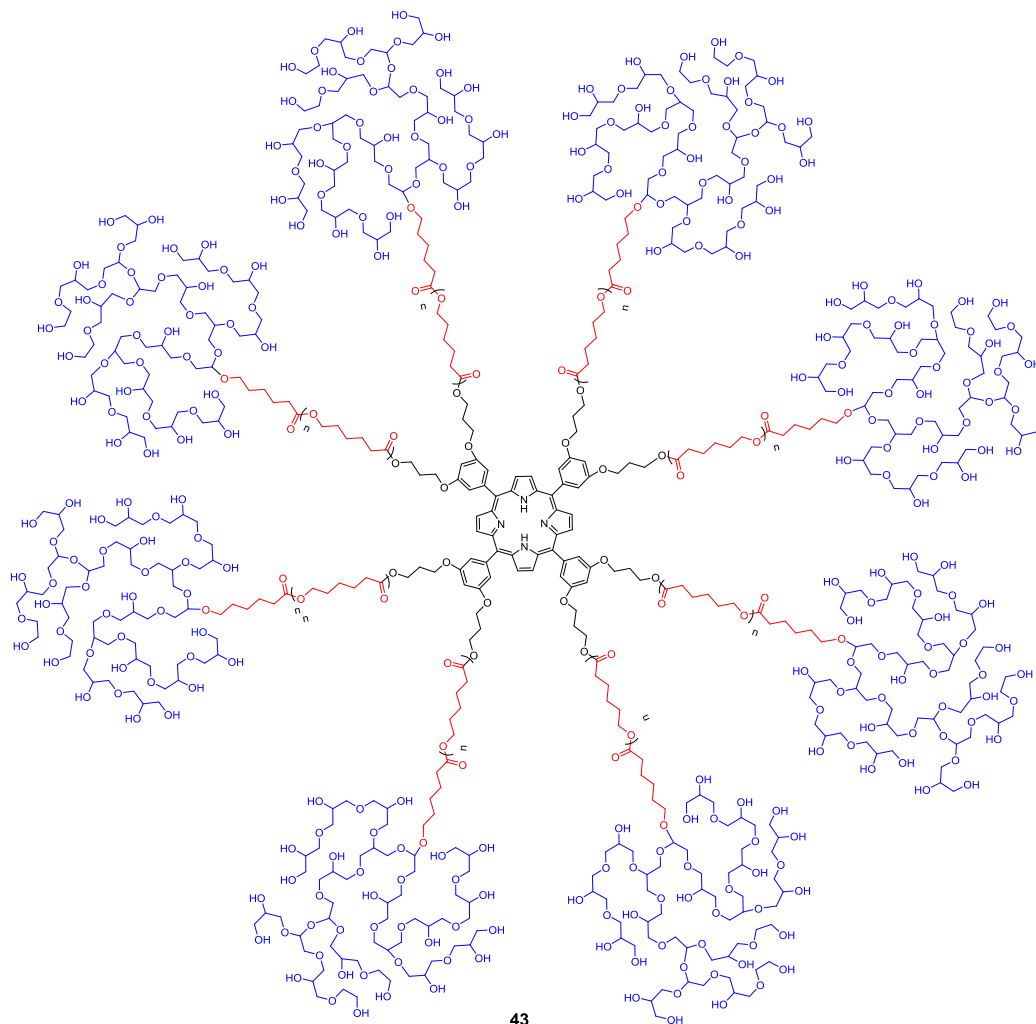
7.8.1.1 TMP1PCL₆₀-HPG₃₀

General procedure was used to synthesis the polymer. The reaction used TMP (60.0 mg, 0.46 mmol), CL (9.4 g, 82.8 mmol), Sn(Oct)₂ (10mg) and glycidol (3.1 g, 40.4 mmol).

Yield: 9.1 g, 72%; ¹H NMR (400 MHz, D₂O) δ_H 2.33 (H, m, α -CH₂), 1.64 (m, β and δ -CH₂), 1.37 (m, γ -CH₂) 3.20-4.21 (br m OH + CH + CH₂); ¹³C NMR (400 MHz, D₂O) δ_C 173.5, 70.9, 64.0, 34.6, 28.4, 25.1, 24.2; IR (cm⁻¹): 3260 (OH), 2859 (CH sp³), 1729 (C=O stretch), 1645, 1332 (C-O-C stretch), 1064 (C-O stretch); GPC (aq.) Mn 4.8K Da, PDI 1.6.

7.8.2 Synthesis of porphyrin cored star poly (caprolactone)-b-hyperbranched

7.8.2.1 Synthesis of TDHPP-PCL-HPG



S-TDHP₁-PCL₁₀-HPG₃₅

General procedure was used to synthesis the polymer. The reaction used S-TDHP (132mg, 0.11mmol), CL (1.0 g, 8.7mmol), Sn(Oct)₂ (10 mg) and glycidol (1.13g, 15.4mmol).

Yield: 0.74 g, 65%; ¹H NMR (400 MHz, D₂O) δ_H 2.33 (H, m, α-CH₂), 1.66 (m, β and δ-CH₂), 1.39 (m, γ-CH₂) 3.20-4.23 (br m OH + CH + CH₂), δ_H 8.32 (br d, aromatic H), 7.73 (br s, aromatic H), 7.35(br s, aromatic H); ¹³C NMR (400 MHz, D₂O) δ_C 173.6, 70.3, 64.2, 34.3, 28.7, 25.4, 24.8; IR (cm⁻¹): 3271 (OH), 2860 (CH sp³), 1720 (C=O stretch), 1652, 1331 (C-O-C stretch), 1060 (C-O stretch); GPC (aq.) Mn 19K Da, PDI 1.2.

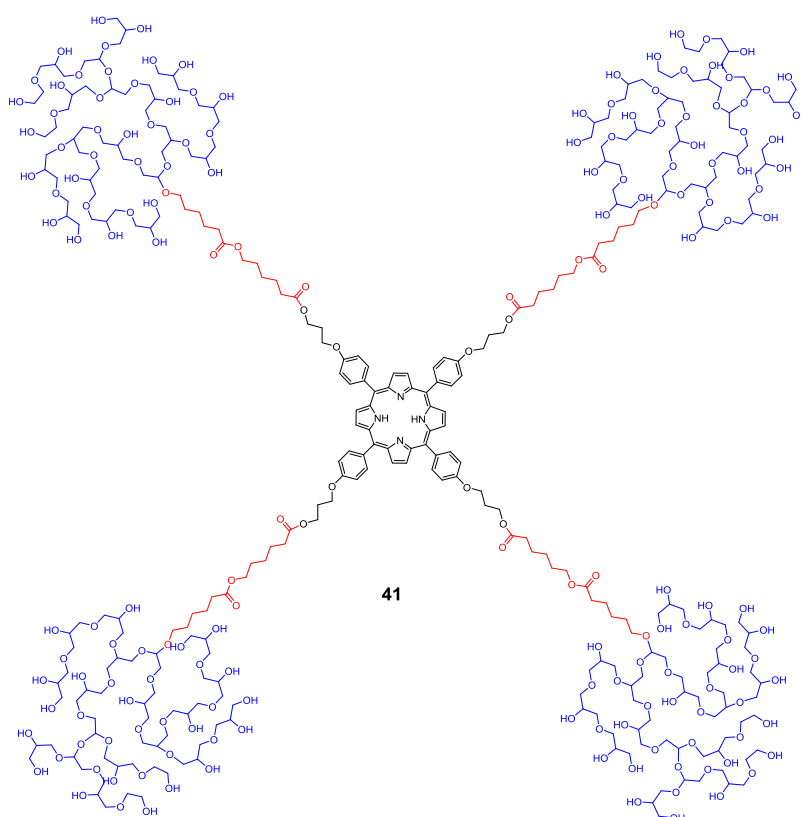
S-TDHPP₁-PCL₃₀-HPG₃₅

The general procedure was used to synthesis the polymer. The reaction used OH-Prop-THPP (132mg, 0.11mmol), CL (4.0 g, 35.2mmol), Sn(Oct)₂ (10 mg) and glycidol (1.13g, 15.4mmol).

Yield: 0.68 g, 60%; ¹H NMR (400 MHz, D₂O) δ_H 2.32 (H, m, α-CH₂), 1.65 (m, β and δ-CH₂), 1.39 (m, γ-CH₂) 3.20-4.21 (br m OH + CH + CH₂), δH 8.32 (br d, aromatic H), 7.73 (br s, aromatic H), 7.37(br s, aromatic H); ¹³C NMR (400 MHz, D₂O) δ_C 173.1, 71.3, 64.1, 34.6, 28.7, 25.5, 24.8; IR (cm⁻¹): 3271 (OH), 2860 (CH sp³), 1725 (C=O stretch), 1651, 1331 (C-O-C stretch), 1061 (C-O stretch); GPC (aq.) Mn 40K Da, PDI 1.1.

7.8.2.2 Synthesis of THPP-PCL-HPG

S-THPP₁-PCL₄₀-HPG₆₀



The general procedure was used to synthesis the polymer. The reaction used OH-Prop-THPP (100mg, 0.11mmol), CL (2.0 g, 17.5mmol), Sn(Oct)₂ (10 mg) and glycidol (1.95g, 26.4mmol).

Yield: 1.5g, 72%; ^1H NMR (400 MHz, D_2O) δ_{H} 2.33 (H, m, $\alpha\text{-CH}_2$), 1.64 (m, β and $\delta\text{-CH}_2$), 1.39 (m, $\gamma\text{-CH}_2$) 3.20-4.23 (br m OH + CH + CH_2), δ_{H} 8.32 (br d, aromatic H), 7.73 (br s, aromatic H), 7.37(br s, aromatic H); ^{13}C NMR (400 MHz, D_2O) δ_{C} 173.0, 71.1, 64.0, 34.5, 28.8, 25.4, 24.8; IR (cm^{-1}): 3270 (OH), 2862 (CH sp^3), 1726 (C=O stretch), 1651, 1335 (C-O-C stretch), 1059 (C-O stretch); GPC (aq.) M_n 22K Da, PDI 1.0.

7.9 Critical aggregation concentration (CAC)

Pyrene was used as a hydrophobic fluorescent probe. Aliquots of pyrene solutions (6×10^{-6} M in acetone, 1ml) were added to the vials and the acetone was allowed to evaporate. Aqueous polymer solutions at different concentrations were then added to the vials which containing pyrene residue. The solutions was left at room temperature for 24 hours to reach the solubilisation equilibriums of pyrene in the aqueous phase. Excitation was carried at 340nm and the emission spectra were recorded over a range of 350 to 600 nm. Both excitation and emission silt widths were 5 nm. From the pyrene emission spectra, the intensities (peak height) ratios (I_3/I_1) of the third band to the first band were analysed as a function of the polymer concentrations. A CMC value was determined from the interaction of the tangent to the curve at the inflection with the horizontal tangent through the point at low concentration.

7.10 Cell Culture

EJ (bladder carcinoma) cells were purchased from American Type Culture Collection–LGC partnership (Teddington, UK) and used within 20 passages of purchase. Cells were cultured using Dulbecco's modified Eagles Medium (DMEM) (Lonza, Cambridge, UK) with 10% fetal calf serum (FCS) (Lonza, Cambridge UK) and cultured in an incubator ($37\text{ }^\circ\text{C}$, 5 % CO_2). The cells were passaged when 70 – 80% confluency was reached and regularly checked for mycoplasma contamination. Stock solutions of compounds were stored in deionised water, or DMSO, at 10 mM aliquoted in small volumes to avoid freeze/thaw cycles.

7.10.1 Imaging

EJ cells were seeded on sterile cover slips (22 x 22 mm) in 6 well dishes at a density of 150,000/well and incubated overnight. Staining solutions of the desired compound were made by dilution into culture media (10 μ M) and added to the cells for 24 hours. Once incubation had taken place the cells were washed (PBS) and fixed (4% paraformaldehyde solution in PBS, 4 $^{\circ}$ C, 20 minutes) before being washed again (PBS) and mounted (IMMU-MOUNT, Life Technologies Ltd, Paisley, UK).

The slides were imaged by confocal microscopy (Inverted Zeiss LSM 510 NLO microscope) using a 60 x lens with activation by helium-neon laser ($\lambda = 633$ nm). Emission was registered in the region 650-710 nm.

7.10.2 Light and dark toxicity – MTT assay

96 Well-plates were seeded with EJ cells at 3000/well and incubated overnight. The wells were treated with compound (1 – 100 μ M) or control (DMSO for porphyrin) and incubated for 24 hours. The media was removed and 40 μ l/well PBS was added to each well. For light toxicity experiments the plate was placed in a foil lined box, 6 cm below the light source (10 minutes, 450 nm/ 630 nm LED array at 4.2 mW 450 nm light and 4.85 mW 630 nm light) while dark toxicity plates were kept in the dark. Following light treatment, media was added to (DMEM, 10 % FCS, 200 μ l/well) and the plates were placed in the incubator. Following 24-hour incubation thiazoyl blue (MTT) solution was added to each well (25 μ L, 3 mg ml⁻¹ in PBS). After 3 hours incubation, the media and MTT solution was removed from each well and DMSO was added (150 μ l/well) and crystals dissolved. The optical density of wells at 540 nm was recorded on a plate reader (Multiskan fc, Thermo Fisher Scientific, Warrington, UK).



Chapter 8

References



8.0 References

1. Thomas G, "Medicinal Chemistry", John Wiley and Sons Ltd, England, 2007, 2nd ed., p. 5.
2. Seymour, L.W., Miyamoto, Y., Maeda, H., Brereton, M., Strohalm, J., Ulbrich, K. and Duncan, R., 1995. Influence of molecular weight on passive tumour accumulation of a soluble macromolecular drug carrier. *European Journal of Cancer*, 31(5), pp.766-770.
3. Ceulemans, F., Baurain, R., Geubel, A., Lesur, B., Rolin-van, D.S. and Trouet, A., 1987. Targeting of anthracyclines and hepatomas. *Pathologie-biologie*, 35(1), pp.61-68.
4. (a): Erdmann, L., Macedo, B. and Urich, K.E., 2000. Degradable poly (anhydride ester) implants: effects of localized salicylic acid release on bone. *Biomaterials*, 21(24), pp.2507-2512. (b): Ringsdorf, H., 1975. Structure and properties of pharmacologically active polymers. In *Journal of Polymer Science: Polymer Symposia* (Vol. 51, No. 1, pp. 135-153). New York: Wiley Subscription Services, Inc., A Wiley Company.
5. Langer, R., 1998. Drug delivery and targeting. *Nature*, 392, pp.5-10.
6. Brouwers, J.R.B.J., 1996. Advanced and controlled drug delivery systems in clinical disease management. *Pharmacy World and Science*, 18(5), pp.153-162.
7. Gavasane, A.J. and Pawar, H.A., 2014. Synthetic biodegradable polymers used in controlled drug delivery system: an overview. *Clin Pharmacol Biopharm*, 3(121), p.2.
8. Wagenaar, B.W. and Müller, B.W., 1994. Piroxicam release from spray-dried biodegradable microspheres. *Biomaterials*, 15(1), pp.49-54.
9. CONFORTI, A., BERTANI, S., LUSSIGNOLI, S., GRIGOLINI, L., TERZI, M., LORA, S., CALICETI, P., MARSILIO, F. and VERONESE, F.M., 1996. Anti-inflammatory Activity of Polyphosphazene-based Naproxen Slow-release Systems. *Journal of pharmacy and pharmacology*, 48(5), pp.468-473.

10. Kalala, W., Kinget, R., Van den Mooter, G. and Samyn, C., 1996. Colonic drug-targeting: *in vitro* release of ibuprofen from capsules coated with poly (ether-ester) azopolymers. *International journal of pharmaceutics*, 139(1-2), pp.187-195.
11. Schierholz, J.M., Rump, A. and Pulverer, G., 1997. New antiinfectious biomaterials. Ciprofloxacin containing polyurethanes as potential drug delivery systems to prevent foreign-body infections. *Arzneimittel-Forschung*, 47(1), pp.70-74.
12. Walter, K.A., Tamargo, R.J., Olivi, A., Burger, P.C. and Brem, H., 1995. Intratumoral chemotherapy. *Neurosurgery*, 37(6), pp.1129-1145.
13. Katayama, N., Tanaka, R., Ohno, Y., Ueda, C., Houjou, T. and Takada, K., 1995. Implantable slow release cyclosporin A (CYA) delivery system to thoracic lymph duct. *International journal of pharmaceutics*, 115(1), pp.87-93.
14. Maniar, M., Domb, A., Haffer, A. and Shah, J., 1994. Controlled release of a local anesthetic from fatty acid dimer based polyanhydride. *Journal of controlled release*, 30(3), pp.233-239.
15. McGee, J.P., Davis, S.S. and Oagan, D.T., 1994. The immunogenicity of a model protein entrapped in poly (lactide-*co*-glycolide) microparticles prepared by a novel phase separation technique. *Journal of controlled release*, 31(1), pp.55-60.
16. Kumar, K.P., Bhowmik, D., Chandira, C.M. and Tripathi, K.K., 2010. Innovations in sustained release drug delivery system and its market opportunities. *J Chem Pharm Res*, 2(1), pp.349-360.
17. Cho, K., Wang, X.U., Nie, S. and Shin, D.M., 2008. Therapeutic nanoparticles for drug delivery in cancer. *Clinical cancer research*, 14(5), pp.1310-1316.
18. Wang, B., Hu, L. and Siahaan, T.J., 2016. *Drug delivery: principles and applications*. John Wiley & Sons.
19. Michael, E.A., 2002. The science of dosage form design. *Translation of Pharmaceutics 2e*.

20. Řihová, B. and Kopeček, J., 1985. Biological properties of targetable poly [N-(2-hydroxypropyl)-methacrylamide]-antibody conjugates. *Journal of Controlled Release*, 2, pp.289-310.
21. Seymour, L.W., Flanagan, P.A., Al-Shamkhani, A., Šubr, V., Ulbrich, K., Cassidy, J. and Duncan, R., 1991. Biological properties of monoclonal antibodies conjugated to synthetic polymeric drug carriers. *Select Cancer Ther*, 7, pp.59-73.
22. Wedge, S.R., Duncan, R. and Kopeckova, P., 1991. Comparison of the liver subcellular distribution of free daunomycin and that bound to galactosamine targeted N-(2-hydroxypropyl) methacrylamide copolymers, following intravenous administration in the rat. *British journal of cancer*, 63(4), p.546.
23. Clegg, J.A., Hudecz, F., Mezo, G., Pimm, M.V., Szekerke, M. and Baldwin, R.W., 1990. Carrier design: biodistribution of branched polypeptides with a poly (L-lysine) backbone. *Bioconjugate chemistry*, 1(6), pp.425-430.
24. Allen, T.M., 2002. Ligand-targeted therapeutics in anticancer therapy. *Nature Reviews Cancer*, 2(10), p.750.
25. Brumlik, M.J., Daniel, B.J., Waehler, R., Curiel, D.T., Giles, F.J. and Curiel, T.J., 2008. Trends in immunoconjugate and ligand-receptor based targeting development for cancer therapy. *Expert opinion on drug delivery*, 5(1), pp.87-103.
26. Miller, K., Erez, R., Segal, E., Shabat, D. and Satchi-Fainaro, R., 2009. Targeting bone metastases with a bispecific anticancer and antiangiogenic polymer–alendronate–taxane conjugate. *Angewandte Chemie International Edition*, 48(16), pp.2949-2954.
27. Qiu, Y. and Park, K., 2001. Environment-sensitive hydrogels for drug delivery. *Advanced drug delivery reviews*, 53(3), pp.321-339.
28. Gupta, P., Vermani, K. and Garg, S., 2002. Hydrogels: from controlled release to pH-responsive drug delivery. *Drug discovery today*, 7(10), pp.569-579.

29. Brocchini, S. and Duncan, R., 1999. Polymer drug conjugates: drug release from pendent linkers. *Encyclopaedia of controlled release*, pp.786-816.
30. Nori, A. and Kopeček, J., 2005. Intracellular targeting of polymer-bound drugs for cancer chemotherapy. *Advanced drug delivery reviews*, 57(4), pp.609-636.
31. Duncan, R., 2003. The dawning era of polymer therapeutics. *Nature reviews Drug discovery*, 2(5), p.347.
32. Ferruti, P., Marchisio, M.A. and Duncan, R., 2002. Poly (amido-amine)s: Biomedical Applications. *Macromolecular Rapid Communications*, 23(5-6), pp.332-355.
33. Ulbrich, K. and Šubr, V., 2004. Polymeric anticancer drugs with pH-controlled activation. *Advanced drug delivery reviews*, 56(7), pp.1023-1050. Duncan R. 2005. Targeting and intracellular delivery of drugs.
34. Duncan, R., 2004, In: Targeting and intracellular delivery of drugs. *In: Encyclopedia of Molecular Cell Biology and Molecular Medicine*, Meyers, R.A., Ed., Weinheim, Germany. Wiley-VCH Verlag, GmbH & Co. KgaA. 163-204.
35. Tong, R. and Cheng, J., 2007. Anticancer polymeric nanomedicines. *Journal of Macromolecular Science, Part C: Polymer Reviews*, 47(3), pp.345-381.
36. Matsumura, Y. and Maeda, H., 1986. A new concept for macromolecular therapeutics in cancer chemotherapy: mechanism of tumoritropic accumulation of proteins and the antitumor agent smancs. *Cancer research*, 46(12 Part 1), pp.6387-6392.
37. Gopinath, P., Kumar, S.U., Matai, I., Bhushan, B., Malwal, D., Sachdev, A. and Dubey, P., 2015. Cancer nanotheranostics. In *Cancer Nanotheranostics* (pp. 1-93). Springer, Singapore.
38. Kwon, G.S., Naito, M., Kataoka, K., Yokoyama, M., Sakurai, Y. and Okano, T., 1994. Block copolymer micelles as vehicles for hydrophobic drugs. *Colloids and Surfaces B: Biointerfaces*, 2(4), pp.429-434.

39. Boddu, S.H., Jwala, J., Chowdhury, M.R. and Mitra, A.K., 2010. *In vitro* evaluation of a targeted and sustained release system for retinoblastoma cells using Doxorubicin as a model drug. *Journal of Ocular Pharmacology and Therapeutics*, 26(5), pp.459-468.
40. Flory P, P. J. 1952, *Journal of the American Chemical Society*, 74, 2718.
41. Cheng, L.; Peng, H.; Luo, J.; Tang, B. Z., 2002, *Polymer Preprints (American Chemical Society, Division of Polymer Chemistry)*, 43, 570.
42. (a): Yamaguchi, N., Wang, J.S., Hewitt, J.M., Lenhart, W.C. and Mourey, T.H., 2002. Acid chloride-functionalized hyperbranched polyester for facile and quantitative chain-end modification: One-pot synthesis and structure characterization, *Journal of Polymer Science Part A: Polymer Chemistry*, 40(16), pp.2855-2867. (b): Urich, K. E.; Hawker, C. J.; Fréchet, J. M. J.; Turner, S. R. *Macromolecules* 1992, 25 (18),4583–4587. (c): Newkome, G. R. *Advances in Dendritic Macromolecules*; Jai Press-Elsevier, 1996; Vol. 3.
43. Kim, Y. H.; Webster, O. W., 1988, *Polymer Preprints (American Chemical Society, Division of Polymer Chemistry)*, 29, 310.
44. Hawker, C.J., Lee, R. and Fréchet, J.M.J., 1991. One-step synthesis of hyperbranched dendritic polyesters, *Journal of the American Chemical Society*, 113(12), pp.4583-4588.
45. Ulery, B.D., Nair, L.S. and Laurencin, C.T., 2011. Biomedical applications of biodegradable polymers. *Journal of Polymer Science Part B: polymer physics*, 49(12), pp.832-864.
46. Mou, L., Chen, N., Zhu, K., Chen, Y. and Luo, X., 2012. Copolymer of star poly (epsilon-caprolactone) and polyglycidols as potential carriers for hydrophobic drugs. *Polymers for Advanced Technologies*, 23(4), pp.748-755.
47. Twyman, L.J. and Ge, Y., 2006. Porphyrin cored hyperbranched polymers as heme protein models. *Chemical Communications*, (15), pp.1658-1660.

48. Saini, R., Lee, N.V., Liu, K.Y. and Poh, C.F., 2016. Prospects in the application of photodynamic therapy in oral cancer and premalignant lesions. *Cancers*, 8(9), p.83.
49. Chen, J., Keltner, L., Christophersen, J., Zheng, F., Krouse, M., Singhal, A. and Wang, S.S., 2002. New technology for deep light distribution in tissue for phototherapy. *The Cancer Journal*, 8(2), pp.154-163.
50. Dougherty, T.J., Gomer, C.J., Henderson, B.W., Jori, G., Kessel, D., Korbélik, M., Moan, J. and Peng, Q., 1998. Photodynamic therapy. *JNCI: Journal of the National Cancer Institute*, 90(12), pp.889-905.
51. Wainwright, M., 1996. Non-porphyrin photosensitizers in biomedicine. *Chemical Society Reviews*, 25(5), pp.351-359.
52. Wainwright, M., 2004. Photodynamic therapy—from dyestuffs to high-tech clinical practice. *Coloration Technology*, 34(1), pp.95-109.
53. Ormond, A.B. and Freeman, H.S., 2013. Dye sensitizers for photodynamic therapy. *Materials*, 6(3), pp.817-840.
54. de Melo, L.S., Gomes, A.S., Saska, S., Nigoghossian, K., Messaddeq, Y., Ribeiro, S.J. and de Araujo, R.E., 2012. Singlet oxygen generation enhanced by silver-pectin nanoparticles. *Journal of fluorescence*, 22(6), pp.1633-1638.
55. Dumoulin, F., 2011. Design and conception of photosensitizers. In *Photosensitizers in medicine, environment, and security* (pp. 1-46). Springer, Dordrecht.
56. Agostinis, P., Berg, K., Cengel, K.A., Foster, T.H., Girotti, A.W., Gollnick, S.O., Hahn, S.M., Hamblin, M.R., Juzeniene, A., Kessel, D. and Korbélik, M., 2011. Photodynamic therapy of cancer: an update. *CA: a cancer journal for clinicians*, 61(4), pp.250-281.
57. Silva, E.F., Serpa, C., Dąbrowski, J.M., Monteiro, C.J., Formosinho, S.J., Stochel, G., Urbanska, K., Simões, S., Pereira, M.M. and Arnaut, L.G., 2010. Mechanisms of Singlet-Oxygen and Superoxide-Ion Generation by Porphyrins and Bacteriochlorins and their

- Implications in Photodynamic Therapy. *Chemistry-A European Journal*, 16(30), pp.9273-9286.
58. Castano, A.P., Demidova, T.N. and Hamblin, M.R., 2004. Mechanisms in photodynamic therapy: part one—photosensitizers, photochemistry and cellular localization. *Photodiagnosis and photodynamic therapy*, 1(4), pp.279-293.
59. Detty, M.R., Gibson, S.L. and Wagner, S.J., 2004. Current clinical and preclinical photosensitizers for use in photodynamic therapy. *Journal of Medicinal Chemistry*, 47(16), pp.3897-3915.
60. Allison, R.R., Downie, G.H., Cuenca, R., Hu, X.H., Childs, C.J. and Sibata, C.H., 2004. Photosensitizers in clinical PDT. *Photodiagnosis and photodynamic therapy*, 1(1), pp.27-42.
61. Mehraban, N. and Freeman, H.S., 2015. Developments in PDT sensitizers for increased selectivity and singlet oxygen production. *Materials*, 8(7), pp.4421-4456.
62. Castano, A.P., Demidova, T.N. and Hamblin, M.R., 2004. Mechanisms in photodynamic therapy: part one—photosensitizers, photochemistry and cellular localization. *Photodiagnosis and photodynamic therapy*, 1(4), pp.279-293.
63. Robertson, C.A., Evans, D.H. and Abrahamse, H., 2009. Photodynamic therapy (PDT): a short review on cellular mechanisms and cancer research applications for PDT. *Journal of Photochemistry and Photobiology B: Biology*, 96(1), pp.1-8.
64. Wei, M.F., Chen, M.W., Chen, K.C., Lou, P.J., Lin, S.Y.F., Hung, S.C., Hsiao, M., Yao, C.J. and Shieh, M.J., 2014. Autophagy promotes resistance to photodynamic therapy-induced apoptosis selectively in colorectal cancer stem-like cells. *Autophagy*, 10(7), pp.1179-1192.
65. Dewaele, M., Maes, H. and Agostinis, P., 2010. ROS-mediated mechanisms of autophagy stimulation and their relevance in cancer therapy. *Autophagy*, 6(7), pp.838-854.

66. Xu, J., Gattacceca, F. and Amiji, M., 2013. Biodistribution and pharmacokinetics of EGFR-targeted thiolated gelatin nanoparticles following systemic administration in pancreatic tumor-bearing mice. *Molecular Pharmaceutics*, 10(5), pp.2031-2044.
67. Huang, P., Xu, C., Lin, J., Wang, C., Wang, X., Zhang, C., Zhou, X., Guo, S. and Cui, D., 2011. Folic acid-conjugated graphene oxide loaded with photosensitizers for targeting photodynamic therapy. *Theranostics*, 1, p.240.
68. Schneider, R., Schmitt, F., Frochot, C., Fort, Y., Lourette, N., Guillemin, F., Müller, J.F. and Barberi-Heyob, M., 2005. Design, synthesis, and biological evaluation of folic acid targeted tetraphenylporphyrin as novel photosensitizers for selective photodynamic therapy. *Bioorganic & Medicinal Chemistry*, 13(8), pp.2799-2808.
69. Van Dongen, G.A.M.S., Visser, G.W.M. and Vrouenraets, M.B., 2004. Photosensitizer-antibody conjugates for detection and therapy of cancer. *Advanced drug delivery reviews*, 56(1), pp.31-52.
70. Yoon, I., Li, J.Z. and Shim, Y.K., 2013. Advance in photosensitizers and light delivery for photodynamic therapy. *Clinical endoscopy*, 46(1), p.7.
71. Josefsen, L.B. and Boyle, R.W., 2008. Photodynamic therapy: novel third-generation photosensitizers one step closer. *British Journal of Pharmacology*, 154(1), pp.1-3.
72. Pavani, C., Uchoa, A.F., Oliveira, C.S., Iamamoto, Y. and Baptista, M.S., 2009. Effect of zinc insertion and hydrophobicity on the membrane interactions and PDT activity of porphyrin photosensitizers. *Photochemical & Photobiological Sciences*, 8(2), pp.233-240.
73. Lo, P.C., Huang, J.D., Cheng, D.Y., Chan, E.Y., Fong, W.P., Ko, W.H. and Ng, D.K., 2004. New amphiphilic silicon (IV) phthalocyanines as efficient photosensitizers for photodynamic therapy: synthesis, photophysical properties, and in vitro photodynamic activities. *Chemistry-A European Journal*, 10(19), pp.4831-4838.

74. Komeda, C., Ikeda, A., Kikuchi, J.I., Ishida-Kitagawa, N., Tatebe, H., Shiozaki, K. and Akiyama, M., 2013. A photo-triggerable drug carrier based on cleavage of PEG lipids by photosensitizer-generated reactive singlet oxygen. *Organic & Biomolecular Chemistry*, 11(16), pp.2567-2570.
75. Bovis, M.J., Woodhams, J.H., Loizidou, M., Scheglmann, D., Bown, S.G. and MacRobert, A.J., 2012. Improved *in vivo* delivery of m-THPC via pegylated liposomes for use in photodynamic therapy. *Journal of Controlled Release*, 157(2), pp.196-205.
76. Choi, Y., Kim, S., Choi, M.H., Ryoo, S.R., Park, J., Min, D.H. and Kim, B.S., 2014. Highly biocompatible carbon nanodots for simultaneous bioimaging and targeted photodynamic therapy *in vitro* and *in vivo*. *Advanced Functional Materials*, 24(37), pp.5781-5789.
77. Castagnos, P., Siqueira-Moura, M.P., Goto, P.L., Perez, E., Franceschi, S., Rico-Lattes, I., Tedesco, A.C. and Blanzat, M., 2014. Catanionic vesicles charged with chloroaluminium phthalocyanine for topical photodynamic therapy. *In vitro* phototoxicity towards human carcinoma and melanoma cell lines. *RSC Advances*, 4(74), pp.39372-39377.
78. Wang, N., Zhao, Z., Lv, Y., Fan, H., Bai, H., Meng, H., Long, Y., Fu, T., Zhang, X. and Tan, W., 2014. Gold nanorod-photosensitizer conjugate with extracellular pH-driven tumor targeting ability for photothermal/photodynamic therapy. *Nano Research*, 7(9), pp.1291-1301.
79. Cheng, Y., Doane, T.L., Chuang, C.H., Ziady, A. and Burda, C., 2014. Near infrared light-triggered drug generation and release from gold nanoparticle carriers for photodynamic therapy. *Small*, 10(9), pp.1799-1804.
80. Fraix, A., Gref, R. and Sortino, S., 2014. A multi-photoresponsive supramolecular hydrogel with dual-color fluorescence and dual-modal photodynamic action. *Journal of Materials Chemistry B*, 2(22), pp.3443-3449.

81. Kesharwani, P., Jain, K. and Jain, N.K., 2014. Dendrimer as nanocarrier for drug delivery. *Progress in Polymer Science*, 39(2), pp.268-307.
82. Yin, M., Ju, E., Chen, Z., Li, Z., Ren, J. and Qu, X., 2014. Upconverting Nanoparticles with a Mesoporous TiO₂ Shell for Near-Infrared-Triggered Drug Delivery and Synergistic Targeted Cancer Therapy. *Chemistry-A European Journal*, 20(43), pp.14012-14017.
83. James, D.A., Arnold, D.P. and Parsons, P.G., 1994. Potency and selective toxicity of tetra (hydroxyphenyl)-and tetrakis (dihydroxyphenyl) porphyrins in human melanoma cells, with and without exposure to red light. *Photochemistry and photobiology*, 59(4), pp.441-447.
84. Flory, P. J. *J. Am. Chem. Soc.* 1941, 63 (11), 3083–3090.
85. Sakamoto, K.; Aimiya, T.; Kira, M. *Chem. Lett.* 1997, 26 (12), 1245–1246.
86. Hawker, C. J.; Fréchet, J. M. J.; Grubbs, R. B.; Dao, J. J. *Am. Chem. Soc.* 1995, 117 (43), 10763–10764.
87. 10763–10764.
88. Weimer, M. W.; Fréchet, J. M. J.; Gitsov, I. J. *Polym. Sci. Part A Polym. Chem.* 1998, 36 (6), 955–970.
89. Matyjaszewski, K.; Gaynor, S. G. *Macromolecules* 1997, 30 (23), 7042–7049.
90. Suzuki, M.; Yoshida, S.; Shiraga, K.; Saegusa, T. *Macromolecules* 1998, 31 (6), 1716–1719.
91. Dworak, A.; Walach, W.; Trzebicka, B. *Macromol. Chem. Phys.* 1995, 196 (6), 1963–1970.
92. Twyman, L.J. and Ge, Y., 2006. Porphyrin cored hyperbranched polymers as heme protein models. *Chemical Communications*, (15), pp.1658-1660.